

Digital Signal Processing Algorithms and Techniques for the Enhancement of Lung Sound Measurements

Thesis submitted to Loughborough University in candidature for the
degree of Doctor of Philosophy.

Thato Tsalaile

Advanced Signal Processing Group
Loughborough University
2008

ABSTRACT

Lung sound signal (LSS) measurements are taken to aid in the diagnosis of various diseases. Their interpretation is difficult however due to the presence of interference generated by the heart. Novel digital signal processing techniques are therefore proposed to automate the removal of the heart sound signal (HSS) interference from the LSS measurements.

The HSS is first assumed to be a periodic component so that an adaptive line enhancer can be exploited for the mitigation of the HSS interference. The utility of the scheme is verified on synthetic signals, however its performance is found to be limited on real measurements due to sensitivity in the selection of a decorrelation parameter.

An improved solution with multiple measurements, that does not require a decorrelation parameter and exploits the spatial dimensions, is therefore proposed on the basis of blind source extraction based upon second-order statistics. This approach is found to have improved performance on both real and synthetic datasets, although the level of departure from true periodicity impacts this improvement.

A new sequential blind extraction algorithm for removing quasi-periodic signals with time-varying period is then developed. Source extraction is performed by sequentially converging to a solution which effectively diagonalizes autocorrelation matrices at time lags corresponding to the

time-varying period, and thereby exploits a key statistic of the nonstationary desired interfering source. The algorithm is shown to have fast convergence and to yield much improvement in signal-to-interference ratio (SIR) as compared to when a fixed period is assumed. Separation of the HSS interference is confirmed on measurement datasets.

To conclude, a complete algorithmic solution for the removal of the HSS interference from the LSS measurements, incorporating automatic peak detection based on particle-filtering to extract the time-varying period of the HSS interference, is proposed and validated on real-world lung sound recordings.

*To my loving.....
and to my parents*

ACKNOWLEDGEMENTS

I would like to express my sincere gratitude to the following people who have contributed tirelessly to rendering this work possible:

- First and foremost, I wish to thank my PhD supervisor Prof. Jonathon Chambers for his great leadership and guidance during my entire PhD studies. Prof. Chambers has always given me the freedom to use my own initiative and to do research in my own way. Discussions that we had during our meetings were never one sided as he allowed me to express my thoughts about any aspect of my studies. Indeed, he is a great mentor who has trained me to think “outside the box”. Besides the specific tasks that I carried out in order to complete my PhD, I have had the opportunity to review conference and transaction papers which were not necessarily in my field of study. I therefore, thank Prof. Chambers for broadening my scope in terms of other disciplines. Two weeks prior to writing of this thesis my son passed away. I thank Prof. Chambers for his support and encouragement during those hard times of my life.
- My supervisor when I was still at Cardiff University, Doctor Saeid Sanei. I thank him for accepting to supervise me and for his suggestions, discussions and pointers to relevant literature during my

first year of study. I also want to thank him for recording and providing the lung sound recording necessary to test my algorithms.

- I would also like to thank my family for their unconditional love and support during my entire studies and especially during the time when I lost my son.
- Members of the advanced signal processing group (ASPG) deserve thanks for making the ASPG laboratory an environment conducive for learning. Our discussions during the PhD period have proved beneficial in many ways.
- Lastly, I wish to express my sincere thanks to Prof. Christian Jutten and Mr Reza Sameni from Institut National Polytechnique de Grenoble for their invaluable input to my transactions paper.

STATEMENT OF ORIGINALITY

The original contributions are focused upon exploiting the periodicity of the source of interest (SoI) in order to extract it from other signals. The novelty of the contributions are supported by one published full journal paper, one full journal paper in preparation, and two published conference papers.

In Chapter 3, an adaptive line enhancement technique is employed to enhance a quasi-periodic heart sound signal (HSS) in a mixture of heart sound signal and lung sound signal (HSS-LSS signal). Since the results are sensitive to adaptive line enhancer parameters selection, the key to achieving good results lies in carefully choosing the parameters of the adaptive line enhancer especially the decorrelation parameter. The results of this approach have been published in:

- **T. Tsalaile** and S. Sanei, “Separation of heart sound signal from lung sound signal by adaptive line enhancer,” in *Proc. Int. Conf. EUSIPCO*, 2007, Poznan, Poland.

In Chapter 4, a procedure based on blind source extraction (BSE) by second-order statistics (SOS) is employed for the extraction of the heart sound signal (HSS) from linear mixtures of the heart sound and lung

sound signals (HSS-LSSs). This procedure works by jointly diagonalizing the autocorrelation matrices at time lags corresponding to integer multiple of the perceived period of the SoI which is assumed fixed. From this approach it is appreciated that any departure from strict periodicity impacts performance. For a quasi-periodic, nonstationary signal such as the HSS or the ECG, the periodic duration generally varies from cycle-to-cycle and hence it has time-varying period. To allow for such signals to be extracted, a method that effectively matches the time variations of the SoI is incorporated in the BSE algorithm, thereby resulting in a new BSE algorithm for quasi-periodic signals with time-varying period. The power of this algorithm lies in detecting the peaks of the source (signal) of interest. The results of both algorithms have been published in:

- **T. Tsalaile**, S. M. Naqvi, K. Nazarpour, S. Sanei and J. A. Chambers, “Blind source extraction of heart sound signals from lung sound recordings exploiting periodicity of the heart sound,” *in Proc. ICASSP*, 2008, Las Vegas, USA.
- **T. Tsalaile**, R. Sameni, S. Sanei, C. Jutten, and J. A. Chambers, “Sequential blind source extraction for quasi-periodic signals with time-varying period,” *IEEE Tran. Biomed. Eng.*,
Doi: 10.1109/TBME.2008.2002141.

In Chapter 5, peak detection of the HSS is automated. A signal which is easy to detect peaks from is derived from the original HSS through sequential Bayesian estimation techniques. Here the HSS is modelled by an AR process whose parameters are tracked by Kalman and particle filtering thereby resulting in an evolution signal of the AR parameters.

A signal made up of the norm of the AR parameters is used in the peak detection algorithm. The ideas developed in Chapter 5 are incorporated into Chapter 4 to form a complete solution (presented in Chapter 6) for the extraction of quasi-periodic signals with time-varying period. The results of the complete solution are to be submitted to:

- **T. Tsalaile**, and J. A. Chambers, “A complete solution to the problem of blind source extraction of quasi-periodic signals with time-varying period,” *EURASIP J. Adv. Sig. Process.*

The results of other contributions which are related to the general approaches adopted in this work are published in:

- S. M. Naqvi, Y. Zhang, **T. Tsalaile**, S. Sanei and J. A. Chambers, “A multimodal approach for frequency domain independent component analysis with geometrically-based initialization,” *in Proc. Int. Conf. EUSIPCO*, 2008, Lausanne, Switzerland.
- S. M. Naqvi, Y. Zhang, **T. Tsalaile**, S. Sanei and J. A. Chambers, “Evaluation of emerging frequency domain convolutive blind source separation algorithms based on real room recordings” *in Proc. IEEE SAM*, 2008, Darmstadt, Germany.

Acronyms

ALE	Adaptive Line Enhancer
AMUSE	Algorithm for Multiple Unknown Signals Extraction
AR	Autoregressive
AV	Atrioventricular
BSE	Blind Source Extraction
BSS	Blind Source Separation
CT	Chirplet transform
CVD	Cardiovascular Diseases
CWT	Continues Wavelet Transform
DWT	Discrete Wavelet Transform
EMSE	Excess Mean Square Error
EM	Expectation Maximizing
FFT	Fast Fourier Transform
FIR	Finite Impulse Response
FT	Fourier Transform

FWT	Fast Wavelet Transform
HOS	Higher-Order Statistics
HSS	Heart Sound Signal
ICA	Independent Component Analysis
KF	Kalman Filter
LMS-ANC	Least Mean Square Adaptive Noise Canceller
LSS	Lung Sound Signal
MLE	Maximum Likelihood Estimation
MMSE	Minimum Mean Square Error
MP	Matching Pursuit
MSD	Method of Steepest Descent
MSE	Mean Square Error
NGA	Natural Gradient Algorithm
PCA	Principal Component Analysis
PDF	Probability Density Function
PF	Particle Filter
PSD	Power Spectral Density
RLS-ANC	Recursive Least Squares Adaptive Noise Canceller
SBE	Sequential Blind Extraction
SNR	Signal-to-Noise Ratio

SOBI	Second-Order Blind Identification
SoI	Source of Interest
SOS	Second-Order Statistics
STFT	Short Time Fourier Transform
WGN	White Gaussian Noise
WT	Wavelet Transform

CONTENTS

ABSTRACT	ii
ACKNOWLEDGEMENTS	v
STATEMENT OF ORIGINALITY	vii
ACRONYMS	x
MATHEMATICAL NOTATIONS	xvii
LIST OF FIGURES	xix
1 INTRODUCTION	1
1.1 Motivation	1
1.2 Scope of this study	2
1.3 The cardiovascular system	4
1.4 The cardiac cycle	5
1.5 ECG and heart sounds	5
1.6 Lung sounds	7
1.7 Organization of the thesis	10
	xiii

2	LITERATURE SURVEY	11
2.1	Fundamentals of blind source separation/extraction	11
2.1.1	Independent component analysis	14
2.1.2	Principal component analysis	15
2.1.3	ICA approaches to BSS/BSE	16
2.2	Previous research	19
2.2.1	Signal processing techniques	19
2.2.2	Adaptive processing	19
2.2.3	Time-frequency techniques	26
2.3	Chapter summary and conclusions	37
3	SEPARATION OF HEART SOUND SIGNAL FROM LUNG SOUND SIGNAL WITH AN ADAPTIVE LINE ENHANCER	39
3.1	Introduction	39
3.2	Simulation results	43
3.2.1	HSS-WGN	44
3.2.2	HSS-LSS	46
3.2.3	Discussions	52
3.2.4	Chapter summary and conclusions	54
4	SEQUENTIAL BLIND SOURCE EXTRACTION OF QUASI-PERIODIC SIGNALS WITH TIME-VARYING PERIOD	55
4.1	Introduction	55

4.2	Problem formulation	59
4.2.1	Signal extraction algorithm	61
4.3	Sequential extraction algorithm for quasi-periodic signals with time-varying period	63
4.3.1	Illustrative examples	64
4.3.2	Proposed method	71
4.4	Simulation results	74
4.4.1	Signal-to-interference ratio and the cost function	74
4.4.2	Extraction of synthetic variable period signal	80
4.4.3	Separation of two periodic signals	83
4.5	Application of the proposed algorithm to separation of the heart beat sound signal from real lung sound recordings	83
4.6	Chapter summary and conclusions	86
5	AUTOMATING PERIOD PICKING BY NONLINEAR SEQUENTIAL BAYESIAN FILTERING	88
5.1	Introduction	88
5.2	Problem formulation	91
5.3	Overview of nonlinear Bayesian filtering	93
5.3.1	Kalman filtering	95
5.3.2	Particle filtering	96
5.4	Deriving a signal suitable for peak-picking from the AR process by Kalman and particle filtering based approaches	100
5.4.1	Simulation results	102

5.4.2	Using Kalman filtering	103
5.4.3	Using particle filtering	107
5.5	Chapter summary and conclusion	109
6	PROPOSED COMPLETE SOLUTION FOR SEQUENTIAL BLIND SOURCE EXTRACTION OF QUASI-PERIODIC SIGNALS WITH TIME-VARYING PERIOD	110
6.1	Introduction	111
6.2	Model of approach	112
6.2.1	Simulation results	115
6.3	Chapter summary and conclusion	117
7	CONCLUSION AND FURTHER RESEARCH	119
7.1	Summary and conclusions	119
7.2	Future research	122
	BIBLIOGRAPHY	124

MATHEMATICAL NOTATIONS

n	Number of source signals
m	Number of mixture signals
t	Discrete time index
t'	Continuous time index
$\mathbf{s}(t)$	Vector of source signals
$\mathbf{x}(t)$	Vector of mixture signals
$\mathbf{y}(t)$	Vector of estimated source signals
\mathbf{A}	Mixing matrix
\mathbf{W}	Unmixing matrix
\mathbf{q}	Extracting vector
$E(\cdot)$	Statistical expectation operator
\mathbf{I}	Identity matrix
\mathbf{V}	Whitening matrix

U	Rotation matrix
R	Correlation matrix
E	Eigenvector matrix
Q	Diagonal matrix
$J(\cdot)$	Cost function
$(\cdot)^T$	Transpose operator
\perp	Orthogonality
$\ \cdot\ $	Euclidean norm
τ_t	Time-varying period
$E_t(\cdot)$	Statistical time average

List of Figures

1.1	Schematic diagram of the human heart [1].	3
1.2	Time correlated ECG (a) showing P, QRS, and T waves and acoustic HSS (b) highlighting the first and the second heart sounds (S1 and S2).	7
1.3	Lung structure showing the key respiratory components [1].	9
2.1	Adaptive noise canceller with primary input $x(t)$ and reference input $n_1(t)$.	22
2.2	Graphical representation of FWT procedure.	30
2.3	Typical spectrograms of the normal lung sound and heart sounds.	34
3.1	Adaptive line enhancer with input $x(t)$.	40
3.2	PSDs of the original HSS and recovered HSS, $SNR_{in} = 27dB$: The PSD of the recovered HSS generally matches that of the original HSS within the whole normalized frequency range.	44

-
- 3.3 PSDs of the original WGN (top) and recovered WGN (bottom), $SNR_{in} = 27dB$: The PSD of the recovered WGN resembles that of the original WGN within the whole normalized frequency range. 45
- 3.4 PSDs of the original HSS and recovered HSS, $SNR_{in} = 5dB$: The PSD of the recovered HSS essentially matches that of the original HSS within the whole normalized frequency range. 46
- 3.5 PSDs of the original LSS (top) and recovered LSS (bottom), $SNR_{in} = 5dB$: The PSD of the recovered LSS closely resembles that of the original LSS within the whole normalized frequency range. 47
- 3.6 PSDs of the original HSS and recovered HSS, $SNR_{in} = -5dB$: The PSD of the recovered HSS matches that of the original HSS within the whole normalized frequency range. 47
- 3.7 PSDs of the original LSS (top) and recovered LSS (bottom), $SNR_{in} = -5dB$: The PSD of the recovered LSS closely resembles that of the original LSS within the whole normalized frequency range. 49
- 3.8 PSD of signal $x(t)$ comprising of HSS and LSS with $SNR_{in} = -5dB$. 49
- 3.9 Time domain signals: the original HSS/LSS (top) and recovered HSS/LSS (bottom), $SNR_{in} = 5dB$. 50
- 3.10 Time domain signals: the original HSS/LSS (top) and recovered HSS/LSS (bottom), $SNR_{in} = -5dB$. 51

3.11	Absolute value of the autocorrelation of the LSS: The function decays to a small value at a lag of approximately 375 samples relative to the zero lag.	53
4.1	Pulsetrain and noise before mixing (top), and the linear mixtures (bottom).	66
4.2	Extracted signals using fixed-period algorithm.	67
4.3	HSS and LSS before mixing (top), and the linear mixtures (bottom)	70
4.4	Extracted HSS using fixed-period algorithm.	71
4.5	Comparison of PSDs for: original HSS, extracted HSS by our method, and extracted HSS using the JADE algorithm.	71
4.6	Demonstration of phase allocation procedure for computing τ_t	73
4.7	SIR(dB) versus number of iterations for both fixed and time-varying extraction algorithms for the case of noise-free BSE	76
4.8	$J(\mathbf{t}, \mathbf{q}, \mathbf{d})/N(K + 1)$ (dB) versus number of iterations for both fixed and time-varying extraction algorithms for the case of noise-free BSE	77
4.9	$J(\mathbf{t}, \mathbf{q}, \mathbf{d})/N(K + 1)$ (dB) and SIR(dB) versus number of iterations using time-varying extraction algorithm for the case of noisy BSE	79
4.10	Synthetic signal with time-varying period as the source of interest	80

4.11	Mixtures of synthetic signal with time-varying period and white Gaussian noise	81
4.12	Extracted synthetic signals using algorithms with fixed and time-varying period	81
4.13	ECG and a zoomed-in portion of a synthetic pure periodic signal whose repetition frequency is not a multiple of that of the ECG	82
4.14	Extracted ECG signals using algorithms with the fixed and time-varying period	82
4.15	Extraction of heart sound signal from lung sound recordings	85
5.1	Power spectral density of noise-free HSS.	92
5.2	A typical noisy heart sound signal.	103
5.3	Unsmoothed evolution of the norm of parameters obtained by Kalman filtering at 20dB SNR.	104
5.4	Smoothed evolution of the norm of parameters obtained by Kalman filtering at 20dB SNR.	104
5.5	Evolution of the innovation signal obtained by Kalman filtering at 20dB SNR.	105
5.6	Unsmoothed evolution of the norm of parameters obtained by Kalman filtering at 5dB SNR.	105
5.7	Smoothed evolution of the norm of parameters obtained by Kalman filtering at 5dB SNR.	106

5.8	Evolution of the innovation signal obtained by Kalman filtering at 5dB SNR	107
5.9	Smoothed evolution of the norm of parameters obtained by particle filtering with SNR of 20dB.	108
5.10	Smoothed evolution of the norm of parameters obtained by particle filtering with SNR of 5dB.	108
6.1	Schematic diagram of the proposed complete solution.	114
6.2	HSS and LSS before mixing (top), and the linear mixtures (bottom) (brought forward from Section 4.3.1 of Chapter 4) for ease of reference)	116
6.3	Extracted HSS by the new algorithm with automatic peak detection incorporated	117
6.4	Extracted HSS by a fixed-period algorithm (brought forward from Section 4.3.1 of Chapter 4 for ease of reference)	117

INTRODUCTION

1.1 Motivation

Lung sound signals (LSSs) are produced in the airways of a human being during inhalation and expiration cycles [2]. The LSSs propagate through lung tissues in the parenchyma and can be recorded over the chest wall using a digital stethoscope. The tissue acts as a spatial frequency filter-like structure whose characteristics can vary according to pathological and indeed physiological changes [2]. Besides the fact that normal and abnormal lung sounds are mixed in the airways, which poses a problem in terms of their potential use for classification of respiratory diseases; the quasi-periodic heart sound signal (HSS), from heart beat activity, invariably interferes with the LSS and therefore masks or inhibits clinical interpretation of LSS particularly over low frequency ranges [3]. The main frequency components of HSS are in the range 20-100 Hz and this is the range in which LSS has major components [4]. Therefore, since HSS and LSS overlap in frequency and they are somewhat statistically non-stationary (due to their dependency on physiological changes), the major problem faced in separating HSS from LSS is, doing so, without degrading the main characteristic features of the LSS. Cardiologists also rely on auscultation of heart sounds for detection and discrimina-

tion of cardiovascular diseases (CVD). Since the HSS and LSS overlap in frequency, the cardiovascular information may be corrupted by the intruding LSS which may lead to misinterpretation of cardiovascular information and could consequently lead to the wrong diagnosis by the cardiologist. Any means that will separate the HSS from LSS without degrading the main characteristics of both HSS and LSS will prove extremely beneficial for cardiologists as well as physicians and clinicians. Although several signal processing techniques have been employed to reduce HSS from LSS recording [5], [6], [7], [8], [9], [10], and [11], none of them exploit the key statistical nonstationary characteristic of the HSS in order to separate it from the lung sound recording. These approaches are briefly reviewed in Chapter 2.

1.2 Scope of this study

The following describes the scope of this study

- To identify and apply available digital signal processing algorithms in the context of separation of heart sound from lung sound recordings.
- To develop novel, robust, statistical signal processing algorithms which exploit the key statistical nonstationary characteristic of the heart sound.
- To test the above developed algorithms with real recorded lung sound data.
- To recommend future research directions.

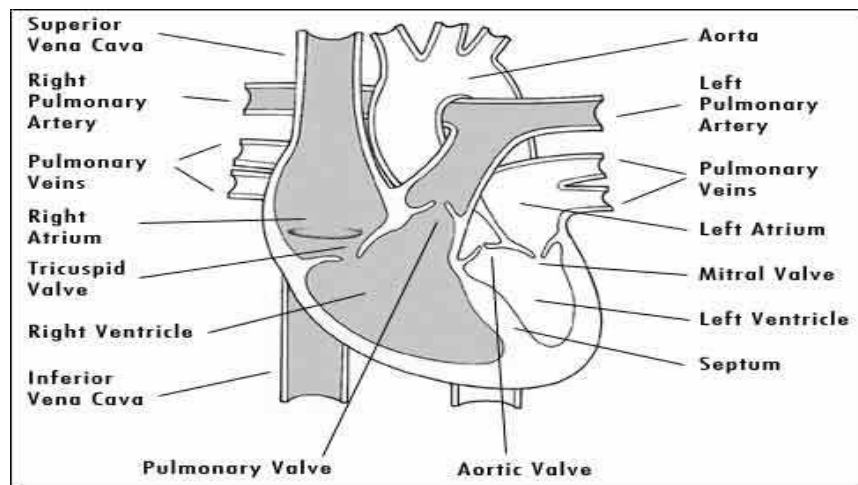


Figure 1.1. A schematic diagram of the human heart showing its major parts. The human heart is a four-chambered muscular organ made up of the left and right atria and the left and right ventricles. Each atrium and its corresponding ventricle is separated by an atrioventricular (AV) valve. The right atrium and right ventricle are separated by the tricuspid valve and the left atrium and left ventricle are separated by the mitral (bicuspid) valve. The two ventricles and arteries are also separated by valves. The right ventricle and the pulmonary artery are separated by the pulmonary valve, while the left ventricle and the aorta are separated by the aortic valve [1].

1.3 The cardiovascular system

The systemic circuit and the pulmonary circuit are two systems through which blood flows in the human body. The pulmonary circuit carries blood to and from the lungs while the systemic circuit carries blood to and from the rest of the body. There are three types of vessels that transport blood namely: *Arteries* which carry blood away from the heart, *veins* which carry blood to the heart and, *capillaries* that permit the exchange of the nutrients and gases between the blood and the surrounding tissues [1].

A schematic diagram of the human heart is shown in Fig.1.1. The human heart is a four-chambered muscular organ: the left and right atria and the left and right ventricles. Each atrium and its corresponding ventricle is separated by an atrioventricular(AV) valve. The right atrium and right ventricle are separated by the tricuspid valve and the left atrium and left ventricle are separated by the mitral (bicuspid) valve. The two ventricles and arteries are also separated by valves. The right ventricle and the pulmonary artery are separated by the pulmonary valve, while the left ventricle and the aorta are separated by the aortic valve.

The right atrium receives deoxygenated blood from the body via the superior and inferior vena cavae. From the right atrium the blood is pumped through the tricuspid valve to the right ventricle, from where it goes through the pulmonary valve into the pulmonary artery, which takes the blood to the lungs where it receives oxygen. The oxygenated blood is transported to the left atrium via the pulmonary vein. The oxygenated blood is pumped through the mitral valve to the left ventricle. When the left ventricle contracts, the blood is pumped through

the aortic valve into the aorta, from where it is distributed to the rest of the body.

1.4 The cardiac cycle

The cardiac cycle is divided into two phases for any of the four chambers of the heart. These are the contraction (systole) and relaxation (diastole) phases. During contraction or systole, the chamber pushes blood into an adjacent chamber; and in relaxation or diastole, the chamber relaxes and is filled with blood.

A cardiac cycle starts with an atrial contraction which fills the ventricles, after which follows an atrial contraction, ventricular contraction, and atrial dilation. During ventricular contraction, the pressure in the ventricles increases and forces the mitral and tricuspid valves to close. The high pressures also forcedly open the pulmonary valve and the aortic valve and the blood flows into the pulmonary artery and aorta. At this point, ventricular relaxation begins and the ventricles as well as the atria are in a dilation phase. The pressures in the ventricles decline and fall below the pressures in the pulmonary artery and aorta, and the pulmonary valve and aortic valve close as a result. As ventricular pressure continues to fall, the pressure drops below the pressure in the atria and the mitral and the tricuspid valve open, allowing blood to flow from the major veins through the atria to the relaxed ventricles.

1.5 ECG and heart sounds

The ECG [12] provides a noninvasive measurement of the electrical activity of the heart. A typical ECG tracing, corresponding to a sin-

gle cardiac cycle is presented in Fig.1.2(a). Distinct electrophysiological events appear as disturbances in the ECG signal. The P wave in Fig.1.2(a) corresponds to the electrical excitation (depolarization) of the top two atrial chambers of the heart. The P wave is associated with blood being pushed by atrial contraction into the lower two ventricular chambers. The Q, R, and S waves together form the QRS complex, which is associated with contraction of the ventricles due to ventricular depolarization. This results in blood being pushed out of the heart into arterial vessels. The T wave corresponds to repolarization of the ventricles, which restores the heart tissue to the normal state and allows the ventricles to relax prior to the next cardiac cycle (Atrial repolarization is typically concealed by the higher-amplitude QRS complex in the normal ECG). The electrical activity of the heart produces mechanical effects that manifest themselves as acoustical signals [12]. Fig.1.2(a) shows time-correlated audio with the ECG in Fig.1.2(b) for a normal heart. The first heart sound, called S1, occurs shortly following the R wave. It is produced as a result of ventricular contraction causing blood to flow back towards the atria, shutting the AV valves between the chambers. The second heart sound, S2, can be heard at the end of the T wave. This is produced by the relaxation of the ventricles causing blood to flow back into these chambers from the arteries, shutting the valves between the ventricles and the arterial vessels. In each case, the closing of valves is associated with vibrations that produce sounds. In the acoustic signal, the period from S1 to S2 is known as systole (ventricular contraction), while the S2-S1 phase corresponds to diastole (ventricular relaxation). Other heart sounds include the third and fourth heart sounds S3 and S4. S3 is due to sudden termination of

the ventricular rapid-filling phase while S4 is due to atrial systole. In this work, S3 and S4 are not considered as they do not occur normally but are indicative of abnormal operation of the heart.

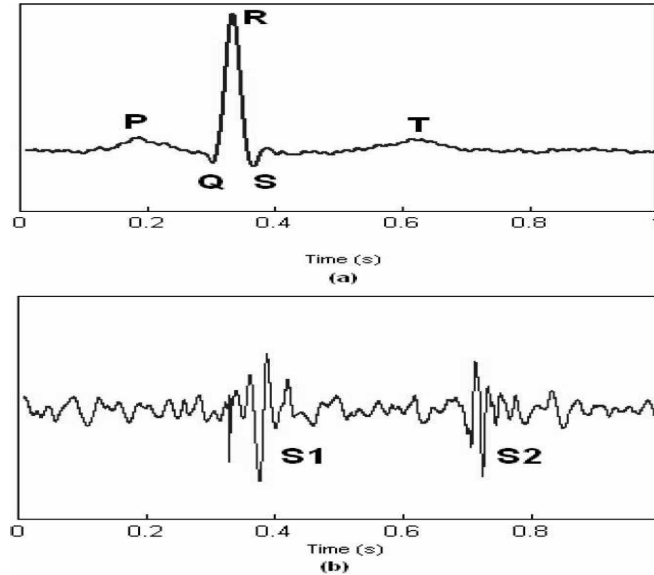


Figure 1.2. Time correlated ECG (a) showing P, QRS, and T waves and acoustic HSS (b) highlighting the first and the second heart sounds (S1 and S2). The ECG signal shown corresponds to a single cardiac cycle. The first heart sound S1 occurs shortly following the R wave. It is produced as a result of ventricular contraction causing blood to flow back towards the atria, shutting the AV valves between the chambers. The second heart sound S2 can be heard at the end of the T wave. This is produced by the relaxation of the ventricles causing blood to flow back into these chambers from the arteries, shutting the valves between the ventricles and the arterial vessels [13].

1.6 Lung sounds

A typical lung structure showing its key components is shown in Figure 1.3. Generally, lung sounds are produced during inspiration and expiration cycles, and are found in the frequency range 20-1200Hz [14]. There are two types of lung sound, namely - normal and abnormal lung sounds. Normal lung sounds originate from within each lobe (made up

of bronchi, bronchioles and alveoli) of the lung during inspiration and from central airways (trachea) during expiration, and they have frequency distribution between 70 and 600Hz [14], [15], and [2].

Abnormal or adventitious sounds are of two types - lung wheeze and crackles. Wheezes are musical or continuous abnormal lung sounds with frequency distribution that extends from less than 100Hz to more than 1000Hz. They originate from air turbulence and oscillations of the walls of narrowed airways (especially the bronchioles) and are heard typically in patients with airway obstruction. Wheezes can further be classified into two categories namely, monophonic and polyphonic wheezes. Monophonic (single tone) wheezes originate from single narrowed airways and are pure tones heard during expiration in patients with airway obstruction. Polyphonic (multi-tone) wheezes have different frequencies. When these frequencies are harmonically related, the wheezing most likely originates from different airways [2]. Crackles on the other hand are non-musical sounds that are essentially short, explosive bursts of sounds that do not have distinct frequencies compared to wheezes. They have broad frequency distribution and originate from airways that open or deform very abruptly in the lung fibrosis when retractile forces of the lung are increased. They may be produced by movement of bubbles in airway fluid and secretions in patients with pulmonary edema or with chronic bronchitis. Crackles may also be classified into two categories: high pitched or fine crackles heard typically in patients with interstitial pulmonary fibrosis, pneumonia, or during early stages of congestive heart failure and the low pitched crackles common in patients with chronic obstructive lung diseases [2].

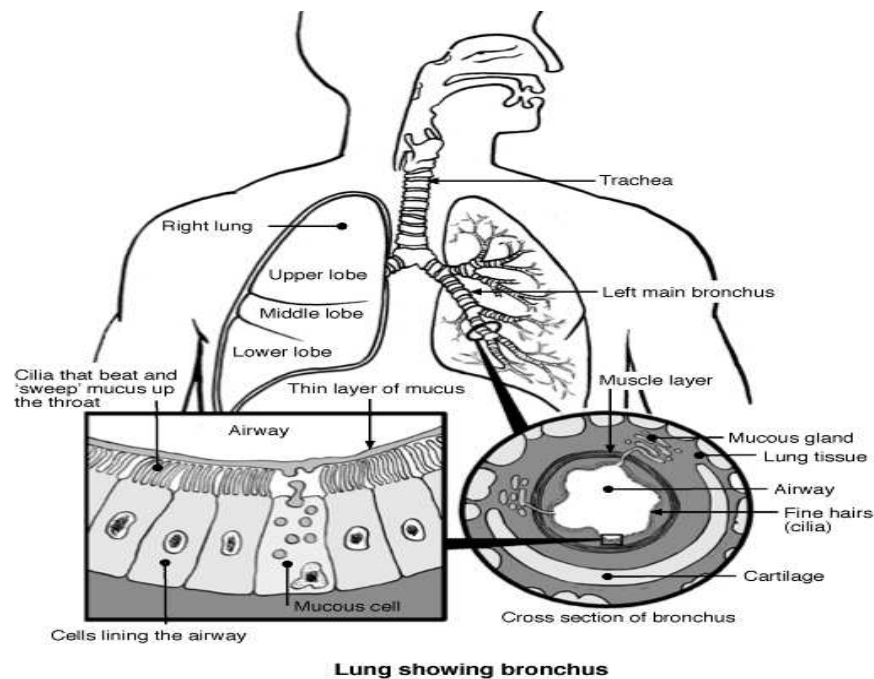


Figure 1.3. Lung structure showing the key respiratory components. Typical sites where normal and abnormal lung sounds originate are shown. Normal lung sounds originate from within each lobe (upper, middle and lower lobe) of the lung during inspiration and from central airways (trachea) during expiration. Abnormal or adventitious sounds from air turbulence and oscillations of the walls of narrowed airways (especially the bronchioles) [1].

1.7 Organization of the thesis

The objective of Chapter 2 is two-fold, notably, to lay the foundation for blind source extraction (BSE) or more generally blind source separation (BSS) and to briefly review signal processing techniques already employed in the literature to solve the problem at hand.

Chapter 3 proposes the adaptive line enhancer (ALE). The basis of this approach stems from the fact that the signal to be removed or extracted has periodic structure which is exploitable through the use of the ALE. The ALE is traditionally used to enhance periodic signals from white or coloured noise.

Chapter 4 introduces a new algorithm, in the context of blind source extraction, for extraction of quasi-periodic signals with time-varying period. The time-varying period is a manifestation of the nonstationarity of the signal of interest. This algorithm is effectively made up of two algorithms. The crucial period or peak information is obtained manually through eye-balling.

Chapter 5 addresses the problem of manually picking the peaks of the signal of interest using sequential Bayesian estimation techniques to introduce a signal suitable for automatic peak-picking.

Chapter 6 presents the complete solution to blind source extraction of quasi-periodic signal with time-varying period. This chapter is effectively made up of material presented in Chapter 5 incorporated in the material presented in Chapter 4.

Chapter 7 concludes the thesis and includes suggestions for future work.

LITERATURE SURVEY

As the main work presented in this thesis is based on blind source extraction, this chapter presents an overview of blind source separation and/or extraction and their general approaches in the context of independent component analysis (ICA). Furthermore, signal processing techniques investigated prior to this research for separation of heart and lung sounds are discussed.

2.1 Fundamentals of blind source separation/extraction

A classical problem in blind source separation (BSS) and blind source extraction (BSE) is to recover the constituent n sources contained within $\mathbf{s}(t)$ given a set of m observable mixture signals collected in $\mathbf{x}(t)$, with minimum assumptions about the mixing medium and the underlying sources. In this work, it is assumed that the dimension m of the observed signals $\mathbf{x}(t)$ is equal to that of the source signals, i.e. $m = n$. The mixtures of sources can be divided into several categories, such as instantaneous mixtures and convolutive mixtures. In the main work presented in Chapter 4, instantaneous mixing is considered instead of the convolutive mixing of sources. This is motivated by the fact that the distances involved (between source signal origin and the sensor) are very small such that the reflections associated with convo-

lutive mixing can be ignored, thereby making the necessity to model convolutive mixing unnecessary. The general noise-free instantaneous BSS problem may be formulated as

$$\mathbf{x}(t) = \mathbf{A}\mathbf{s}(t) \quad (2.1.1)$$

where $\mathbf{x}(t) = [x_1(t), \dots, x_m(t)]^T$ is a vector of observed mixed signals measured at m spatially distinct locations, $\mathbf{s}(t) = [s_1(t), \dots, s_n(t)]^T$ is a vector of source signals assumed to be either statistically independent and /or have different temporal structures, \mathbf{A} is an unknown full column rank mixing matrix, and $[\cdot]^T$ denotes vector transpose. Throughout this thesis all signals are assumed to be real valued and zero mean, and only linear mixing models are considered. The temporal structure of the source signals is very attractive in this research as shall be seen in Chapter 4, wherein it is shown to be possible to exploit this structure of the signals to extract them from their mixtures. In practice, it is possible for the model in Equation (2.1.1) to have a noise term that represents additive white observation noise. In this work however, only the noise-free model (Equation (2.1.1) is assumed but the effect of additive noise is demonstrated in the simulation section of Chapter 4). In general, two approaches are available for recovering the original sources from the instantaneous mixtures: the simultaneous separation approach [16], [17], [18], [19], [20], and [21] and the extraction approach [22], [23], [24], [25], [26], [27], and [28], widely known in the literature respectively as the blind source separation (BSS) and blind source extraction (BSE) approaches. In BSS, all sources are separated simultaneously as

$$\mathbf{y}(t) = \mathbf{W}\mathbf{x}(t) \quad (2.1.2)$$

where $\mathbf{y}(t) = [y_1(t), \dots, y_n(t)]^T$ is the vector of recovered or estimated source signals, and \mathbf{W} is known as the unmixing or separating matrix. On the other hand, in the BSE approach the objective is to extract the sources sequentially one-by-one from the available mixtures $\mathbf{x}(t)$ according to the extraction model

$$y(t) = \mathbf{q}^T \mathbf{x}(t) \quad (2.1.3)$$

where \mathbf{q} is a vector designed to extract the source of interest (SoI) at each extraction stage and $y(t)$ is the output of the extraction algorithm (a single extracted source). Normally, a deflation operation [29] follows the extraction stage in order to remove the extracted source from the mixtures before the next source is extracted. The extraction of each source signal is generally achieved subject to having some *a priori* knowledge about the signals of interest (for example, its stochastic properties, temporal structure or sparseness). This is a major attraction of BSE, since in many applications a large number of sensors (electrodes, microphones or transducers) is available but only a few source signals are of interest. A typical example is the “so-called” cocktail party problem, where it is usually desired to extract the voice of a specific person rather than to separate all the available source signals from an array of microphones. Moreover, in biomedical signal-processing applications such as electroencephalogram/magnetoencephalogram (EEG/MEG) data processing, in which the number of sensors (observations) can be very large, it is desired to recover only some components matched to the

problem of interest.

A common approach to solving BSS and BSE problem is to use some kind of objective function in the context of independent component analysis (ICA) [30]. Independent component analysis estimates statistically independent sources albeit with scaling and permutation ambiguities in the extracted sources. Attempts to solve the permutation problem have been addressed in [31] (using audio-visual information) and the references therein for convolutive mixing of source signals. In the instantaneous mixing and especially when employing blind source extraction, permutation problem is less important and therefore is not considered in this work. ICA is reviewed next.

2.1.1 Independent component analysis

Independent component analysis is a statistical approach designed to decompose multivariate data into components that are as statistically independent as possible. In the literature [30] and [32], ICA normally refers to using a linear transform, i.e. as in the instantaneous BSS model. Nevertheless, within the same literature, some authors address convolutive BSS and implicitly convey the idea that these convolutive BSS algorithms form part of the ICA family. For simplicity in this thesis, ICA refers to the techniques which solve BSS and BSE based on the assumption of statistical independence of the sources. In effect, ICA implies that the joint probability density function $p(\mathbf{s}(t))$ of the sources can be factorized as:

$$p(\mathbf{s}(t)) = \prod_{j=1}^n p_j(s_j(t)) \quad (2.1.4)$$

where $p_j(s_j(t))$ is the marginal distribution of the j th source. Furthermore, the statistical independence of the sources implies the uncorrelatedness of the sources, but the reverse is not necessarily true. As a pre-processing step, most ICA algorithms decorrelate (pre-whiten) the mixtures via spatial whitening, before optimizing their separating objective or cost functions. This spatial whitening is achieved by employing the well-known principal component analysis (PCA), which is explained next.

2.1.2 Principal component analysis

Generally, in the context of BSS, principal component analysis (PCA) seeks to remove the cross-correlation between the observed signals, and ensures that they have unit variance. PCA operates by finding the projections of the mixture data in orthogonal directions of maximum variance [30]. A vector $\mathbf{v}(t)$ is said to be spatially white if

$$E(\mathbf{v}(t)\mathbf{v}^T(t)) = \mathbf{I} \quad (2.1.5)$$

where $E(\cdot)$ denotes the statistical expectation operator and \mathbf{I} is the identity matrix. The unmixing matrix, \mathbf{W} , can be decomposed into two components, i.e.

$$\mathbf{W} = \mathbf{U}\mathbf{V} \quad (2.1.6)$$

where \mathbf{V} is the whitening matrix and \mathbf{U} is the rotation matrix [33]. For $m = n$, there are n^2 unknown parameters in \mathbf{W} . PCA requires the n diagonal elements of the whitened data covariance matrix \mathbf{C}_v to be unity, and due to the symmetry property of \mathbf{C}_v , it suffices that only

$(n^2 - n)/2$ of its off-diagonal terms be zero. Therefore, spatial whiteness imposes $n(n + 1)/2$ constraints. This leaves $n(n - 1)/2$ unknown parameters. Hence, as described by Cardoso, *prewhitening only does half of the BSS job* [33]. The whitening matrix \mathbf{V} can be computed as follows:

$$\mathbf{V} = \mathbf{Q}^{-\frac{1}{2}} \mathbf{E}^T \quad (2.1.7)$$

where \mathbf{E} is the eigenvector matrix of the covariance matrix of $\mathbf{v}(t)$, \mathbf{C}_v . This matrix projects the data into the n -dimensional source space. \mathbf{Q} is a diagonal matrix storing the eigenvalues of \mathbf{C}_v . $\mathbf{Q}^{-\frac{1}{2}}$ ensures the projections have unit variance. It is however important to note that the whitening matrix \mathbf{V} is not unique because it can be pre-multiplied by an orthogonal matrix to obtain another version \mathbf{V} .

2.1.3 ICA approaches to BSS/BSE

ICA relies on fundamentally two factors: 1) a statistical criterion expressed in terms of a cost function $J(\mathbf{y}(t))$, which requires to be either minimized or maximized, 2) an optimization technique to perform the minimization or maximization of the cost function.

Many researchers have focused mainly on formulating new cost functions to propose novel BSS/BSE algorithms. In doing so, it is common in the BSS community to employ either the traditional steepest descent/ascent algorithm, or those more specific to the BSS field such as the natural gradient algorithm (NGA) [34]. The natural gradient can be expressed as:

$$\nabla \mathbf{W} = \frac{\partial J(\mathbf{y}(t))}{\partial \mathbf{W}} \mathbf{W}^T \mathbf{W} \quad (2.1.8)$$

where $J(\mathbf{y}(t))$ is the cost function to be either minimized or maximized, and $\nabla \mathbf{W}$ is the natural gradient with respect to the unmixing matrix \mathbf{W} . This gradient is derived based on the fact that the optimization is Riemannian or curved [34]. The concept of Riemannian is intrinsically related to differential geometry, which is the mathematics of curved spaces. The NGA has been shown to work more efficiently in terms of convergence than the normal gradient approach [34], and therefore it has been used extensively [29].

In general, the statistical criteria employed by the majority of ICA-type algorithms are summarized as

- Many algorithms use second-order statistics (SOS) and thereby exploit the time structure of the sources, mainly the temporal correlation of the sources. Thus, in these methods, the nonGaussianity assumption on the sources, generally required by HOS based approaches, is replaced by assumptions on the time structure of the signals. Typical examples include the famous second-order blind identification (SOBI) algorithm [35], and an algorithm for multiple unknown signal extraction (AMUSE) [36]. Other second-order based techniques such as Parra's algorithm [37] exploit the statistical non-stationarity of the source signals. These techniques are particularly attractive, as they involve only second-order statistics, which are computationally less intensive and less sensitive to data length than the methods based on higher-order statistics (HOS).
- Another class of ICA algorithms utilizes knowledge about stochastic properties (notably the higher-order statistics (HOS)) of the source signals to maximize the statistical independence or non-

Gaussianity. These are based on fourth-order cumulants or kurtosis which is a measure of nonGaussianity. For instance, the joint approximate diagonalization of eigenmatrices (JADE) algorithm jointly diagonalize a set of fourth-order cumulant matrices, such that the sum of squared cross-cumulants is minimized [38]. Similarly, in [29], Cichocki *et al.* proposed an extraction algorithm which extracts a source of interest, whose absolute normalized kurtosis value is the largest amongst all the mixed source signals. Furthermore, in [39] an extraction algorithm is proposed that extracts a source signal whose kurtosis value lies within a specific range. The reason why these algorithms employ higher-order statistics (HOS) lies in the fact that the sources are statistically independent. In other words, uncorrelatedness in terms of higher-order statistics entails statistical independence, whilst uncorrelatedness in terms of second-order statistics does not imply independence, except for sources that are Gaussian [30].

- The last class of ICA algorithms is derived from an information theoretic perspective. This family of ICA algorithms exploits concepts borrowed from information theory such as entropy and mutual information. It is noted that two variables are said to be statistically independent whenever their mutual information is zero [40]. Examples of this ICA category are the Infomax algorithm of Bell and Sejnowski [41], which attempts to maximize the entropy of the estimated sources, and FastICA of Hyvarinen *et al.* that utilizes differential entropy, negentropy [30].

In this research, the stochastic properties of the signals in question are not readily known. However, information regarding the temporal

structure is available in the literature. Therefore, algorithms based on second-order statistics are adopted in this work.

2.2 Previous research

2.2.1 Signal processing techniques

Several different techniques have been implemented to remove or reduce the level of heart sound signals (HSSs) within lung sound recording. These include classical band-pass filtering, adaptive processing techniques (such as the least mean square adaptive noise canceller (LMS-ANC) [5] and the recursive least squares adaptive noise canceller (RLS-ANC)) [9], together with wavelet [10] and Fourier transform-based [11] methods.

2.2.2 Adaptive processing

There are applications where a particular band of frequencies needs to be filtered from a wider range of mixed signals. The band-pass filter is a suitable candidate for achieving this task. Methods based on linear band-pass fixed filtering are not suitable for separation of the heart sound signal (HSS) from the lung sound signal (LSS) because of spectral overlap of these two signals. Given the time-variance or nonstationarity of the signals in question, time-domain adaptive noise cancelling techniques have been implemented instead to remove the interfering noise (HSS) from the signal (LSS).

Adaptive noise cancellation

Adaptive noise cancellation is an approach used to remove background noise from useful signals. Usually, the background noise does not remain statistically stationary. In this case, the noise canceller must be adaptive or exploit an algorithm that is able to adjust to the changing conditions.

A typical adaptive noise canceller is shown in Figure 2.1. The basic idea of the adaptive noise cancellation algorithm is to pass the corrupted signal through a filter that tends to suppress the noise while leaving the signal unchanged. Since this is an adaptive process, it does not require *a priori* knowledge of the signal or noise characteristics.

In order to realize the adaptive noise cancellation, two inputs $x(t)$ (primary input) and $n_1(t)$ (secondary input) where t denotes the discrete time index) are used in conjunction with an adaptive filter. The signal $x(t)$ is information bearing which is corrupted by additive interfering noise $n_0(k)$. Thus, $x(t) = s(t) + n_0(t)$. The signal $n_1(t)$ is the reference noise input which is related in some way to the interference noise in the primary input but ideally uncorrelated with the signal. The noise reference input passes through the adaptive filter and an output $y(t)$ is produced which is as close a replica as possible to $n_0(t)$. The structure of filter employed for adaptive filtering is almost invariably finite impulse response because of the inherent stability and mathematical tractability for computation of its coefficients. The filter, through an adaptive algorithm, readjusts its coefficients $\mathbf{w}(t)$ at each time sample such that the actual filter output $y(t)$ is as close to the interference component $n_0(t)$ of the primary input signal as possible in the mean square error (MSE) sense [42]. Then the output $y(t)$ is subtracted from

the primary input to produce the system output $e(t) = x(t) - y(t)$, which becomes an estimate of the source $s(t)$, denoted as $\hat{s}(t)$, of the information bearing component of the primary signal $x(t)$:

$$\hat{s}(t) = e(t) = x(t) - y(t) = (s(t) + n_0(t) - y(t)) \quad (2.2.1)$$

Using (2.2.1) and assuming jointly wide-sense stationarity inputs $x(t)$ and $n_1(t)$, the MSE is determined as

$$\begin{aligned} E(e(t)^2) &= E(\{x(t) - y(t)\}^2) \\ &= E(\{s(t) + n_0(t) - y(t)\}^2) \\ &= E(s(t)^2) + E(\{n_0(t) - y(t)\}^2) + 2E(s(t)\{n_0(t) - y(t)\}) \end{aligned} \quad (2.2.2)$$

where $E(\cdot)$ denotes statistical expectation. Clearly, the first term is independent of the adaptive noise canceller. Since all signals in the third term of (2.2.2) have been filtered to remove DC and hence have zero-mean, and $s(t)$ is uncorrelated from $n_0(t)$ and $n_1(t)$, this term reduces to zero. Therefore, when the filter coefficients are adjusted so that $E(e(t)^2)$ is minimized, importantly $E(\{n_0(t) - y(t)\}^2)$ is also minimized. In the steady state therefore, theoretically, the system output $e(t)$ serves as the noise-free information bearing signal. Several adaptation algorithms can be used for adjusting the filter coefficients. The most widely used are the least mean square (LMS) and the recursive least squares (RLS) families of algorithms.

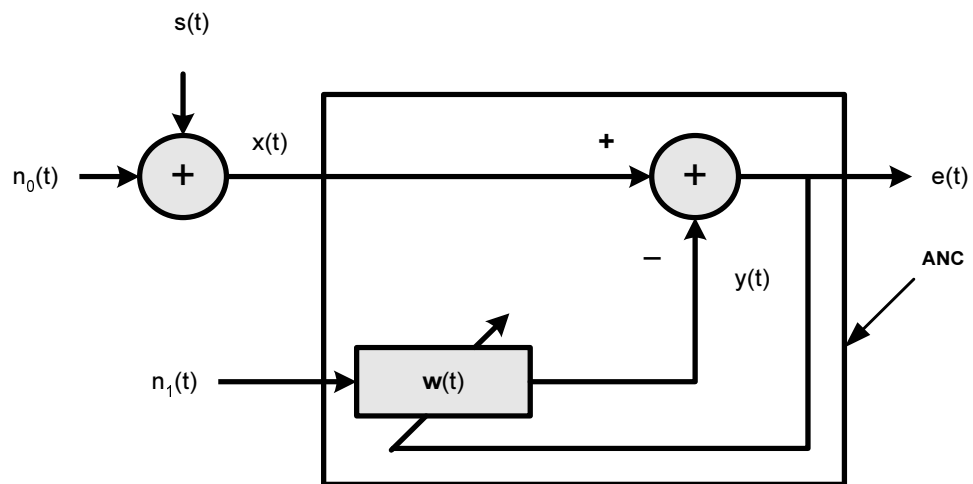


Figure 2.1. Adaptive noise canceller with primary input $x(t)$ and reference input $n_1(t)$.

Least mean square adaptive noise canceller

Generally, the LMS algorithm operates by automatically setting the filter coefficients $\mathbf{w}(t)$ so that the square of the instantaneous error signal $e(t)^2$ is minimised. The optimum minimum mean square error filter coefficients may be obtained by solving the Wiener-Hopf equation [42] to yield

$$\mathbf{w}_{opt} = \mathbf{R}^{-1} * \mathbf{p} \quad (2.2.3)$$

where \mathbf{R} and \mathbf{p} are the auto-correlation matrix and cross correlation vector respectively. The LMS algorithm attempts to approximate this solution. In practice, the computational burden of finding the inverse of the autocorrelation matrix \mathbf{R} is high, requiring $O(M^2)$ operations for a length M filter when \mathbf{R} is Toeplitz. An iterative search method is therefore preferred. One such method is the method of steepest descent (MSD) [42]. If an objective function is defined as: $J = E(e(t)^2)$. The aim of the MSD is to try to find the optimum filter coefficients that minimize this objective function. A recursive way to obtain the filter coefficients based on the MSD is through [42]

$$\mathbf{w}(t+1) = \mathbf{w}(t) + \mu_{MSE} E(e(t)\mathbf{x}(t)) \quad (2.2.4)$$

where μ_{MSE} is called the learning rate of the algorithm, $\mathbf{w}(t+1)$ and $\mathbf{w}(t)$ are the next and present coefficient vectors respectively. Instead of minimizing the mean square error $J = E(e(t)^2)$, the LMS algorithm adapts the filter coefficients so that the instantaneous squared error $e(t)^2$ is minimized. The LMS algorithm is a stochastic approximation of the MSD algorithm in that it replaces the cost function $E(e(t)^2)$ by its instantaneous coarse estimate $\hat{J} = e(t)^2$. If \hat{J} is substituted for J in

the development of the method of steepest descent recursion formula, the recursive formula for the weight updates within the LMS algorithm becomes [42]:

$$\mathbf{w}(t+1) = \mathbf{w}(t) + \mu_{LMS}e(t)\mathbf{x}(t) \quad (2.2.5)$$

where μ_{LMS} refers to the learning rate when the LMS algorithm is used and $\mathbf{w}(0) = 0$.

Recursive least squares adaptive noise canceller

The adaptation algorithm of Figure 2.1 may instead be the recursive least squares algorithm (RLS). For this case, the recursive algorithm for updating the coefficients takes the form [42]

$$\mathbf{w}(t) = \mathbf{w}(t-1) + \mathbf{k}(t)(x(t) - \mathbf{w}^T(t-1)\mathbf{u}(t)) \quad (2.2.6)$$

The filter output is given by:

$$y(t) = \mathbf{w}^T(t-1)\mathbf{u}(t) \quad (2.2.7)$$

where $\mathbf{w}^T(t-1)$ is a transpose of the filter coefficients (tap-weight) vector calculated for the iteration $t-1$, $\mathbf{u}(t) = [u_1(t), u_1(t-1), \dots, u_1(t-M+1)]$ and, M is the filter length.

For every $\mathbf{u}(t)$, the Kalman gain vector, $\mathbf{k}(t)$, is determined as:

$$\mathbf{k}(t) = \frac{\mathbf{P}(t-1)\lambda^{-1} * \mathbf{u}(t)}{(1 + \mathbf{u}(t)^T * \mathbf{P}(t-1)\lambda^{-1} * \mathbf{u}(t))} \quad (2.2.8)$$

The matrix $\mathbf{P}(t)$, which is a sample estimate of the inverse of the adaptive filter input covariance matrix, is initialized as $\mathbf{P}(0) = \mathbf{I}\delta$, where \mathbf{I} is the identity matrix, and δ is the regularization parameter, chosen as

less than 0.01 times the variance of the primary input [9]. The parameter $\lambda \in [0, 1]$ is the forgetting factor and is related to the memory of the algorithm, given by $\frac{1}{1-\lambda}$.

In the literature reviewed, LMS-ANC and RLS-ANC have been used to remove HSS from lung sound recordings. In [5], researchers have used an adaptive filter based on the LMS algorithm to remove heart sound (HS) interferences. In this work, the HSS recorded from above the person's heart location (to maximize the presence of the heart sound) was used as the reference signal $n_1(t)$ for the adaptive system. The HSS recorded this way is not without the LSS and this is a discrepancy in the method since the adaptive scheme requires a 'noise only' (HSS in this case) reference signal. The presence of such signal leakage into the reference degrades the performance of the ANC. Similarly, researchers in [6] and [7] have used an adaptive system with the ECG signal as the reference signal. The noise signals $n_1(t)$ and $n_0(t)$ of the adaptive noise canceler (Fig.2.1), corresponding to the contaminating HSS in the LSS and the reference HSS respectively, are assumed to be correlated in time. Thus, their time alignment is crucial to successful reduction of the contaminating HSS which is assumed additive to the LSS. Apart from the fact that the ECG signal does not occur at exactly the same time as the HSS, it has only one spike or significant peak (the R-wave) corresponding to the first heart sound $S1$ (contraction of the heart), while the contaminated LSS (with HSS) has two heart sounds $S1$ and $S2$ corresponding to the contraction and relaxation of the heart. While a new reference signal may be designed by adding to the ECG a delayed version of itself to account for the occurrence of $S2$, the delay used will be subject to error because it may be chosen to be approxi-

mately the time between the two heart sounds. Thus, the error of the estimate of this delay between the two heart sounds plays a pivotal role in successfully removing or reducing the second heart sound. The statistical nonstationary nature of the HSS makes estimation of the delay a challenging task. Efforts to eliminate the use of a reference signal, by using a single recording (eliminating the use of the reference signal) have proved futile due to improper identification of the HSS sounds within the long sound recording [8]. An RLS-based adaptive noise cancellation filtering technique has also been implemented to separate or reduce the HSS from the LSS where the reference signal was derived through band-pass filtering and segmentation of the LSS recording (see for instance [9]). For similar reasons presented above, the reference HSS signal was not free of LSS. Thus, generally, the major challenge in using the ANC has been to identify the appropriate choice of the reference signal. In this work therefore, proceeding with the ANC is abandoned due to its inherent use of the reference signal.

2.2.3 Time-frequency techniques

Wavelet transform

Computing the wavelet transform consists of breaking up a signal into shifted and scaled versions ($\psi_{a,b}(t')$) of an original (mother) wavelet ($\psi(t')$), where t' denotes continuous time, and is similar to the Fourier transform which breaks up the original into sinusoids of different frequencies. The continuous wavelet transform (CWT) is calculated as:

$$\psi_{a,b}(t') = \frac{1}{\sqrt{a}}\psi\left(\frac{t' - b}{a}\right), a > 0, b \in \Re \quad (2.2.9)$$

where a is the dilation (scale) parameter and b is the translation parameter. An original mother wavelet is chosen from a pre-defined set of wavelets, or alternatively, a custom wavelet can be constructed. The wavelet is then stepped through the signal, multiplied with the signal at every time instant of interest and integrated to yield a wavelet coefficient. The scale of the wavelet is then changed to compress or dilate it. The new wavelet undergoes the same process of stepping through the signal, multiplication and integration to yield wavelet coefficients. This process is repeated for the set of scales chosen. If the coefficient that has been calculated is relatively large, the signal contains a component that is similar to the wavelet of the specific scale.

The discrete wavelet transform (DWT) computes coefficients for a dyadic scale sequence. This means that the wavelet coefficients are only calculated for scales based on the power of two. The resolution of the DWT is not as good as the resolution of the CWT, but its computation time is highly reduced since the coefficients are not calculated for every scale and integration is replaced by summation, which is more easily implemented. The analysis can be equally accurate as the CWT nonetheless [43].

Mallat developed an efficient way to implement the DWT by using the subband coding scheme [44] known as the fast wavelet transform (FWT). With this scheme, the signal is broken down into low-frequency (approximation) and high-frequency (detail) components by passing the signal through low and high-pass finite impulse response (FIR) filters respectively. At each breakdown level, the signal bandwidth is split in half. For example, if a signal is sampled at 4000Hz, the maximum frequency present in the signal is 2000Hz according to the Nyquist

criterion. This implies that after the first set of filters in the DWT, the approximation will essentially contain the components between 0-1000Hz and the detail will essentially contain the components between 1000-2000Hz. In the next breakdown level, the approximations of the previous level are broken down further, yielding another set of approximations and details. The approximation of this level essentially contains the frequency components between 0-500Hz and the detail the frequency components between 500-1000Hz. The signal has to be down sampled at each level to ensure that the number of samples at the breakdown level is half the amount of samples contained in the signal that is passed through the filters. The FWT process is explained graphically in Fig.2.2.

In the reviewed literature, wavelet-based filtering has been implemented to separate respiratory signals as well as in reducing phonocardiogram signals from lung sound recording. The wavelet-based filter was first proposed by Hadjileontiadis and Panas [45] with the assumption that the nonstationary part of the signal in the time domain produces large WT coefficients over many wavelet scales, a_s (from Equation (2.2.9)) whereas for the stationary part, the coefficients die out quickly with increasing scale. They applied the method to separate discontinuous adventitious sounds (crackles) from vesicular sounds based on the significant wavelet transform (WT) coefficients at each scale - most significant coefficients at each scale with amplitude above some predetermined threshold correspond to nonstationary signals (crackles) in the time domain and the rest correspond to a stationary signal (the vesicular). Researchers in [10] have applied a wavelet-based filter to separate the HSS from the LSS. These researchers suggested that generally the

HSS has larger peaks in HSS-LSS recording, and therefore they considered the HSS as nonstationary and the LSS as a stationary signal. However, the HSS peak is not always larger than that of LSS. Making such a conclusion about the HSS and LSS, and using a wavelet-based filter to separate the two signals, could lead to failing to completely remove the HSS from the LSS, primarily due to ambiguity in determining the threshold amplitude. In fact, according to reported results, the HSS was not completely removed [11].

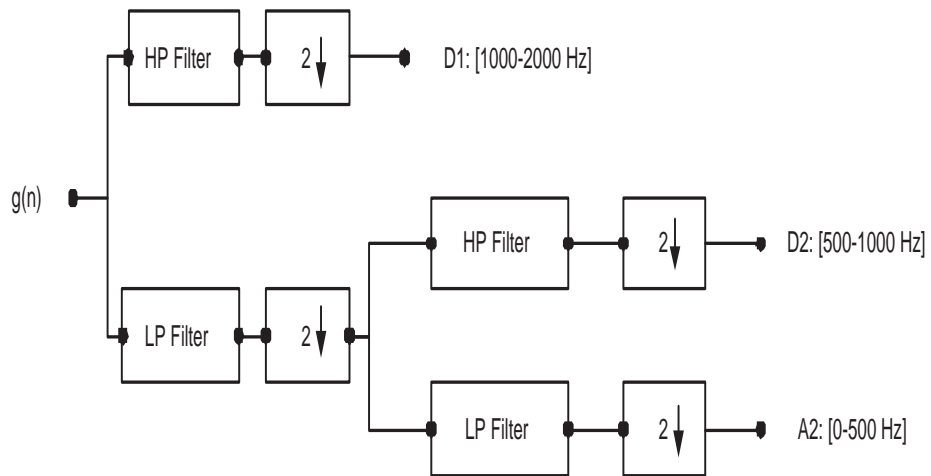


Figure 2.2. Graphical representation of FWT procedure. With this scheme, the signal is broken down into low-frequency (approximation) and high-frequency (detail) components by passing the signal through low and high-pass finite impulse response (FIR) filters. At each breakdown level, the signal bandwidth is split in half.

Short-time Fourier transform

A time-domain signal may be transformed into a frequency-domain signal by applying the Fourier transform (FT). The resulting Fourier coefficients are indicative of which frequencies are contained in a given time-domain signal. In practice, the discrete Fourier transform (DFT) is implemented to obtain the frequency-domain signal for discrete time-domain signals. In order to compute the FT of a signal in a more fast and efficient manner, in 1965, Cooley and Tukey developed the fast Fourier transform (FFT) algorithm. The details of the FFT algorithm can be found in [46]. The spectrum or the frequency information of a signal is of vital importance, since for a composite signal like the lung sound recording, which comprises of the breath sound (LSS) and the HSS, it is possible to deduce the occurrence of each one of them and possibly use this information to separate them.

The major setback in performing the FT is the fact that if the signal under analysis is nonstationary all the temporal information in the signal is lost [47]. The FT can only be properly applied if the signal being analyzed is assumed stationary [48]. A stationary signal is a signal whose statistical characteristics do not change with time [49]. HSS and LSS signals vary according to pathological and physiological changes and therefore exhibit extremely nonstationary properties. The FT is thus not suitable for the analysis of these signals [50]. To determine how the frequency content of a signal changes over time, a signal is cut into blocks and the spectrum of each block is computed. In an effort to avert the disadvantage (of losing temporal information) of the FT, the short time Fourier transform (STFT) was developed. The STFT is implemented by cutting the signal of interest into smaller blocks, where

each block is assumed stationary and the FT is performed on each one of them. In order to improve the results, blocks overlap each other and each block is multiplied by a window function that is tapered at its endpoints (this is called windowing) to mitigate spectral smearing. The spectrum is thus determined by computing spectra of overlapping signal blocks. The discrete STFT is computed as:

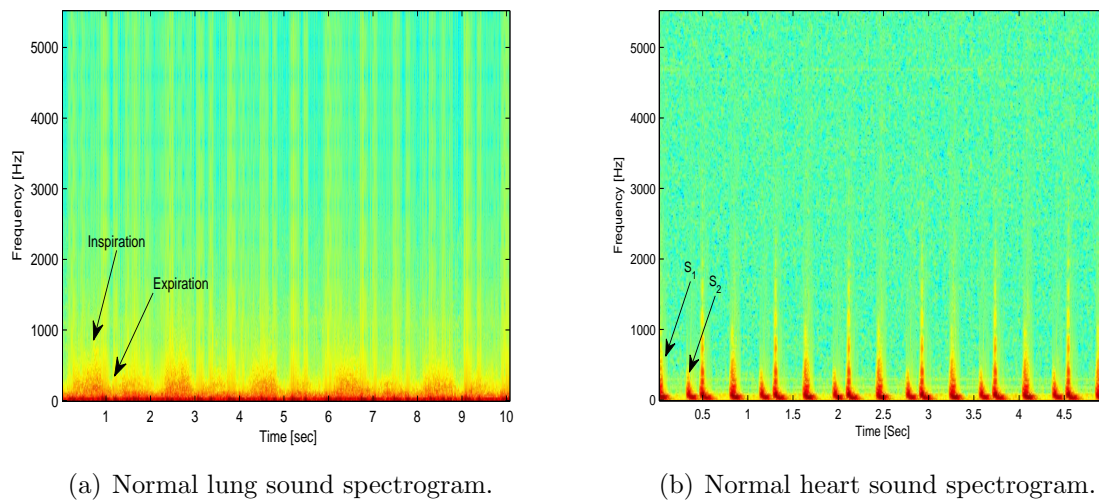
$$STFT(t, f_k) = \sum_{l=t*D-(T/2)}^{t*D+(T/2)-1} w(t*D-l)x(l)e^{-j*2\pi*f_k*l/T} = \mathfrak{S}(w(t * D - 1)x(l)) \quad (2.2.10)$$

where $x(l)$ is the sampled signal, t and f_k are the time and frequency sample indices respectively, $w(t*D-l)$ is a time domain window whose location is a multiple of D samples in time, and \mathfrak{S} corresponds to evaluation of T uniformly spaced samples via the discrete-time Fourier transform.

Typical LSS and HSS spectrograms, computed using the STFT are shown in Figs.2.3(a) and 2.3(b) respectively. The STFT cannot track very sensitive changes in the time direction [51] and hence is not suitable for the analysis of nonstationary and rapidly changing HSS and LSS. However, a method based on the adaptive thresholding of the spectrum (of the HSS-LSS signal) obtained through the STFT was proposed in [11] for detection of segments which include HSS. Finally, these segments were removed by band-stop filtering. Although the main components of HSS are in the range of the chosen band-stop filter (20-100Hz), there are still some HSS components (weak) at frequencies higher than this range. Therefore, this technique could not completely remove the HSS signal from the LSS signal.

The main deficiency of STFT is that the length of the window is fixed

and, thus, is not an effective way to describe structures much smaller than the window length. Although the wavelet transform overcomes this limitation by allowing for a variable window length, there is fundamental reciprocal relation that exists between the central frequency of a wavelet and its window length. Thus, the wavelet transform does not provide precise estimates of low frequency components with short duration or narrow-band high frequency components. In view of the above disadvantages in time-frequency techniques (WT, FT, STFT), they are not considered further in this thesis.



(a) Normal lung sound spectrogram.

(b) Normal heart sound spectrogram.

Figure 2.3. Typical spectrograms of the normal lung sound and heart sounds are shown on Figs. 2.3(a) and 2.3(b). This shows the prevalent frequency components during breathing (inspiration and expiration) and those due to heart activity (S₁ and S₂).

Chirplet transform

A chirp function is a rapidly swept wave. Just as the short time Fourier transform (STFT) is a windowed Fourier transform (FT), a chirplet function is a windowed chirp function. The STFT and the wavelet transform (WT) may be considered as special cases of the chirplet transform (CT). The basis function for a Gaussian CT is derived from a single Gaussian function through four operations namely: scaling, chirping, time and frequency shifting, which lead to a family of wave packets with four adjustable parameters [52].

$$g_{t_c, w_c, c, \Delta_{t'}}(t') = \frac{1}{\sqrt{\sqrt{\pi} \Delta_{t'}}} e^{-1/2 \left(\frac{t' - t_c}{\Delta_{t'}} \right)^2} e^{j[c(t' - t_c) + w_c](t' - t_c)} \quad (2.2.11)$$

where $j = \sqrt{-1}$, t_c , is the time center, w_c is the frequency center, $\Delta_{t'}$ is the effective time spread, and c is the chirp rate that characterizes how quickly the frequency changes. The chirplet transform of a signal $f(t')$ is defined as the inner product between the signal and the Gaussian chirplet defined in (2.2.11)

$$a_{t_c, w_c, c, \Delta_{t'}} = \int_{-\infty}^{\infty} f(t') g_{t_c, w_c, c, \Delta_{t'}}^*(t') dt' \quad (2.2.12)$$

where $*$ denotes the complex conjugate operation. The coefficient $a_{t_c, w_c, c, \Delta_{t'}}$ represents the signal energy content in the time-frequency region specified by the chirplet, and the absolute value of the coefficient is the amplitude of the projection. If the set of parameters is defined by a continuous index set $I = (t_c, w_c, c, \Delta_{t'})$, then an arbitrary signal $f(t')$ can be constructed as a linear combination of Gaussian

chirplets, thus,

$$f(t') = \sum_{n=1}^P a_{I_n} g_{I_n}(t') + R^{P+1}f(t') = f_P(t') + R^{P+1}f(t') \quad (2.2.13)$$

where I_n is the parameter set of the n^{th} chirplet, $R^{P+1}f(t')$ denotes the residue and $f_P(t')$ is the P^{th} -order approximation of the signal. The optimal estimation of the a_{I_n} , and I_n corresponding to the decomposition of a signal into the basis functions g_{I_n} , is a nondeterministic-polynomial time (NP) hard problem [53]. Thus, there is no known existing polynomial time algorithm to solve this problem. However, suboptimal techniques have been developed [54], [55], and [56]. One such technique involves obtaining initial coarse estimates by the matching pursuit (MP) algorithm; the estimates obtained undergo progressive refinement with maximum likelihood estimation (MLE); the values obtained from MLE are optimized through the Newton-Raphson method; the estimates obtained are further refined by the expectation maximizing (EM) algorithm.

The main deficiency of the STFT is that the length of the window is fixed. Therefore, it is not an effective way to describe structures much smaller or much larger than the window length. The discrepancy with the WT is that it does not provide precise estimates of low frequency components with short-time duration or narrow-band high frequency components. This is because of the reciprocal relationship between central frequency of the wavelet and its window length. The Chirplet transform overcomes the deficiencies in the STFT and WT by allowing for adjustment of four parameters of time-spread, chirp rate, time center and frequency center giving a more compact representation of

the signal under analysis. The CT has also found applications in the analysis of biomedical signals such as visual evoked potentials [57].

To this end, HSS and LSS in the lung sound recording could be modelled by Gaussian chirplets and the lung sound recording by a linear combination of these chirplets. However, as noted in the discussion above, the solution requires greedy algorithms which are computationally demanding because they perform exhaustive search along the signal to estimate each chirplet. Furthermore, in modeling HSS and LSS, critical parameter information I_n has to be estimated in order to construct chirplets dictionary. Due to computational constraints and possible errors in parameters estimation, the CT method is not considered in this thesis.

2.3 Chapter summary and conclusions

In this chapter the fundamentals of blind source separation/extraction (BSS/E) algorithm have been presented. It has been noted that, compared with blind source separation (BSS), blind source extraction (BSE) provides more flexibility and has some advantages over BSS such as relative low computational complexity and extraction of sources of interest (when *a priori* knowledge of the source of interest is available). In general, BSS/E solutions include methods based on either second-order statistics (SOS) or higher-order statistics (HOS). Methods based on SOS that exploit the temporal structure of the signal of interest are preferred in this thesis.

Furthermore, in this chapter, signal processing techniques such as adaptive noise cancellation (ANC), time-frequency techniques and time-scale-frequency (TSF) are reviewed. It is suggested not to proceed

with ANC methods due to their inherent use of a noisy reference signal. Time-frequency techniques are also abandoned because of limitations in transforms used (FT, STFT, WT). It is suggested that the TSF (chirplet transform) could be used to mitigate HSS from lung sound recording. However, the major setback of this technique lies in its relatively high computation burden and the need to design a dictionary of chirplets corresponding to the HSS and LSS. New techniques are therefore required, and the following chapters contain new contributions to the field.

SEPARATION OF HEART SOUND SIGNAL FROM LUNG SOUND SIGNAL WITH AN ADAPTIVE LINE ENHANCER

In this chapter, the adaptive line enhancer (ALE) is employed for reducing heart sound signal (HSS) from lung sound recordings. The ALE is tested on both synthetic and real recorded data mixed with the HSS. This is the first time the ALE is used in this application.

3.1 Introduction

The adaptive line enhancer (ALE) was originally introduced by Widrow *et al.* [58]. It was coined adaptive line enhancer because of its ability to ‘enhance’ narrowband signals in the presence of wide-band noise [59] and [60]. The adaptive line enhancer has also been used to enhance sinusoidal signals in “coloured” noise [59]. This technique has also found applications in spectral estimation, frequency estimation and detection [58], [61], [60], interference rejection [58], predictive deconvolu-

tion [62], and adaptive linear predictive coding [63].

The time domain representation of the ALE structure is shown in Fig.3.1. The ALE comprises of an M -weight linear predictive finite impulse response (FIR) filter. The ALE adaptively filters the delayed version of the input signal in accordance with the well known least mean square (LMS) adaptation algorithm of [42].

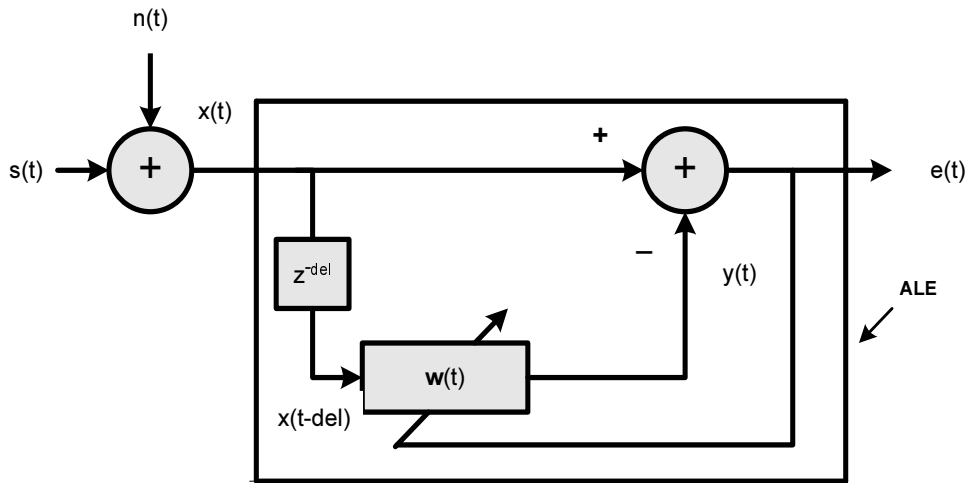


Figure 3.1. Adaptive line enhancer with input $x(t)$.

The time domain analysis of the structure is as follows:

$$x(t) = s(t) + n(t) \quad (3.1.1)$$

where $s(t)$ is the periodic narrowband signal and $n(t)$ is the broad-band noise signal.

At any time instance t , the output $y(t)$ of the ALE is defined as:

$$y(t) = \sum_{l=0}^{M-1} w_l(t)x(t-l-del) \quad (3.1.2)$$

where del is the prediction distance of the filter in terms of the normalized sampling interval, M is the filter length, and $w_l(t), l = 0, 1, \dots, M-1$

are the ALE coefficients (FIR filter weights).

According to Widrow *et al.* [58], $y(t)$ is an estimate of $s(t)$ provided the delay del exceeds the correlation time of $n(t)$. The delay del should be chosen equal to a lag, τ , for which the autocorrelation function of $n(t)$, $z_n(\tau)$ can be considered small relative to $z_n(0)$. Suffice to note that when dealing with sinusoidal signals in ‘coloured’ noise, a relatively large value of the delay del is often chosen [58]. The adaptive filter weights $w_l(t)$, $l = 0, \dots, M - 1$, are chosen to minimise approximately the mean square error (MSE) defined as:

$$\xi = E(\{x(t) - y(t)\}^2) \quad (3.1.3)$$

Now, since the only correlated component with $x(t)$ and its delayed versions, $x(t - del), \dots, x(t - del - M + 1)$ is the underlying narrowband signal $s(t)$ the MSE is minimized when $y(t) = x(t)$ [64]. In order to adjust the ALE coefficients the LMS algorithm is preferably used due to its low computational complexity and robustness.

$$\mathbf{w}(t + 1) = \mathbf{w}(t) + \mu_{ALE} \mathbf{x}(t - del)(x(t) - \mathbf{w}(t)^T \mathbf{x}(t - del)) \quad (3.1.4)$$

where $\mathbf{w}(t) = [w_0(t), \dots, w_{M-1}(t)]^T$, and M is the length of the adaptive filter $\mathbf{x}(t - del) = [x(t - del), \dots, x(t - del - M + 1)]^T$ is the ALE input vector, and μ_{ALE} is the ALE convergence rate.

The use of the LMS algorithm for the ALE and its properties have been discussed extensively in [64]. There are three parameters that determine the performance of the LMS-ALE algorithm for a given application. These are the ALE adaptive filter length M , the prediction distance del , and the LMS convergence parameter μ . Several perfor-

mance criteria may be considered in choosing ALE parameters. These include: adaptation rate, excess mean square error (EMSE) or misadjustment, and finally the frequency resolution. The adaptation rate is controlled by the choice of μ , M , and the condition of the data autocorrelation matrix [42]. Typically, the MSE for the LMS-ALE converges geometrically with a time constant $\tau_{LMS-ALE}$ [65] as:

$$\tau_{LMS-ALE} \approx \frac{1}{4\mu_{ALE}\lambda_{min}} \quad (3.1.5)$$

where λ_{min} is the minimum eigenvalue of the input vector autocorrelation matrix. Clearly, the convergence speed is proportional to the convergence rate μ_{ALE} . The EMSE ξ_{mis} , resulting from the noisy estimate of the MSE gradient in the LMS algorithm is approximately given by [65]

$$\xi_{mis} \approx \frac{\mu_{ALE}M\lambda_{av}}{2} \quad (3.1.6)$$

where λ_{av} is the average eigenvalue of the input vector autocorrelation matrix. Since the user has no control over λ_{av} (determined by input data), EMSE may be controlled by choosing values of μ_{ALE} and M . Smaller values of μ_{ALE} and M reduce the EMSE, while larger values increase the EMSE. The frequency resolution f_{res} , of the ALE is given in [65] as:

$$f_{res} = \frac{F_s}{M} \quad (3.1.7)$$

where F_s is the sampling frequency. Hence, clearly, f_{res} may be controlled by M . Equation (3.1.6) in concert with Equation (3.1.7) show that larger values of M improve f_{res} at the expense of increased EMSE, and smaller values reduce the EMSE at the expense of the reduced f_{res} . The choice of the three parameters of μ , M , and del when the ALE is

used in this chapter is largely motivated by the performance criteria discussed above.

An expression for the signal-to-noise ratio (SNR) gain due to processing by the ALE for sinusoids in white noise has been given in [66]. For large M , the expression is simplified to

$$\frac{SNR_{out}}{SNR_{in}} = \frac{1}{\frac{2}{M} + \mu_{ALE}\xi_{min}M(1 + SNR_{in})} \quad (3.1.8)$$

where ξ_{min} is the minimum MSE. Clearly, decreasing μ_{ALE} increases the SNR gain at the expense of slower adaptation rate.

The ALE operation may be summarized as follows; the introduced delay, del , causes decorrelation between the noise components within the input signal $x(t)$ and that contained in the delayed input signal $x(t - del)$. The adaptive filter responds by forming a transfer function equivalent to that of a narrow-band filter centred at the frequency of the sinusoidal components. The noise component of the delayed input is rejected, while the phase difference of the periodic components is readjusted so that the components cancel each other at the summing point, producing a minimum error signal composed of the noise component of the instantaneous input data alone.

3.2 Simulation results

The objective of this section is to show the use of the ALE in mitigating, for the first time, the HSS in LSS measurement. The section demonstrates the ability of the ALE to recover the HSS signal from the combined heart sound signal and white Gaussian noise (HSS-WGN) signal as well as from the combined HSS-LSS signal. The aforementioned

composite signals are applied sequentially to the ALE. Evaluation is performed by comparing the power spectral densities (PSDs) at the input of the adaptive line enhancer and those of the recovered signals at the output of the adaptive line enhancer after convergence. The normalized frequency ranges from 0 to 1, where 1 corresponds to the normalized Nyquist frequency, this convention is used throughout the thesis. The effectiveness of the ALE is further evaluated by listening to the resulting recovered HSS and LSS to detect any artefacts. HSS and LSS data are obtained from R.A.L.E. data sets [67]. Reference is made to Fig. 3.1 for discussions in the following section.

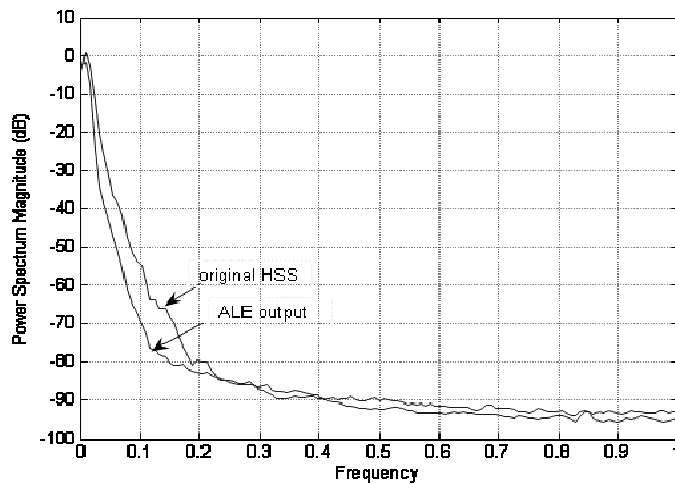


Figure 3.2. PSDs of the original HSS and recovered HSS, $SNR_{in} = 27dB$: The PSD of the recovered HSS generally matches that of the original HSS within the whole normalized frequency range.

3.2.1 HSS-WGN

The purpose of this subsection is to demonstrate that processing by the ALE does not affect the signal to be enhanced therefore a low level noise component is added. The input signal to the ALE $x(t)$, is the noise-free HSS signal $s(t)$, corrupted by synthetic WGN $n(t)$, with SNR

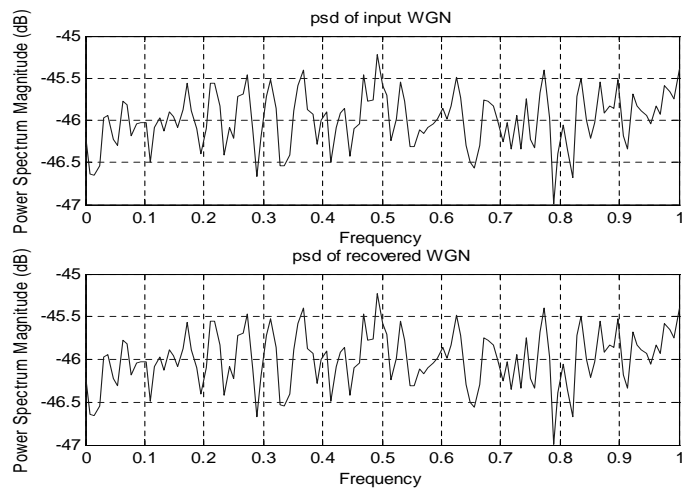


Figure 3.3. PSDs of the original WGN (top) and recovered WGN (bottom), $SNR_{in} = 27dB$: The PSD of the recovered WGN resembles that of the original WGN within the whole normalized frequency range.

equal to 27dB. The signal $x(t)$ was applied to the ALE of Fig. 3.1 with ALE parameters $\mu = 0.0001$, $M = 256$, and $del = 15$. The PSDs of the recovered HSS $y(t)$ -ALE output, and that of $s(t)$ are compared in Fig. 3.2. In Fig. 3.3, the PSD of the recovered WGN $e(t)$, is compared with that of $n(t)$. From Figs. 3.2 and 3.3, it is observed that at SNR of 27dB, the PSD of the recovered HSS generally matches that of the original, noise-free HSS. Also, the PSDs of the recovered WGN and that of the original synthetic WGN match. Thus, the PSDs of both the original signals and the recovered signals are generally the same within the entire frequency range. This confirms that the ALE introduces essentially no distortion to the HSS signal.

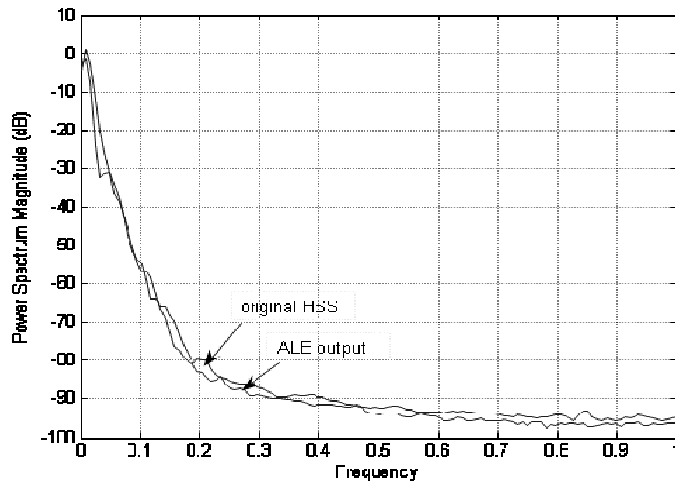


Figure 3.4. PSDs of the original HSS and recovered HSS, $SNR_{in} = 5dB$: The PSD of the recovered HSS essentially matches that of the original HSS within the whole normalized frequency range.

3.2.2 HSS-LSS

The procedure outlined in Section 3.2.1 above was repeated with WGN replaced by LSS and SNR adjusted to 5dB and -5dB with initial ALE parameter settings of $\mu = 0.0001$, $M = 256$, and $del = 15$. Figs. 3.4

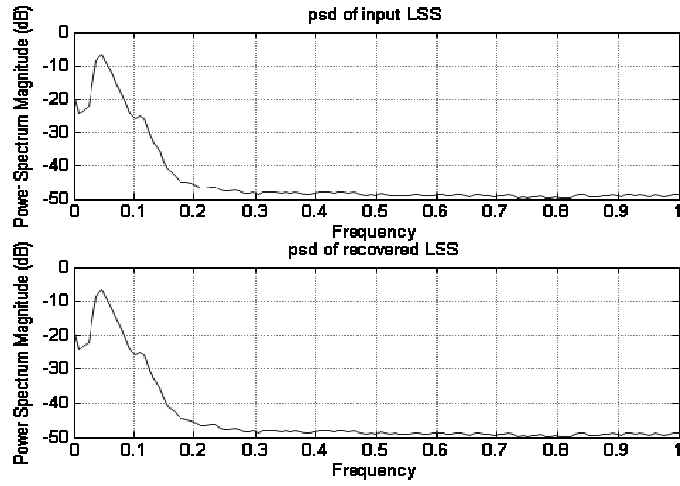


Figure 3.5. PSDs of the original LSS (top) and recovered LSS (bottom), $SNR_{in} = 5dB$: The PSD of the recovered LSS closely resembles that of the original LSS within the whole normalized frequency range.

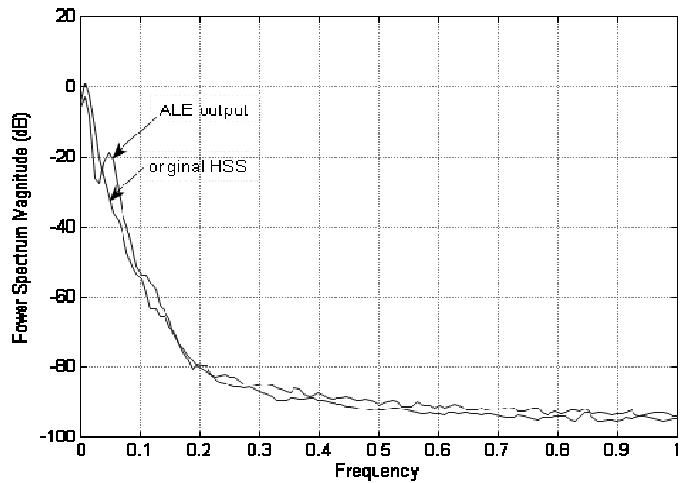


Figure 3.6. PSDs of the original HSS and recovered HSS, $SNR_{in} = -5dB$: The PSD of the recovered HSS matches that of the original HSS within the whole normalized frequency range.

and 3.5 show PSD comparison for when the SNR equals 5dB and Figs. 3.6 and 3.7 show PSD comparison for a case when SNR equals -5dB, in this case all parameters were identical to the 5dB case except the delay parameter $del = 375$. This increase is motivated by better matching the correlation properties of the LSS signal and is discussed in more detail later in this section. For both cases, the PSDs show close resemblance in the entire frequency range. The PSD of the signal $x(t)$, which in this case comprises of HSS and LSS with SNR of -5dB is shown on Fig. 3.8. The mixing of the two signals is shown most clearly below normalized frequency 0.1, for normalized frequencies above 0.2, $x(t)$ is dominated by LSS. The success of the ALE is confirmed in Fig 3.6 which represents the PSD of $y(t)$. The PSD of the ALE output clearly matches very closely the PSD of the original HSS. Moreover, the PSD of $e(t)$ as shown in the bottom plot of Fig. 3.7 matches the original LSS signal very well. Comparing Fig. 3.8 with Fig. 3.6 shows that processing has improved $x(t)$ to better match the original HSS. Figs. 3.9 and 3.10, included for completeness, depict the comparison between the input HSS/LSS time domain signals and HSS-LSS output time domain signals for both cases of SNR equal to 5 and -5dB respectively. Clearly, the two signals are separated however the definition of the recovered time domain signals degrades as the input SNR decreases.

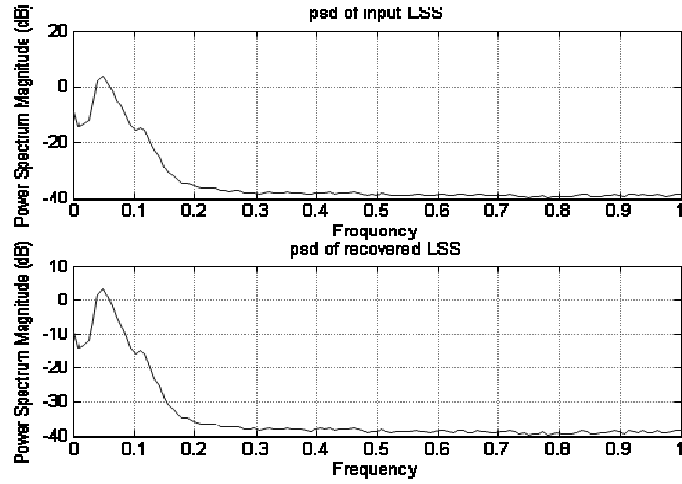


Figure 3.7. PSDs of the original LSS (top) and recovered LSS (bottom), $SNR_{in} = -5dB$: The PSD of the recovered LSS closely resembles that of the original LSS within the whole normalized frequency range.

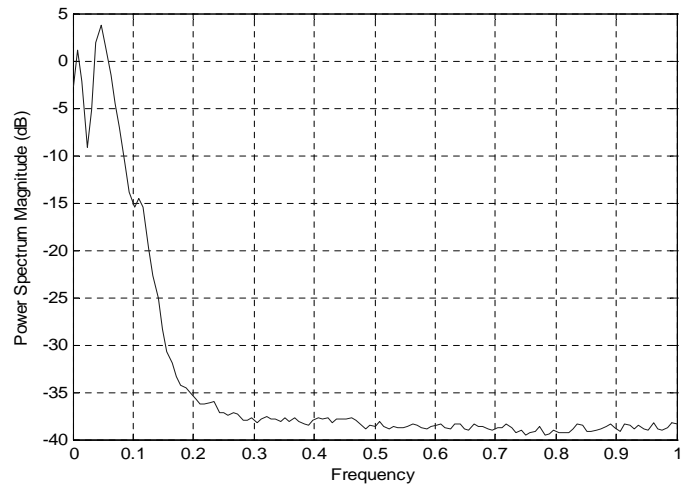


Figure 3.8. PSD of signal $x(t)$ comprising of HSS and LSS with $SNR_{in} = -5dB$.

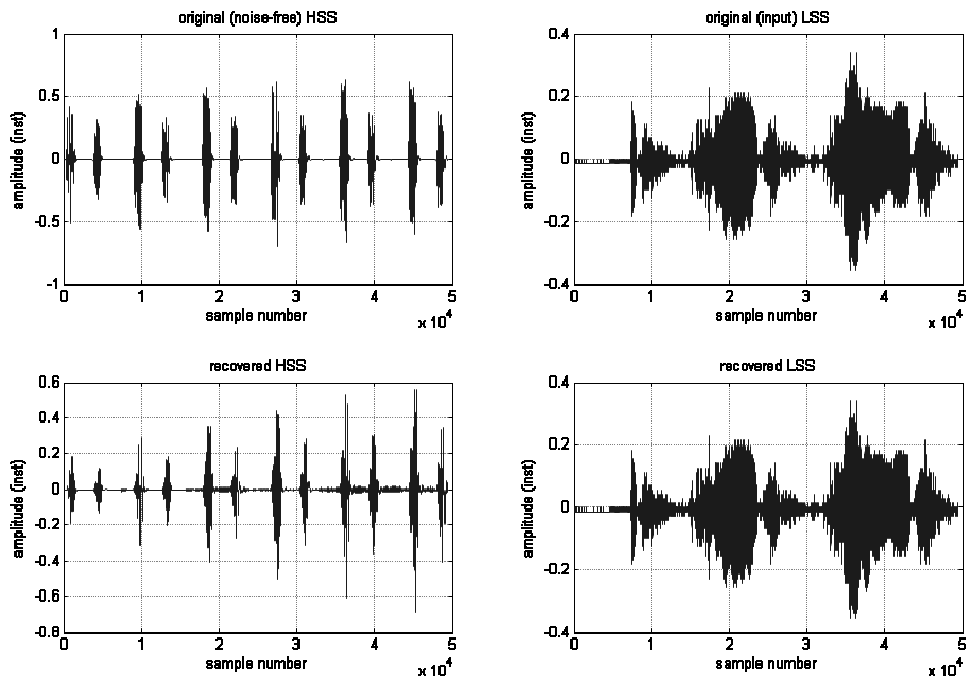


Figure 3.9. Time domain signals: the original HSS/LSS (top) and recovered HSS/LSS (bottom), $SNR_{in} = 5dB$.

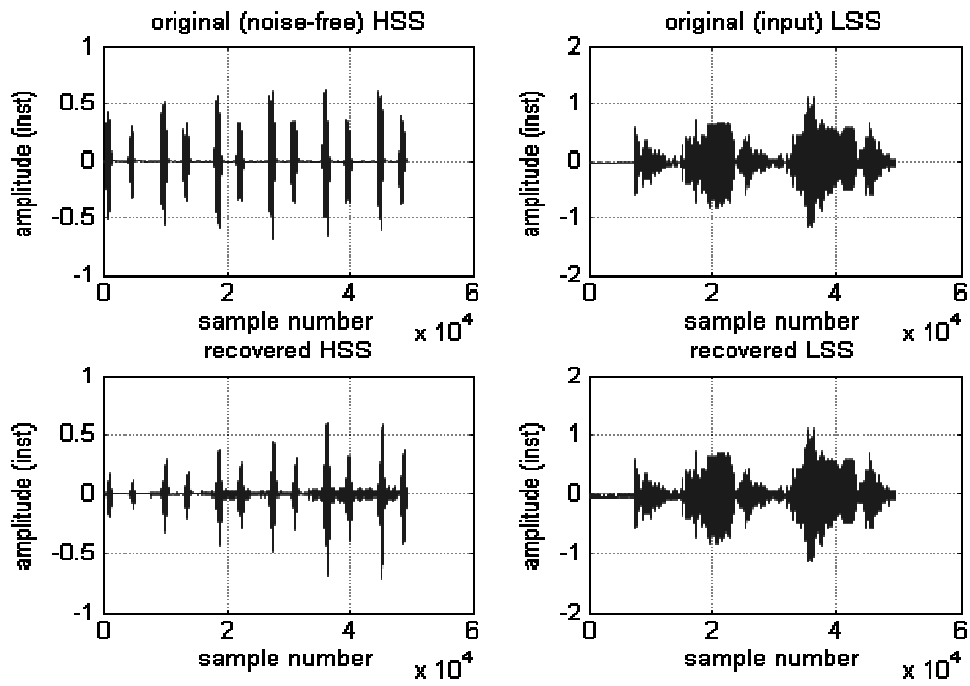


Figure 3.10. Time domain signals: the original HSS/LSS (top) and recovered HSS/LSS (bottom), $SNR_{in} = -5dB$.

3.2.3 Discussions

The ALE is primarily used to extract a periodic signal component from additive white background noise without any knowledge of constituent frequencies of the periodic component and without making any assumptions *a priori* about the stationarity of the signal. The ALE can also be applied to periodic signals in “coloured” noise.

Application of the ALE to periodic signals in “coloured” noise is characterized by longer prediction distances [59]. Fig. 3.11 shows the autocorrelation function of the LSS. It can be seen that the autocorrelation function decays to a small value at a lag of approximately 400 samples relative to the zero lag $z(0)$. Consistent with the discussion on choosing the prediction distance (decorrelation parameter) del , it is clear that for this particular signal choosing the prediction distance equal to approximately 375 would be best for ALE-based HSS-LSS processing. This result is likely to change however for a new signal, and further computational load would be required for its recalculation. Therefore, any method that does not depend upon a decorrelation parameter would be desirable. To this end, other approaches need to be explored.

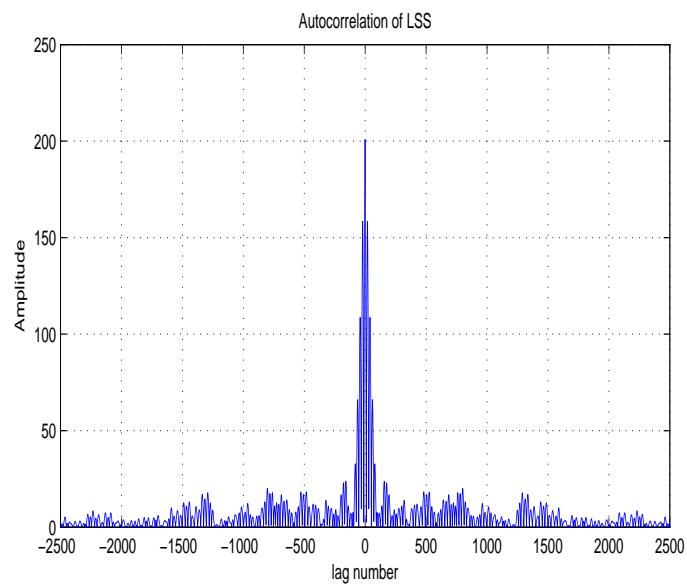


Figure 3.11. Absolute value of the autocorrelation of the LSS: The function decays to a small value at a lag of approximately 375 samples relative to the zero lag.

3.2.4 Chapter summary and conclusions

The ALE has been used as a new technique for separation of the HSS from HSS mixed with synthetic white Gaussian noise and from an HSS-LSS mixed signal. It goes without saying that ALE may be used in a single channel recorded HSS-LSS signal for separation of the two. For HSS in the presence of LSS (noise), the ALE performs even at low SNRs when the delay del is chosen to match the correlation properties of the LSS signal. However, in this thesis the target is next to avoid the need for the selection of this delay parameter.

SEQUENTIAL BLIND SOURCE EXTRACTION OF QUASI-PERIODIC SIGNALS WITH TIME-VARYING PERIOD

In this chapter, a novel sequential blind source extraction algorithm for the extraction of quasi-periodic signals with time-varying period is presented. The algorithm is a combination of the sequential blind source extraction (BSE) algorithm introduced in [68] and the time-varying lag (period) calculation procedure proposed in [69]. The proposed algorithm is tested on both synthetic and real-world recorded data.

4.1 Introduction

Blind source extraction (BSE) has received much research attention because of its potential utility in a wide range of applications including many in biomedical signal processing [70]. The problem arises when

linear, instantaneous mixtures or observations, generated as a set of signals are mixed by traversing an unknown medium, essentially without delay, need to be processed to estimate or recover a number or all of the original sources. One of the important and challenging issues in BSE is how to extract specific sources of interest. This requires the proper use of prior information about the sources or the mixing operation in forcing the algorithm to extract the sources of interest rather than any arbitrary sources. The objective of blind source separation (BSS), on the other hand, is to recover or estimate simultaneously all the original sources from their mixtures. Compared with BSS, BSE provides more flexibility and has some potential advantages over BSS, in terms of computational complexity and extraction of only the sources of interest.

Over the last decade or so, several approaches have been developed for the solution of both BSS and BSE problems, which are based on either second or higher-order statistics of the data. Typically, the higher-order techniques consist of two steps: a whitening step for exploiting the second order statistics, and a rotation step for exploiting the higher order statistics. They require few assumptions aside from the statistical independence of the sources, and therefore, have generally been the preferred approach to the solution of BSE and BSS. Higher-order statistics based solutions include [16], [38], [71] and [34]. Second-order statistics methods, on the other hand, have the advantage of requiring shorter data records due to their reduced sensitivity to small sample estimation errors, and do not limit the number of Gaussian sources that can be separated to one (see for instance [37], [72], [73] and [74]). As opposed to higher-order methods, second-order methods operate in a

semi-blind context, since their derivation usually requires that certain additional assumptions are made on the nature of the original signals, such as statistical nonstationarity of the sources, presence of temporal structure in stationary signals, or cyclostationarity [37], [72], [73] and [74]. Such information is usually available in certain biomedical applications, for instance in physiological signals such as the electrocardiogram (ECG), and should be exploited.

Several algebraic block-based methods exist that exploit the temporal correlations of the source signals, and perhaps the best known is the second-order blind identification (SOBI) algorithm [35]. Consistent with the operation of batch algorithms, the original SOBI algorithm entails prewhitening the data; followed by the (approximate) joint diagonalization of a set of covariance matrices at different time lags, thus potentially allowing separation of sources based on their temporal structure. However, in the SOBI algorithm, the time lags at which the covariance matrices are jointly diagonalized, are fixed, and are not matched to the extraction of a quasi-periodic signal with time-varying period. Furthermore, computational complexity of this algorithm is generally substantially greater than sequential algorithms due to the need to diagonalize a number of sample covariance matrices and therefore will not be considered further in this work. Related algorithms that are essentially based on a similar principle can be found in [75] and [76].

Recently, a sequential algorithm was developed for a class of periodic signals in [77]. In that work however, the signals, although periodic, have a constant or fixed period. *In this work, the combination of the sequential blind source extraction (BSE) algorithm using second-order statistics based on the approximate joint diagonalization (AJD) of auto-*

correlation matrices [68] and the time-varying lag (period) calculation procedure recently proposed in [69] is exploited, and thereby a novel sequential blind source extraction algorithm for the extraction of quasi-periodic signals with time-varying period is introduced. This work is motivated by the observation that the majority of physiological signal measurements (for example, ECG) exhibit some degree of periodicity and statistical nonstationarity. The nonstationarity manifests itself as variations in period as a function of time. This makes the assumption of a fixed period (as in [77]) invalid for the ECG signal, and perhaps many other biomedical signals. To the best of the author's knowledge, a sequential blind source extraction algorithm that is matched to such variations in the signal period has not previously been discussed. Using a time-varying period can moreover help with extraction of a specific desired source.

To this end, a time-varying period τ_t , which is estimated for each new cycle-to-cycle interval of the quasi-periodic source to be extracted, is incorporated in the sequential blind extraction algorithm. Source extraction is performed by sequentially converging to a solution which effectively diagonalizes the autocorrelation matrices, at lags τ_t corresponding to the different periods.

The rest of the chapter is organized as follows. Problem formulation, in the context of BSE using second-order statistics is presented in Section 4.2. In Section 4.3, the concept of time-varying period is presented and incorporated in the problem formulated in Section 4.2. Simulation results are presented in Section 4.4. In Section 4.5, results of applying the new algorithm to extraction of a heart sound signal (HSS) from real lung sound recordings are provided. A summary and concluding

remarks are given in Section 4.6.

4.2 Problem formulation

Consider the real valued signal generating model:

$$\mathbf{x}(t) = \mathbf{A}\mathbf{s}(t) + \mathbf{n}(t) \quad (4.2.1)$$

where $\mathbf{s}(t) = [s_1(t), s_2(t), \dots, s_N(t)]^T$ is a column vector of N mutually uncorrelated zero-mean unknown source signals, $\mathbf{A} = [\mathbf{a}_1, \mathbf{a}_2, \dots, \mathbf{a}_N]$ is an $N \times N$ invertible unknown mixing matrix, $\mathbf{x}(t) = [x_1(t), x_2(t), \dots, x_N(t)]^T$ is a column vector of N observed sensor signals, $\mathbf{n}(t) = [n_1(t), n_2(t), \dots, n_N(t)]^T$ denotes a column vector of additive white Gaussian zero-mean measurement noise, \mathbf{a}_i is the i -th column of \mathbf{A} , $[\cdot]^T$ and t denote respectively the vector transpose and the discrete time index. In the discussion that follows, the noise term $\mathbf{n}(t)$ in (4.2.1) is dropped, but the effect of the noise on the algorithm is shown in the simulation section (Section 4.4). Based on the assumption that the sources are spatially uncorrelated and wide sense stationary, the time lagged autocorrelation matrix \mathbf{R}_k , can be defined as

$$\mathbf{R}_k = E(\mathbf{x}(t)\mathbf{x}^T(t - \tau_k)) \quad , \quad k = 1, 2, 3, \dots, K \quad (4.2.2)$$

where K is the index of the maximum time lag, i.e., τ_K and $E(\cdot)$ denotes the statistical expectation operator.

The vector $\mathbf{x}(t)$ in (4.2.1) (ignoring the noise term) is a linear combination of the columns of matrix \mathbf{A} , i.e., the \mathbf{a}_i s. Therefore, the most intuitive way to extract the i -th source is to project $\mathbf{x}(t)$ onto

the space in \mathbb{R}^N orthogonal to, denoted by \perp , all of the columns of \mathbf{A} except \mathbf{a}_i , i.e., $\{\mathbf{a}_1, \dots, \mathbf{a}_{i-1}, \mathbf{a}_{i+1}, \dots, \mathbf{a}_N\}$. Henceforth, by defining a vector $\mathbf{q} \perp \{\mathbf{a}_1, \dots, \mathbf{a}_{i-1}, \mathbf{a}_{i+1}, \dots, \mathbf{a}_N\}$ and setting $\mathbf{t} \equiv \mathbf{a}_i$, together with adopting oblique projector notation [78], gives

$$y(t)\mathbf{t} = \mathbf{E}_{\mathbf{t}|\mathbf{q}^\perp}\mathbf{x}(t) \quad (4.2.3)$$

where $y(t)$ is an estimate of one source, \mathbf{q}^\perp is a subspace in \mathbb{R}^N orthogonal to \mathbf{q} , i.e. the space spanned by $\{\mathbf{a}_1, \dots, \mathbf{a}_{i-1}, \mathbf{a}_{i+1}, \dots, \mathbf{a}_N\}$ and $\mathbf{E}_{\mathbf{t}|\mathbf{q}^\perp} = (\mathbf{t}\mathbf{q}^T)/(\mathbf{q}^T\mathbf{t})$ is the oblique projection of \mathbf{t} onto the space \mathbf{q}^\perp . By omitting the scalar $1/(\mathbf{q}^T\mathbf{t})$ and dropping \mathbf{t} from both sides of equation (4.2.3) results in

$$y(t) = \mathbf{q}^T\mathbf{x}(t) \quad (4.2.4)$$

In BSE based on second-order statistics, both vectors \mathbf{t} and \mathbf{q} are unknown. In order to extract one source, the same approach and assumptions as in Section III of [68] are adopted, that is, the following cost function is exploited to find these vectors

$$[\hat{\mathbf{t}}, \hat{\mathbf{q}}, \hat{\mathbf{d}}] = \arg \min_{\mathbf{t}, \mathbf{q}, \mathbf{d}} J(\mathbf{t}, \mathbf{q}, \mathbf{d}) \quad (4.2.5)$$

where $J(\mathbf{t}, \mathbf{q}, \mathbf{d}) = \sum_{k=1}^K \|\mathbf{R}_k\mathbf{q} - d_k\mathbf{t}\|^2$, $\mathbf{d} = [d_1, d_2, \dots, d_K]^T$ is the column vector of unknown scalars, and $\|\cdot\|$ denotes the Euclidean norm. The cost function in (4.2.5) utilizes the fact that for BSE, $\mathbf{R}_k\mathbf{q}$ should be collinear with \mathbf{t} incorporating the coefficients d_k which provides \mathbf{t} with proper scaling. The trivial answer for (4.2.5) is its immediate global minimum point when $\mathbf{t} = \mathbf{q} = \mathbf{d} = \mathbf{0}$. This solution has been avoided by imposing the condition $\|\mathbf{t}\| = \|\mathbf{d}\| = 1$. Minimization of the

cost function (4.2.5) with respect to \mathbf{q} leads to the identification of vector \mathbf{q} in equation (4.2.4) which can thereby be used to extract one of the sources. It is however worth noting that the actual extracting vector is given by $\mathbf{q}/(\mathbf{q}^T \mathbf{t})$ due to earlier omission of the scaling factor $1/(\mathbf{q}^T \mathbf{t})$ in order to arrive at (4.2.4). The convergence of (4.2.5) is rather difficult to prove analytically in the time domain due to the product term $d_k \mathbf{t}$ in (4.2.5). The formal analytical proof of the convergence is left as a subject of future research.

4.2.1 Signal extraction algorithm

By employing the sequential approximate diagonalisation algorithm (SDA) proposed in [68], the cost function (4.2.5) is minimized by adjusting its parameters alternatively as follows:

- Stage 1 : Freeze both \mathbf{t} and \mathbf{d} and adjust \mathbf{q} . Taking the gradient of J with respect to \mathbf{q} leads to analytical solution for \mathbf{q} as $\partial J/\partial \mathbf{q} = 2 \sum_{k=1}^K \mathbf{R}_k (\mathbf{R}_k \mathbf{q} - d_k \mathbf{t}) = 0$ to yield a new value of \mathbf{q} :

$$\mathbf{q} \leftarrow \mathbf{H} \left(\sum_{k=1}^K d_k \mathbf{R}_k \right) \mathbf{t} \quad (4.2.6)$$

where $\mathbf{H} = [\sum_{k=1}^K \mathbf{R}_k^2]^{-1}$, and $e \leftarrow f$ denotes replacing e by f .

- Stage 2: Freeze both \mathbf{t} and \mathbf{q} and adjust \mathbf{d} . Utilizing the property that $\|\mathbf{d}\| = 1$ and considering the Lagrangian function

$$J_{\lambda_d} = J + \lambda_d \left(\sum_{k=1}^K d_k^2 - 1 \right) \quad (4.2.7)$$

where λ_d is the Lagrange multiplier, to obtain a new value of \mathbf{d}

$$\mathbf{d} \leftarrow \frac{\mathbf{u}}{\|\mathbf{u}\|} \quad ; \quad \mathbf{u} = [\mathbf{r}_1^T \mathbf{t}, \mathbf{r}_2^T \mathbf{t}, \dots, \mathbf{r}_K^T \mathbf{t}]^T \quad (4.2.8)$$

where $\mathbf{r}_k = \mathbf{R}_k \mathbf{q}$.

- Stage 3: Freeze both \mathbf{q} and \mathbf{d} and adjust \mathbf{t} . Using $\|\mathbf{t}\| = 1$ and exploiting the Lagrangian function

$$J_{\lambda_t} = J + \lambda_t (\mathbf{t}^T \mathbf{t} - 1) \quad (4.2.9)$$

to obtain the adjustment for \mathbf{t}

$$\mathbf{t} \leftarrow \frac{\mathbf{v}}{\|\mathbf{v}\|} \quad ; \quad \mathbf{v} = \sum_{k=1}^K d_k \mathbf{r}_k \quad (4.2.10)$$

These three stages are repeated until the cost function (4.2.5) converges, and one source can be extracted according to (4.2.4). For the later presented results on ECG signals, five iterations are typically sufficient and no problem with ill-convergence has been experienced. This, however, depends on the dimensions of the subspace that is being extracted [79]. After extracting one source a deflation procedure is employed to remove it from the mixture as follows [29]:

$$\mathbf{x}_{i+1}(t) = \mathbf{Z}^T \mathbf{x}_i(t) \quad , \quad \mathbf{x}_1(t) = \mathbf{x}(t) \quad (4.2.11)$$

where $\mathbf{x}(t)$ is the original observation signal defined in (4.2.1), and

$$\mathbf{Z} = \mathbf{I} - \frac{\mathbf{R}_{0(i)} \mathbf{w} \mathbf{w}^T}{\sigma_y^2} \quad (4.2.12)$$

where $\mathbf{R}_{0(i)} = E(\mathbf{x}_i(t) \mathbf{x}_i^T(t))$, \mathbf{I} is the $N \times N$ identity matrix, and $\sigma_y^2 = E(y^2)$.

The autocorrelation matrix is then updated as

$$\mathbf{R}_{0(i+1)} = \mathbf{Z}^T \mathbf{R}_{0(i)} \mathbf{Z} \quad (4.2.13)$$

before another source can be extracted following the same procedure, using equations (4.2.6)-(4.2.13). An alternative way to obtain a deflation matrix is to design a matrix $\mathbf{Z} = [\mathbf{z}_1, \mathbf{z}_2, \dots, \mathbf{z}_{N-1}]$ whose columns \mathbf{z}_i span the subspace orthogonal to the estimated source direction \mathbf{t} , i.e., $\mathbf{z}_i \perp \mathbf{t}$ for $1 \leq i \leq N - 1$. This latter approach can speed up the algorithm in the case of slow convergence.

This extraction algorithm is computationally simple when compared with one stage of other algorithms such as those proposed in [22] which extract the sources one-by-one by using fourth-order cumulants. It is worth noting, however, that the iterative extraction algorithm for estimating one source at a time in this work in fact replaces the joint diagonalization procedure in the SOBI algorithm [35], whereby the computation is simplified since full eigen-decomposition is not required. Nonetheless, performing the iterative procedure in this method is very similar to the procedure that is carried out within techniques which calculate the first (or the first few) eigenvalues [80]. In the next section this algorithm is extended to the extraction of periodic signals with time-varying period.

4.3 Sequential extraction algorithm for quasi-periodic signals with time-varying period

Successful minimization of the cost function (4.2.5) in concert with (4.2.4) leads to the extraction of any one source. It is not possible to

extract the source of interest (SoI) unless some additional information is known *a priori*. The SoI in this case is a quasi-periodic signal of varying period duration. If the fundamental period, or its approximation, of the SoI is fixed and known, then the algorithm can be made to focus only on this specific source. This is based on the fact that if the fundamental period is, say, τ samples, then its autocorrelation matrix will have the same value at time lags corresponding to integer multiples of τ . Hence, the autocorrelation matrices \mathbf{R}_k s as computed in (4.2.2) can jointly be diagonalized at time lags $\tau, \dots, K\tau$ along with the constraint $d_1 = d_2 = \dots = d_K$.

However, if the SoI has a period that varies from period to period (see, for instance Fig. 4.10), then to jointly diagonalize the \mathbf{R}_k s, at the time lags $\tau, \dots, K\tau$ and applying the extraction algorithm, would invariably result in erroneous results. Before proceeding on to develop a method that effectively matches the variations in the period of the SoI, illustrative examples are presented, which have been published in [81], showing the performance of the extraction algorithm outlined in Section 4.2.1 when exploiting knowledge about the periodicity of the SoI.

4.3.1 Illustrative examples

In this section, two examples are considered. In the first example a deterministic periodic signal and WGN that have been mixed by a mixing matrix \mathbf{A} with elements drawn from a standardized Gaussian distribution are considered, and the second example considers two real HSS and LSS measurement signals that have been mixed in the same manner. The HSS and LSS signals are obtained from the R.A.L.E. data

sets [67]. Qualitative evaluation is performed in the second example by comparing power spectral densities (PSDs) of the signals before and after mixing for the proposed method and for the *JADE* algorithm, a benchmark BSS algorithm [82].

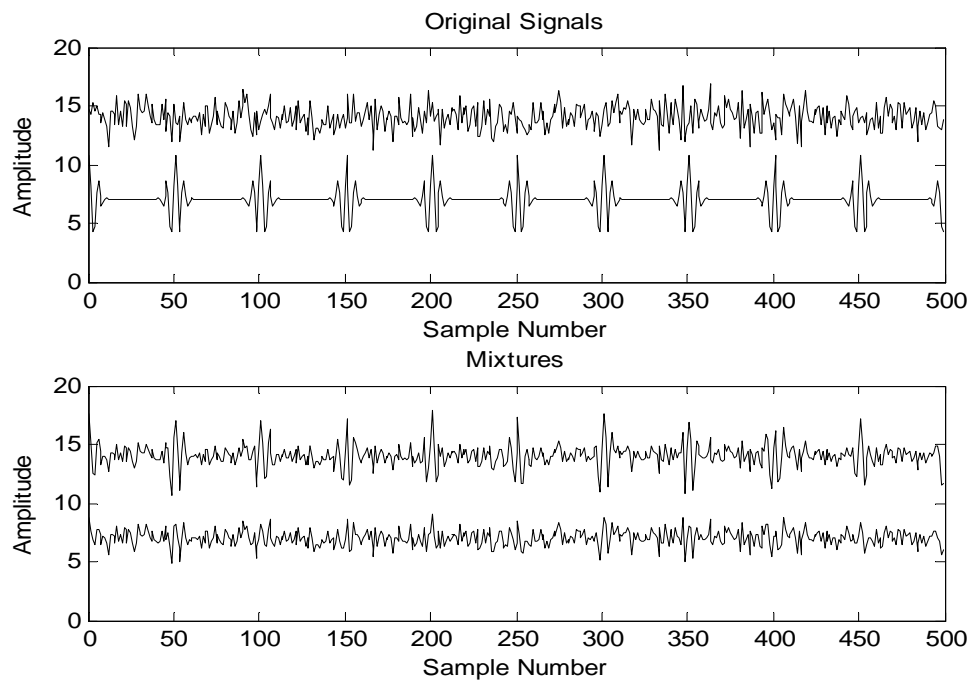


Figure 4.1. Pulsetrain and noise before mixing (top), and the linear mixtures (bottom).

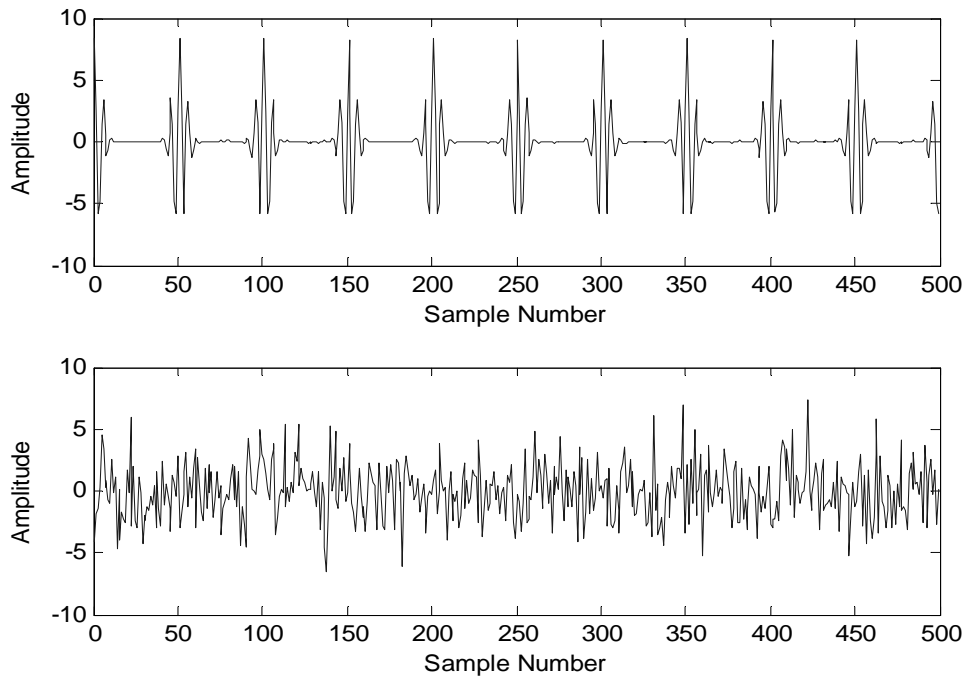


Figure 4.2. Extracted signals using fixed-period algorithm. The signal of interest is the pulse train with a period of 50 samples. Setting this period in the algorithm results in the extracted pulse train (top), and when no period information is specified the algorithm locks onto the noise component (bottom).

Blind source extraction of a periodic signal of known period

In this example two source signals are considered. One is the periodic pulsetrain signal of known period and the other is a white Gaussian noise (WGN) signal, a portion of which is shown in Fig. 4.1 (top subplot). The SoI is the periodic signal whose period is 50 samples. The two signals are mixed as shown in the same Fig. 4.1 (bottom subplot). By setting the period to 50 samples, and K , the number of autocorrelation matrices, to 30, the algorithm is run and the SoI is obtained as in Fig. 4.2 (top subplot), confirming an accurate reconstruction. As seen from Fig. 4.2 (bottom subplot), when no information about the periodicity is incorporated in the algorithm, the algorithm locks onto

the noise component.

Blind source extraction of the HSS

In this example, the two source signals are the HSS and the LSS signals, shown in Fig. 4.3 (top subplot). The SoI in this case, is the HSS signal. The knowledge of the HSS periodicity is exploited in order to extract it from the HSS-LSS mixtures. By using a technique such as the one introduced in [83], the cycle frequency of HSS may be estimated and hence its period. This method, called heart instantaneous frequency (HIF), was developed for the extraction of the instantaneous heart rate from non-stationary electrocardiogram (ECG) signals, the value of which varies over time due to pathological and physiological changes.

In practice, any lung sound recording performed invariably contains both HSS and LSS. However, if the recording transducer is placed closer to the person's heart location, then HSS spectral components would be more dominant in the recorded signal than LSS. The method outlined above can then be used to estimate the period of the HSS dominant signal.

The two signals are mixed by a matrix \mathbf{A} with random elements drawn from a standardized Gaussian distribution to yield the mixtures in Fig. 4.3 (bottom subplot). Fig. 4.4 shows the recovered HSS signal obtained after running the algorithm. As seen from Fig. 4.4, the HSS has also been recovered from the mixture though it is slightly corrupted in the regions of low signal-(HSS)-to-noise (LSS) ratio. The PSDs in Fig. 4.5 show that the frequencies of the original HSS signal have been preserved in the recovered signal for both cases, although there is a

change in magnitude of the extracted signal, but this is a result of scale ambiguity and can easily be mitigated. Moreover, the performance is as good as the full benchmark *JADE* blind source separation algorithm which extracts all the sources, but suffers from the problem of reliably estimating fourth order statistics.

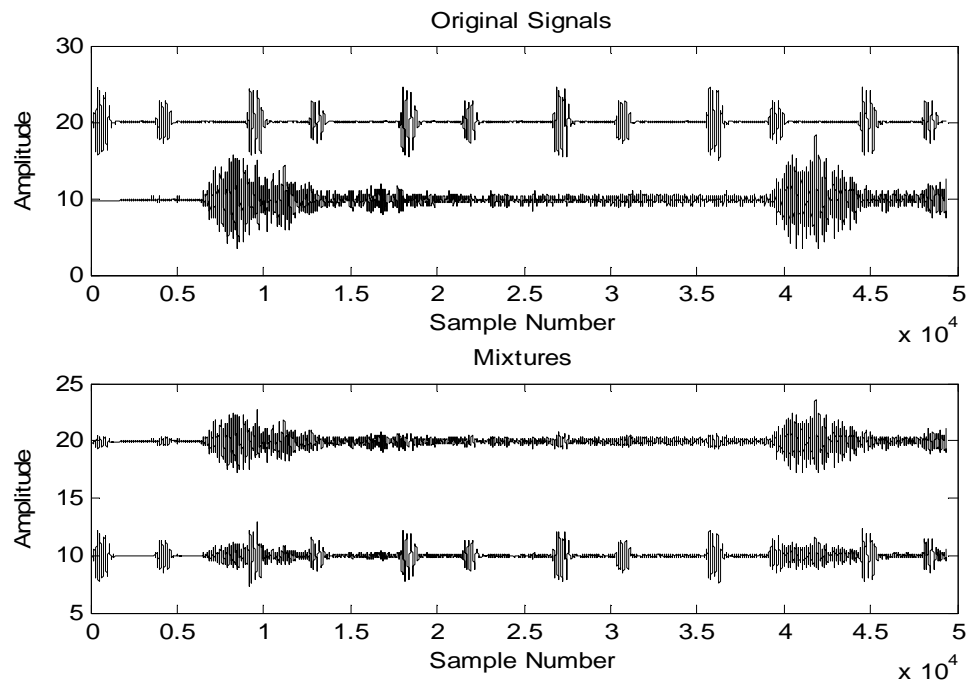


Figure 4.3. HSS and LSS before mixing (top), and the linear mixtures (bottom)

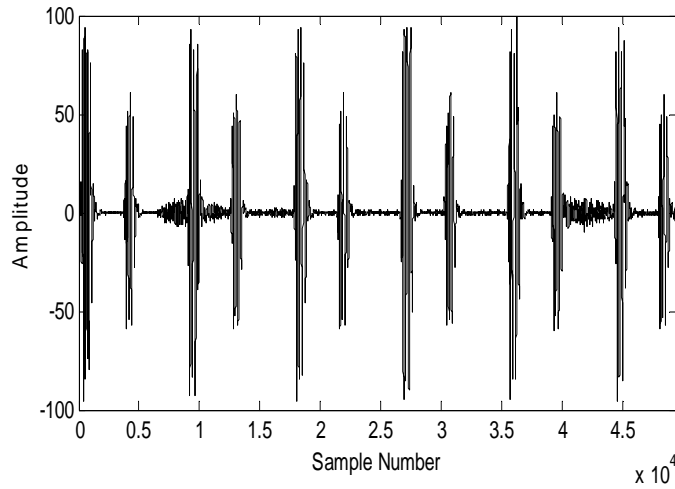


Figure 4.4. Extracted HSS using fixed-period algorithm. The HSS is extracted. However, since HSS is not completely periodic, the algorithm also locks on to the noise component.

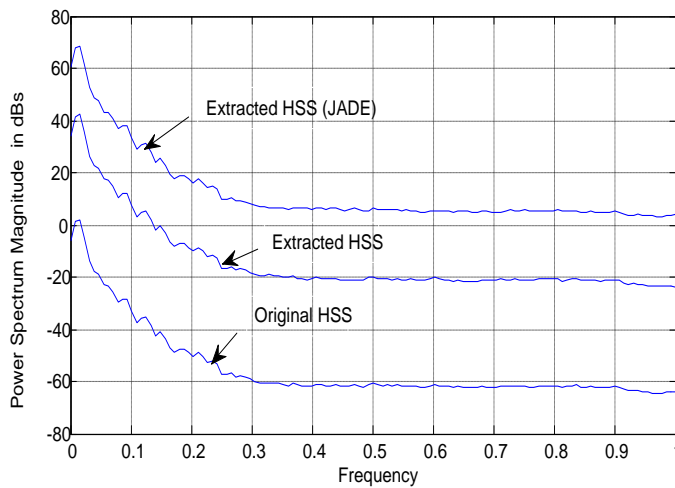


Figure 4.5. Comparison of PSDs for: original HSS, extracted HSS by our method, and extracted HSS using the JADE algorithm.

4.3.2 Proposed method

The method, recently proposed in [69] for multichannel ECG decomposition, entails detecting the peaks of the quasi-periodic signal which are assumed to define the period of the SoI, as is the case in ECG signals, and allowing a linear phase signature $\theta(t)$, to span the range from $-\pi$

to π , between the peaks. The phase signature is then allocated to each sample of the signal, with the positions of the R-peaks being fixed at $\theta(t) = 0$ as shown in Fig. 4.6. It follows that the samples corresponding to a certain specific phase angle are compared along the signal. For example, in Fig. 4.6, for the phase angle of 2rads, the samples at time instant t and $t + \tau_t$ are compared accordingly. Therefore, in the sequential algorithm explained in Section 4.2, the following key equations can be redefined:

- The autocorrelation matrix in (4.2.2)

$$\tilde{\mathbf{R}}_{\tau_t} = E_t(\mathbf{x}(t)\mathbf{x}^T(t - \tau_t)) \quad (4.3.1)$$

where $E_t(\cdot)$ denotes averaging over t , and

$$\tau_t = \min\{\tau | \theta(t + \tau) = \theta(t), \tau > 0\}. \quad (4.3.2)$$

- The cost function in (4.2.5) is again exploited

$$[\hat{\mathbf{t}}, \hat{\mathbf{q}}, \hat{\mathbf{d}}] = \arg \min_{\mathbf{t}, \mathbf{q}, \mathbf{d}} J(\mathbf{t}, \mathbf{q}, \mathbf{d}) \quad (4.3.3)$$

where $J(\mathbf{t}, \mathbf{q}, \mathbf{d}) = \sum_{p=1}^K \|\tilde{\mathbf{R}}_{p\tau_t} \mathbf{q} - d_p \mathbf{t}\|^2$. where the $\tilde{\mathbf{R}}_{p\tau_t}$ terms are also calculated as time averages.

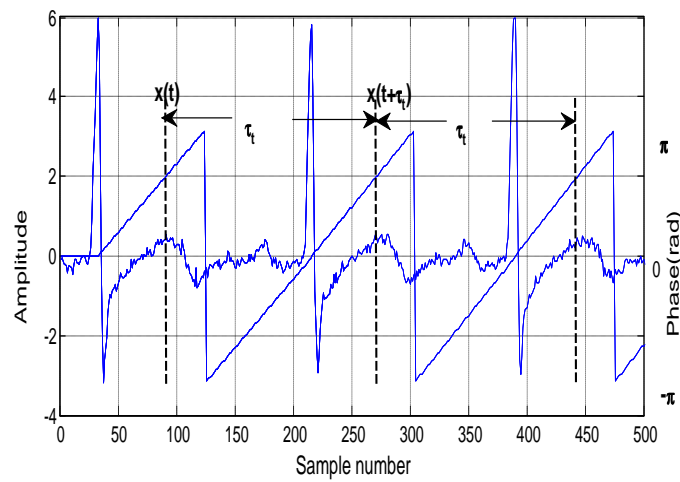


Figure 4.6. Demonstration of phase allocation procedure first proposed in [69] for computing τ_t . The sawtooth signal depicts the phase signature $\theta(t)$ ranging from $-\pi$ to π . The peaks positions are assigned to $\theta(t) = 0$. For each period of the signal, half of the signal samples are assigned to $\theta(t)$ ranging from $-\pi$ to 0 and the other half is assigned to $\theta(t)$ ranging from 0 to π . Typically, a sample at time instant t is compared with the sample at $t + \tau_t$. τ_t is recalculated on a period-by-period basis.

Therefore, the autocorrelation matrix and the cost function, now take into account the variable period τ_t , that is calculated from $\theta(t)$ from cycle-to-cycle of the signal. This leads to a new algorithm for extracting SoI with a variable period duration. The main difference in the algorithm of Section 4.2, and the one proposed in this chapter is the way in which the time lagged autocorrelation matrix $\tilde{\mathbf{R}}$ is computed, which in turn, leads to the re-definition of the cost function (4.2.5).

In this algorithm, the autocorrelation matrices are calculated at varying time lags τ_t rather than at fixed time lags. Thus, after performing peak detection, and calculating the $\theta(t)$ and the time-varying τ_t , each autocorrelation matrix is calculated by computing correlations between sample points t and their dual samples $t + \tau_t$ across the entire signal length and then averaging over the number of correlation and phase angle points. The resulting $\tilde{\mathbf{R}}$ s are used in the sequential algorithm of Section 4.2 to extract the SoI from multichannel mixtures.

4.4 Simulation results

Computer simulations were carried out to illustrate the performance of the proposed method, and were compared to the one proposed recently in [81], which is based on a fixed period of the SoI.

4.4.1 Signal-to-interference ratio and the cost function

The performance of the algorithm was evaluated by both:

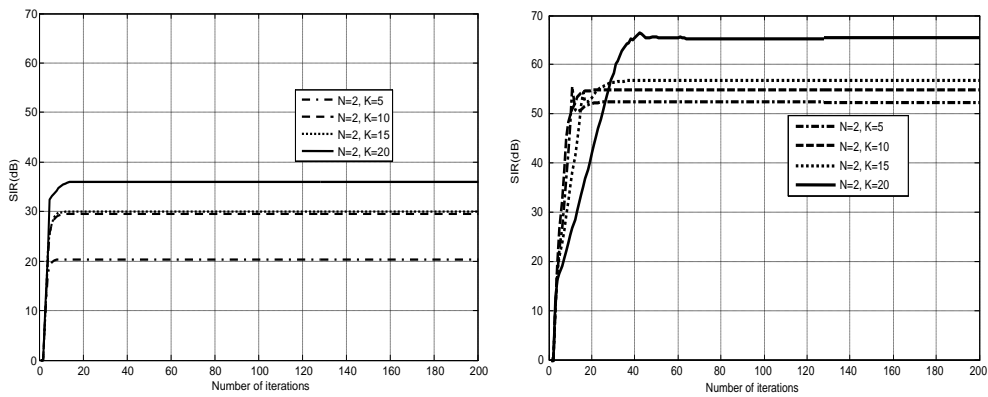
- The peak signal-to-interference ratio (SIR) in decibels (dB) given by

$$\text{SIR}(\text{dB}) = 10 \log_{10} \frac{\max(|v_i|^2)}{\sum_{i=1}^N |v_i|^2 - \max(|v_i|^2)} \quad (4.4.1)$$

where $[v_1, v_2, \dots, v_N] = \mathbf{q}^T \mathbf{A}$ is the global transform vector, and (4.4.1) is evaluated by first calculating the average of SIR in a linear scale, and then converting to dBs. For completeness, note that from (4.2.1) and (4.2.4)

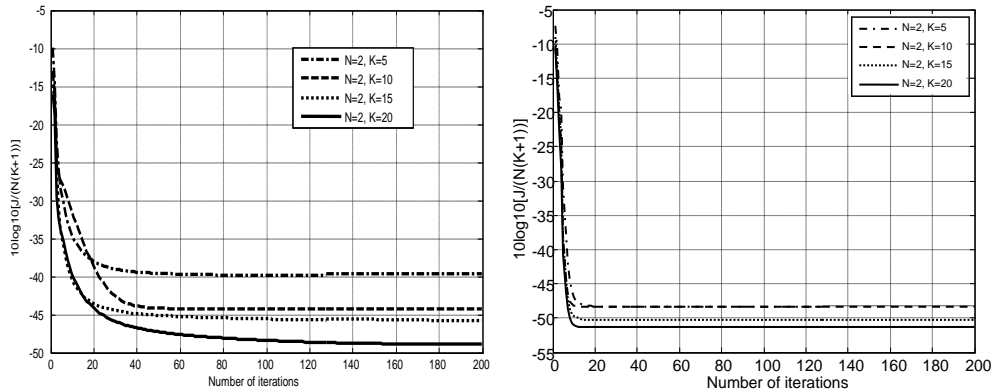
$$y(t) = \mathbf{q}^T \mathbf{A} \mathbf{s}(t) = v_1 s_1(t) + v_2 s_2(t) + \dots + v_N s_N(t) \quad (4.4.2)$$

- The cost function in dBs given by $J(\mathbf{t}, \mathbf{q}, \mathbf{d})/N(K+1)$.



(a) SIR(dB) for extraction algorithm using fixed period algorithm. (b) SIR(dB) for extraction algorithm using time-varying period, notice the range on the SIR axis.

Figure 4.7. SIR(dB) versus number of iterations for both fixed and time-varying extraction algorithms for the case of noise-free BSE, averaged over 250 independent runs when extracting the first source signal. N represents the number of signals while K represents the number of autocorrelation matrices used. SIR performance improves as the number of matrices increases. The SIR performance of the time-varying period algorithm almost doubles that of the fixed period algorithm.



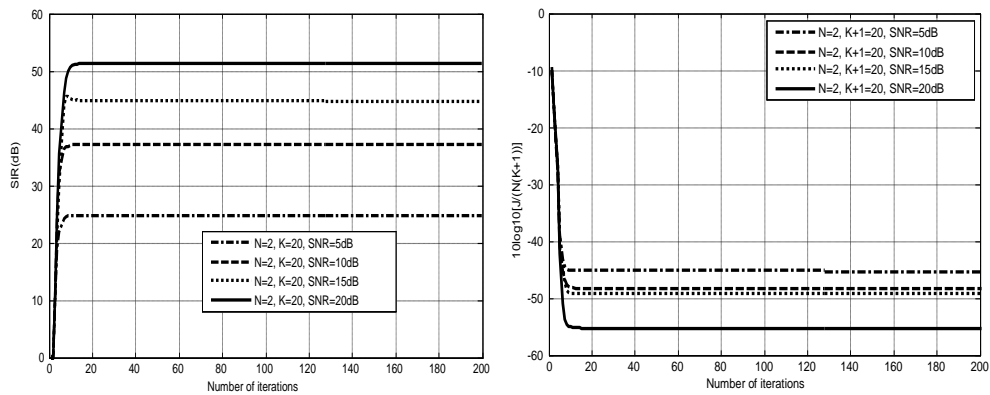
(a) $J(\mathbf{t}, \mathbf{q}, \mathbf{d})/N(K+1)$ (dB) for extraction algorithm using the fixed period algorithm. (b) $J(\mathbf{t}, \mathbf{q}, \mathbf{d})/N(K+1)$ (dB) for extraction algorithm using the time-varying period algorithm.

Figure 4.8. $J(\mathbf{t}, \mathbf{q}, \mathbf{d})/N(K+1)$ (dB) versus number of iterations for both fixed and time-varying extraction algorithms for the case of noise-free BSE, averaged over 250 independent runs when extracting the first source signal. N represents the number of signals while K represents the number of autocorrelation matrices used. The proposed algorithm converges faster than the fixed-period algorithm.

In the simulation, blind extraction of the ECG signal obtained from the DaISY database (available at: <http://homes.esat.kuleuven.be/smc/daisy/>) was considered. The 2500 samples long clean ECG signal, sampled at 500Hz, was concatenated to form a 7500 sample long signal. It is worth noting that no discontinuity problems were experienced when concatenating the signal. The ECG signal was mixed with white Gaussian noise (WGN) by a mixing matrix \mathbf{A} with elements drawn from a standardized Gaussian distribution. Figs. 4.7(a) and 4.7(b) show the SIR(dB) versus number of iterations averaged over 250 independent runs when extracting the SoI assuming a fixed and time-varying period respectively. Figs. 4.8(a) and 4.8(b) represent the corresponding cost function performance in dBs for both cases. N and K , shown in the figures represent the number of original signals and the number of autocorrelation matrices used respectively. Thus, the performance cri-

teria were evaluated for $N = 2$ and K set to 5, 10, 15, 20, accordingly. It is seen from Figs. 4.8(a) and 4.8(b) that the proposed algorithm converges faster than the fixed-period algorithm, with convergence improving with the number of matrices used. The SIR performance also improves as the number of matrices is increased. As seen from Fig. 4.7(b), there is a marked increase in SIR performance for the proposed algorithm. In fact, the SIR performance of the proposed algorithm almost doubles that of the algorithm using a fixed period. For instance, from Figs. 4.7(a) and 4.7(b), the maximum SIR when assuming fixed and time-varying period, and using 20 matrices is 33dB and 65dB, respectively. This underlines the motivation for the work in this chapter, since by exploiting the nonstationarity of the source, captured in the varying period, improved SIR performance is achieved for the same fast convergence performance.

The performance of the algorithm was also investigated using different signal-to-noise ratios (SNRs) on mixture signals for the case of the noisy model given by (4.2.1). Figs. 4.9(a) and 4.9(b) show SIR(dB) and convergence performance as a function of SNR(dB), respectively. It is seen from the figures that the performance degrades as more independent noise is added to the mixtures, i.e. as SNR(dB) reduces. It is however seen (from Figs. 4.7(a) and 4.9(a)) that the algorithm, when applied to the noisy BSE, still outperforms (at least at SNR of 10dB) the one using a fixed period in terms of SIR(dB), when applied to noise-free BSE.



(a) SIR(dB) for the extraction algorithm using time-varying period algorithm for different signal-to-noise ratios on observations. Notice the degradation in SIR(dB) performance as a function of SNR(dB). (b) $J(\mathbf{t}, \mathbf{q}, \mathbf{d})/N(K+1)$ (dB) for the extraction algorithm using the time-varying period algorithm for different signal-to-noise ratios on observations, notice degradation in convergence performance as a function of reduction in signal-to-noise ratio SNR(dB).

Figure 4.9. $J(\mathbf{t}, \mathbf{q}, \mathbf{d})/N(K+1)$ (dB) and SIR(dB) versus number of iterations using time-varying extraction algorithm for the case of noisy BSE, averaged over 250 independent runs when extracting the first source signal. N represents the number of signals while K represents the number of autocorrelation matrices used.

4.4.2 Extraction of synthetic variable period signal

This simulation considers extraction of a synthetic, deterministic signal, with time-varying period (Fig. 4.10). The signal is mixed with white Gaussian noise in the same manner as above. Both algorithms are run to extract the periodic signal. Figs. 4.11(a) and 4.11(b) show the mixtures while Figs. 4.12(a) and 4.12(b) show the extracted periodic signal using algorithms employing the fixed and the time-varying periods, respectively. As seen from the latter figures, when a fixed period is used in the algorithm, the algorithm recovers the signal, but also heavily locks onto the noise component. When running the proposed algorithm, however which incorporates the time-varying period, accurate reconstruction is achieved as confirmed by Fig. 4.12(b).

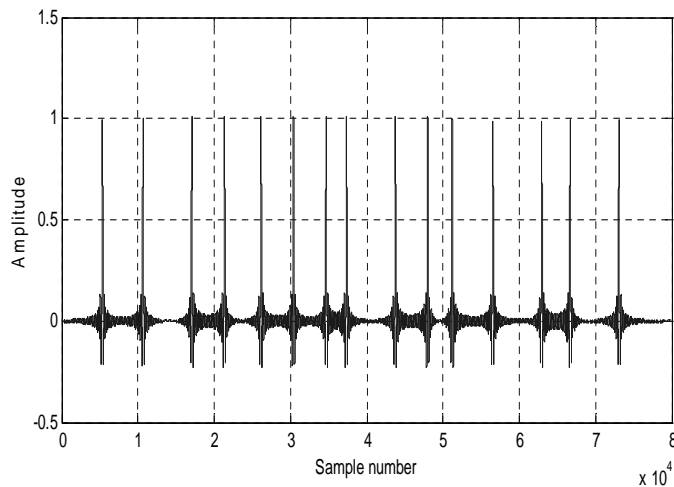
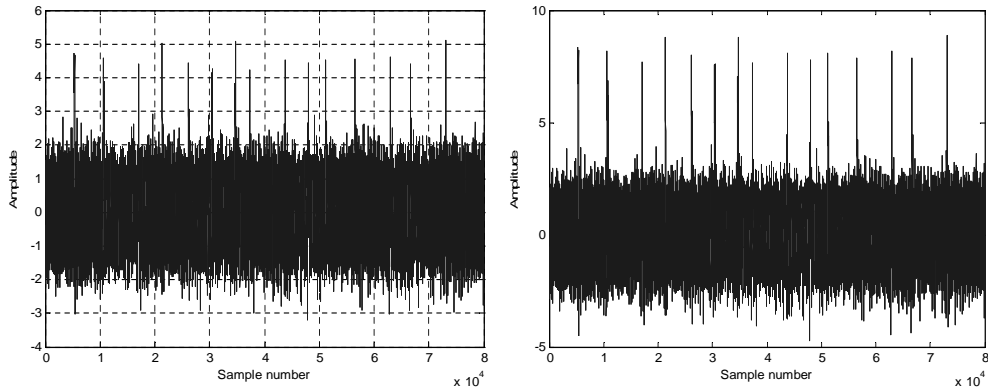
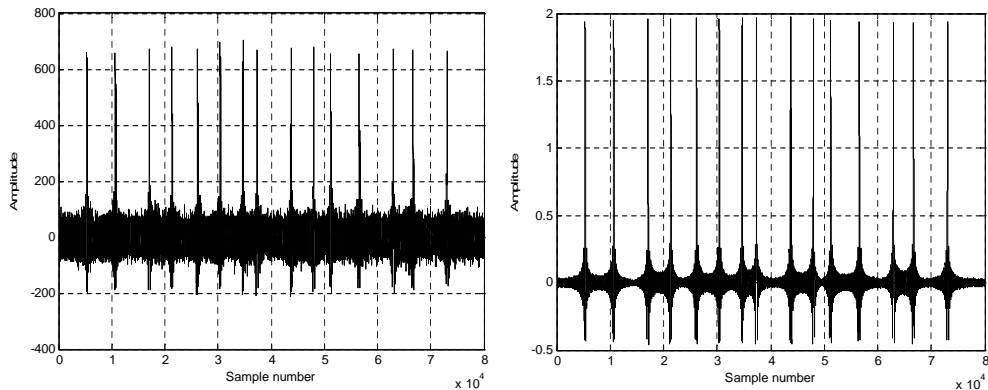


Figure 4.10. Synthetic periodic signal designed to have considerable period variations. This signal acts as a source of interest (SoI) after mixing it with white Gaussian noise.



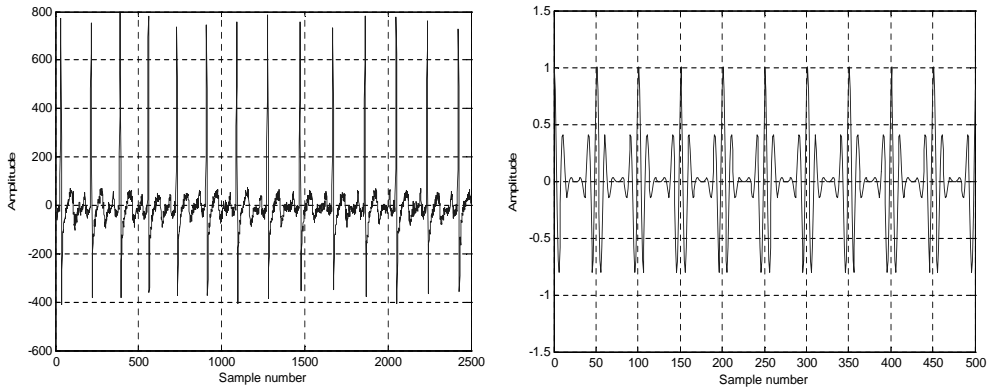
(a) Mixture 1 of synthetic signal with time-varying period and white Gaussian noise. (b) Mixture 2 of synthetic signal with time-varying period and white Gaussian.

Figure 4.11. Mixtures of synthetic periodic signal with time-varying period and white Gaussian noise, generated by a mixing matrix \mathbf{A} with elements drawn from a standardized Gaussian distribution: The synthetic periodic signal is designed to have significant period variations. The aim is to extract the synthetic periodic signal (Fig. 4.10).



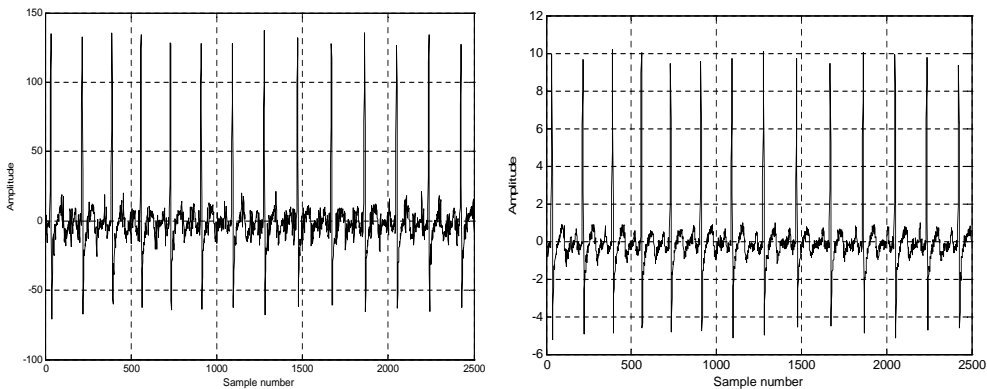
(a) Extracted synthetic signal using the algorithm with fixed period. (b) Extracted signal using the algorithm with time-varying period.

Figure 4.12. Extracted synthetic signals using algorithms with the fixed and time-varying period. Clearly, the algorithm employing time-varying period much better reconstructs the synthetic signal and we can see the variations in the signal period. The algorithm using the fixed period locks onto the noise component and results in a poorly reconstructed signal.



(a) ECG signal which is to be extracted after mixing it with a synthetic pure periodic signal. The signal has slight variations in period durations. (b) Synthetic pure periodic signal which is mixed with the ECG signal. It is designed to be non harmonically related to the ECG signal.

Figure 4.13. ECG and a zoomed-in portion of a synthetic pure periodic signal whose repetition frequency is not a multiple of that of the ECG. These signals are combined by a mixing matrix \mathbf{A} with elements drawn from standardized Gaussian distribution. The aim was to extract the ECG signal which has a time-variant period.



(a) Extracted ECG using the algorithm employing fixed period. (b) Extracted ECG using the algorithm employing time-varying period.

Figure 4.14. Extracted ECG signals using algorithms with fixed and time-varying period. The algorithm employing time-varying period reconstructs the ECG signal perfectly. Although the algorithm using the fixed period reconstructs the ECG, it is also affected by the noise component.

4.4.3 Separation of two periodic signals

Another investigation was performed considering separation of two non-harmonically related periodic signals, i.e. the ECG signal having varying period duration (see Fig. 4.13(a)), mixed with a synthetic purely periodic signal shown in Fig. 4.13(b). The signal of interest in this case is the ECG signal. The recovered ECG signals are shown in Fig. 4.14(a) and 4.14(b) for algorithms employing fixed and time-varying periods, respectively. As seen in Fig. 4.14(b), the proposed algorithm recovers the ECG completely. This shows that the algorithm works, not only for a periodic signal contaminated with WGN, but also for separating periodic signals. This can be likened to biomedical applications, such as the extraction of the heart sound signal (HSS) from lung sound recordings, where both the HSS and lung sound signal (LSS) have distinct periodicity but are generally not harmonically related. Another example is the extraction of fetal ECG signals from maternal abdominal sensors that are highly contaminated with the maternal ECG [84].

4.5 Application of the proposed algorithm to separation of the heart beat sound signal from real lung sound recordings

In this section, the applicability of the proposed algorithm to extraction of the HSS from real recorded lung sound recordings is demonstrated. The data set comprised of two synchronized recordings obtained from channel (1), front left chest (heart location), and channel (2), front right chest, by digital stethoscopes sampled at 44,100Hz with 16-bits resolution. It is worth noting that, in order to use the algorithm, a

clean reference signal with clear distinct peaks is required such that the peaks could automatically be detected using the readily available peak detection algorithm. The clean reference signal in this case would be the ECG signal that is synchronized with the two channel recordings. However, since this ECG was not available, ‘manual’ peak detection was used where data from channel (1) was pre-filtered prior to using an individual judgement about the occurrence of the peaks in the data. Using the resulting peak locations, both the $\theta(t)$ and the τ_t were calculated, which are necessary to compute the $\tilde{\mathbf{R}}\mathbf{s}$ for two channel data. The algorithm was run with the two raw recordings as mixture signals. The two recordings are shown in Figs. 4.15(a) and 4.15(b). The recovered HSSs for when both the fixed and time-varying algorithms are used, are shown in Figs. 4.15(c) and 4.15(d), respectively. The HSS recovered from using the time-varying algorithm has clear distinct peaks depicting a better estimate of the actual HSS. Using the fixed period algorithm results in a noisy reconstructed HSS. These results have been further corroborated by listening tests. In the listening tests, five subjects of normal hearing ability were asked to listen to both the recovered HSSs, and to comment on their intelligibility. All subjects observed that although it was evident that the recovered signals were HSSs, the one recovered when using the fixed period was less intelligible due to the presence of noise.

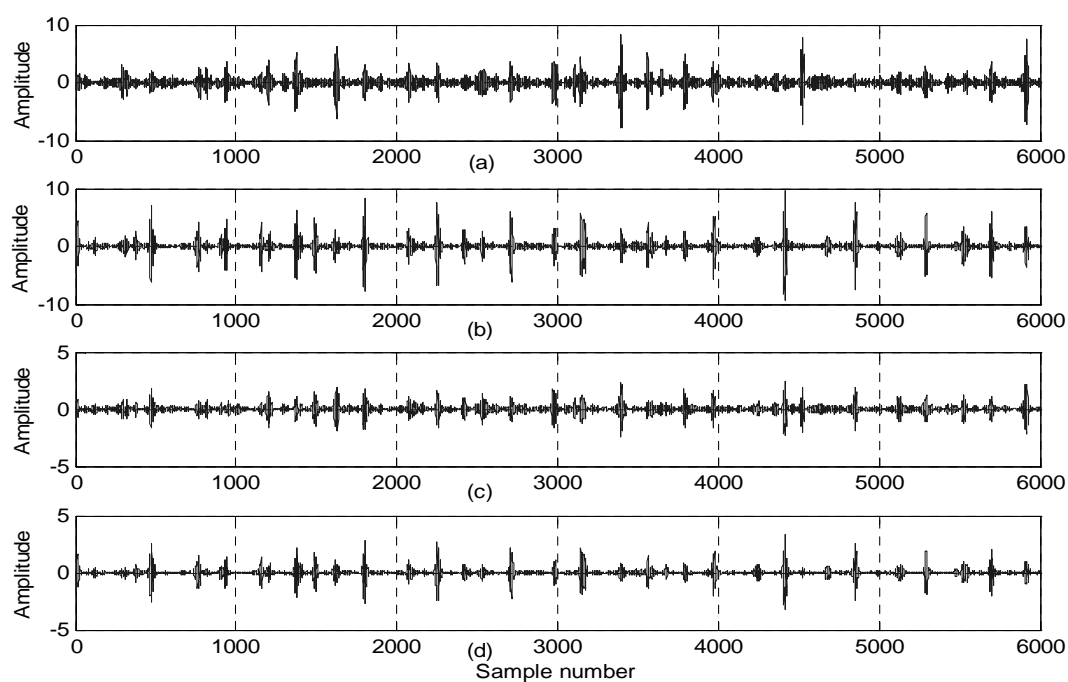


Figure 4.15. Extraction of heart sound signal from lung sound recordings. (a) & (b) are the lung sound recordings (also called mixtures since each contain both heart and lung sound signals). The aim is to extract the heart sound signal from the recordings. Subplots (c) & (d) depict the resulting extracted heart sound signal for algorithms employing fixed and time-varying period respectively, the definition of the signal in subplot (d) is much improved.

4.6 Chapter summary and conclusions

The performance of the BSE algorithm depends on *a priori* knowledge of the source signal. Knowledge of the period of the signal of interest helps to extract the source signal of interest from the mixtures. In this chapter, a novel sequential algorithm using second-order statistics for the BSE of quasi-periodic source signals, which exploits the temporal, time-varying, quasi-periodicity of the source signals, was introduced. The algorithm was based on partial approximate joint diagonalization of autocorrelation matrices at time-varying lag τ_t , which is recalculated on a cycle-by-cycle basis. The algorithm is suitable for multichannel decomposition of periodic signals with or without a time-varying period. Simulation results suggest that if the signal of interest has a time-varying period, then using an algorithm employing a fixed period results in erroneous results. Results from other investigations show that the algorithm is suitable for removing a heart sound signal from lung sound recordings where the periodic variation in the heart beat has been extracted manually. However, with the availability of a suitably clean ECG signal, which would be synchronous with the underlying heart sound within the phonocardiogram signals, significant improvements might be possible and the heart beat period extraction could then be automated. Furthermore, due to the multidimensional nature of the ECG, the results for multichannel recordings may be improved by using more ECG reference signals [84] which could thereby better exploit the sub-components of the ECG recording, i.e. the P, QRS, and the T waves.

The cost function in (4.2.5), proposed in [68] has some limitations. Firstly, its convergence is rather difficult to prove analytically in the

time domain. Secondly, there are some questions regarding its exact formulation and constraints imposed on the associated vector norms. This, together with increasing the number of channels for lung sound recordings and exploring other algorithms based on cost functions that do not exhibit the aforementioned shortcomings could be future work. In conclusion, this work is nonetheless a step forward in overcoming the time-varying periodic characteristic of many nonstationary biomedical measurements such as the heart sound signals, thereby allowing separation using information about a signal's periodicity.

AUTOMATING PERIOD PICKING BY NONLINEAR SEQUENTIAL BAYESIAN FILTERING

In this chapter nonlinear sequential Bayesian filtering techniques, in particular the Kalman filter and the particle filter are proposed to derive a much cleaner and more reliable signal from the HSS for the purpose of *automating* heart sound signal peak-picking for subsequent use by the peak detection algorithm.

5.1 Introduction

Many biomedical signals including the heart sound signal (HSS), lung sound signal (LSS) and the electrocardiogram (ECG) exhibit some degree of nonstationarity and quasi-periodicity. Several algorithms have been developed that rely on period information of the signal of interest (SoI) to extract it from other signals or noise (see for instance [77]). It has been shown in [81] that assuming strict periodicity for a signal

of interest which is, in actual fact, quasi-periodic, invariably impairs performance. Recently, a sequential blind source extraction algorithm, based on variable period information, to account for nonstationarity of the signal of interest was proposed [85]. This algorithm, to a larger extent, was based on the ECG signal, which has clear, distinct peaks necessary for detection of period information. Although the algorithm performed well in the extraction of the HSS, the period information was captured manually through eye-balling, which, needless to say, is not convenient for automatic period detection necessary for on-line processing. The reason for eye-balling heart signal period information was because, normally, unlike the ECG, the HSS, due to its acoustic nature, exhibits multiple peaks during each heart beat and, in such a scenario, the detection algorithms fail to perform. Therefore, the heart sound signal needs some prior processing or to be modified in some way before it can be used in the established peak detection algorithms to detect its peaks.

It is common in many science and engineering situations to estimate the hidden state of the system that changes over time using a sequence of noisy observations made on the system. Normally, the state-space approach, which focuses attention on the state vector of the system, is adopted for modelling a dynamic system. In state-space formulation, at least two joined signal models are required: the state model which describes the evolution of the system state with time and the observation model relating the noisy observations to the system state. Proceeding with these models in their probabilistic form provides a basis for dynamic state estimation with a Bayesian-type approach to state estimation. In the Bayesian approach to stochastic state estima-

tion, the idea is to construct the posterior probability density function (pdf) of the state based on all the available information, including the received observations. Since such a pdf contains all the available statistical information, it can be considered to be the complete solution to the estimation problem.

For many problems, some sort of recursive processing is required in that each time an observation is received, an estimate is required based on that observation. This may be achieved by the use of a recursive filter. Essentially, such a filter comprises of prediction and update stages. During the prediction stage, the state pdf is predicted using the state model. Since the state is usually subject to some unknown disturbances (modelled as random noise), prediction generally deforms the state pdf. The predicted pdf, resulting from the prediction stage, is modified by the latest observation during the update stage. The update operation is achieved through Bayes' rule.

The purpose of this chapter is to use nonlinear sequential Bayesian filtering techniques, in particular the Kalman filter and the particle filter, to derive a much cleaner and reliable signal from the HSS itself for the purpose of *automating* heart sound signal peak picking for ultimate use by the peak detection algorithm. The proposed approach entails tracking the time-varying autoregressive (AR) parameters of the AR model fitted to the HSS information. The so-called “Kalman filter autoregressive (KF-AR)” model is a widely adopted approach for estimating and tracking the AR parameters of a nonstationary time series [42]. The conventional Kalman filter itself assumes linear state and observation models as well as Gaussian pdfs. In order to extend the idea of the conventional Kalman filter to nonlinear systems, with approximate

Gaussian pdfs, several variants of the conventional Kalman filter have been developed and documented in the literature (see for example [86]). Particle filtering on the other hand is a versatile algorithm in that it can be applied to almost any type of problem where signal variations are present including models with high nonlinearities and with pdfs that are not necessarily Gaussian.

This chapter is organized as follows: The problem is formulated, in the context of Kalman filter and particle filtering approaches, in Section 5.2. In Section 5.3 an overview of nonlinear sequential Bayesian filtering is presented. In the same section Kalman and particle filtering algorithms are reviewed. Examples of suitable signals for peak-picking by Kalman and particle filtering based approaches are presented in Section 5.4. Chapter conclusions are presented in Section 5.5.

5.2 Problem formulation

The heart sound signal (HSS) is modelled by a time-varying AR process. The AR model fits the spectral characteristics of the HSS since its power spectral density (PSD) possesses distinctive peaks. This model is arrived at by using the heart sound information which is free of noise and respiratory sounds (see Fig.5.1). The time-varying part accounts for the nonstationarity nature of the HSS.

Consider the observed data $\{y(t), t \in \mathbb{N}\}$ representing an M th order time-varying AR process

$$y(t) = \sum_{m=1}^M a_m(t)y(t-m) + u(t) \quad (5.2.1)$$

where $\{a(m)\}_{m=1}^M$ are the parameters of the AR process at each time instant t , $u(t)$ is independently and identically distributed (i.i.d.) driving noise which could take the form of either a Gaussian or non-Gaussian distributed signal and $y(t)$ models the heart sound signal. A nonGaussian-type driving noise may be modelled as either a Gaussian mixture with two mixands, thus,

$$u(t) \sim (1 - \gamma)\mathcal{N}(0, \sigma_1^2) + \gamma\mathcal{N}(0, \sigma_2^2) \quad (5.2.2)$$

where $0 < \gamma < 1$, and $\sigma_2^2 \gg \sigma_1^2$, or as a Laplacian distribution, thus,

$$u(t) \sim \frac{\alpha}{2}e^{-\alpha|u(t)|} \quad (5.2.3)$$

where $\alpha > 0$

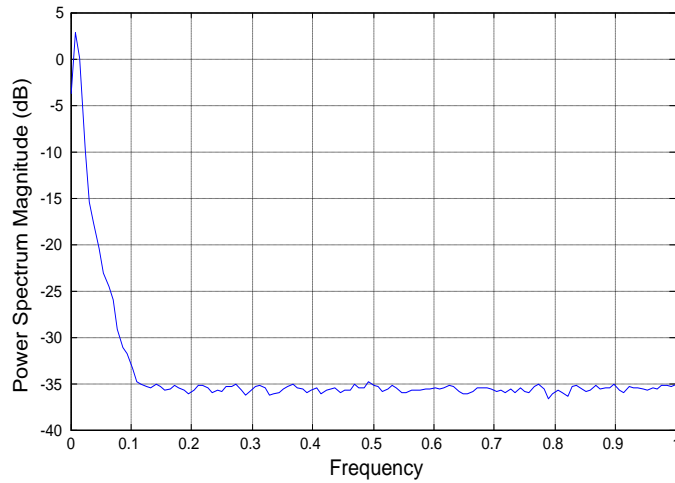


Figure 5.1. Power spectral density of noise-free HSS.

Based on the premise that the AR parameters evolve according to the changes in $y(t)$, and hence maybe used to explicitly show changes in $y(t)$, the objective is to track the evolution of the AR parameters $\{a(m)\}_{m=1}^M$ for all t and to represent the heart sound signal by a new signal composed of the evolution of the norm of these parameters.

Bayesian filtering techniques are suitable candidates for the problem at hand. In particular, Kalman and particle filtering algorithms are chosen to track the AR parameters. This is motivated by the fact that the noise term $u(t)$ in (5.2.1) could be considered to have been drawn from either Gaussian or non-Gaussian distributions.

5.3 Overview of nonlinear Bayesian filtering

A classical problem in nonlinear filtering theory is to estimate recursively the state sequence $\{\mathbf{x}(t), t \in \mathbb{N}\}$ of a system, from noisy observation sequence $\{y(t), t \in \mathbb{N}\}$ made on the system.

Let $\mathbf{x}(t)$ evolve according to the dynamic model:

$$\mathbf{x}(t) = \mathbf{g}(\mathbf{x}(t-1), \mathbf{v}(t-1)), \quad (5.3.1)$$

and the observation sequence $y(t)$ be related to the state sequence via the observation model:

$$y(t) = \mathbf{h}(\mathbf{x}(t), e(t)), \quad (5.3.2)$$

where $\mathbf{g}(\cdot)$ is the state evolution function and $\mathbf{h}(\cdot)$ is the observation function that represents the relationship between the state and observation sequences. The signals $\mathbf{v}(t-1)$ and $e(t)$ are the system and observation noises respectively.

The state sequence $\mathbf{x}(t)$ is characterized by its probability density function estimated from a sequence of observations $y(t)$. In the sequential Bayesian filtering framework, the conditional density of the state sequence given the observations is propagated through prediction and update stages;

$$p(\mathbf{x}(t)|y(1:t-1)^1) = \int_{-\infty}^{+\infty} p(\mathbf{x}(t)|\mathbf{x}(t-1))p(\mathbf{x}(t-1)|y(1:t-1))d\mathbf{x}(t-1). \quad (5.3.3)$$

$$\begin{aligned} p(\mathbf{x}(t)|y(1:t)) &= p(\mathbf{x}(t)|y(t), y(1:t-1)) \\ &= \frac{p(y(t)|\mathbf{x}(t), y(1:t-1))p(\mathbf{x}(t)|y(1:t-1))}{p(y(t)|y(1:t-1))} \\ &= \frac{p(y(t)|\mathbf{x}(t))p(\mathbf{x}(t)|y(1:t-1))}{p(y(t)|y(1:t-1))} \end{aligned} \quad (5.3.4)$$

where $p(y(t)|y(1:t-1)) = \int p(y(t)|\mathbf{x}(t))p(\mathbf{x}(t)|y(1:t-1))d\mathbf{x}(t-1)$ is a normalization constant independent of $\mathbf{x}(t)$. $p(\mathbf{x}(t-1)|y(1:t-1))$ is the prior probability density function, $p(\mathbf{x}(t)|y(1:t-1))$ is the predicted probability density function and $p(y(t)|\mathbf{x}(t))$ is the observation likelihood function. The posterior probability density function at time instant t , $p(\mathbf{x}(t)|y(1:t))$, is used as the prior probability density function at time instant $t+1$.

When the system dynamics and observation models (Equations (5.3.1) and (5.3.2)) are known and linear, the solution to relations (5.3.3) and (5.3.4) is provided by the Kalman filter, which can be proved to be the optimal filter under certain general constraints. Suboptimal algorithms have been developed for nonlinear systems including the particle filter, a thorough treatment of both optimal and suboptimal algorithms can be found in [86]. The particle filter approximates the posterior densities by samples (particles) and their associated weights. The Kalman and the particle filters are summarized in the following sections.

¹ $y(1:t-1) = y(1), y(2), \dots, y(t-1)$ as in MATLAB notation.

5.3.1 Kalman filtering

Under the standard assumptions that the noise terms $\mathbf{v}(t-1)$ and $e(t)$ are white and Gaussian, the state dynamics function $\mathbf{g}(\cdot)$ is known and linear with respect to both $\mathbf{x}(t-1)$ and $\mathbf{v}(t-1)$ and, the observation function $\mathbf{h}(\cdot)$ is known and linear with respect to both $\mathbf{x}(t)$ and $e(t)$ the prediction and update problems (5.3.3) and (5.3.4) are optimally resolved by the Kalman filter [87]. Hence, in the Kalman filtering framework, (5.3.1) and (5.3.2) can be written as:

$$\mathbf{x}(t) = \mathbf{G}\mathbf{x}(t-1) + \mathbf{v}(t) \quad (5.3.5)$$

$$y(t) = \mathbf{h}^T \mathbf{x}(t) + e(t) \quad (5.3.6)$$

where \mathbf{G} is a known matrix and \mathbf{h} is a known vector defining the linear functions of the state and observation respectively, $\mathbf{v}(t)$ and $e(t)$ are assumed i.i.d. $\sim \mathcal{N}(0, \mathbf{Q}(t-1))$ and i.i.d. $\sim \mathcal{N}(0, r(t))$ where $\mathbf{Q}(t-1)$ and $r(t)$ are covariances of the system state and observation noises respectively.

Given the assumptions about $\mathbf{v}(t)$ and $e(t)$, the state of the system can be recursively estimated, accordingly to

$$\hat{\mathbf{x}}(t|t) = \hat{\mathbf{x}}(t|t-1) + \mathbf{k}(t)(y(t) - \mathbf{h}^T \hat{\mathbf{x}}(t|t-1)) \quad (5.3.7)$$

where the Kalman gain $\mathbf{k}(t)$ is obtained by the Kalman recursion [88]

$$\mathbf{P}(t|t-1) = \mathbf{Q}(t) + \mathbf{G}\mathbf{P}(t-1|t-1)\mathbf{G}^T \quad (5.3.8)$$

$$\mathbf{k}(t) = \mathbf{P}(t|t-1)\mathbf{h}c^{-1}(t) \quad (5.3.9)$$

$$\mathbf{P}(t|t) = \mathbf{P}(t|t-1) - \mathbf{k}(t)c(t)\mathbf{k}^T(t) \quad (5.3.10)$$

where $c(t) = \mathbf{h}^T\mathbf{P}(t|t-1)\mathbf{h} + r(t)$ defines the covariance of the innovation term $y(t) - \mathbf{h}^T\hat{\mathbf{x}}(t|t-1)$.

5.3.2 Particle filtering

The fundamental idea in particle filtering is to represent the density of interest $p(\mathbf{x}(0:t)|y(1:t))$ as in (5.3.3) by a set of samples (particles) $\{\mathbf{x}^i(0:t), i = 1, 2, \dots, N\}$, and their associated weights $\{w^i(t), i = 1, 2, \dots, N\}$. The weights are normalized such that $\sum_i w^i(t) = 1$. The density of interest $p(\mathbf{x}(0:t)|y(1:t))$, at time t , based on particles and their weights, can be approximated as

$$p(\mathbf{x}(0:t)|y(1:t)) \approx \sum_{i=1}^N w^i(t)\delta(\mathbf{x}(0:t) - \mathbf{x}^i(0:t)) \quad (5.3.11)$$

where $\delta(\cdot)$ is the Dirac delta function. The weights $w^i(t)$ are chosen according to the principle of importance sampling [89] whereby if the samples $\{\mathbf{x}^i(0:t), i = 1, 2, \dots, N\}$ cannot be directly taken from the posterior $p(\mathbf{x}(0:t)|y(1:t))$, then they are drawn from a so-called ‘importance density’ $q(\mathbf{x}(0:t)|y(1:t))$ and then the weights $w^i(t)$, can be defined as

$$w^i(t) \propto \frac{p(\mathbf{x}^i(0:t)|y(1:t))}{q(\mathbf{x}^i(0:t)|y(1:t))} \quad (5.3.12)$$

If at time $t - 1$ an approximation of the posterior density $p(\mathbf{x}(0 : t)|y(1 : t))$ subject to having density $p(\mathbf{x}(0 : t - 1)|y(1 : t - 1))$, then the importance density is chosen to be factorized such that

$$q(\mathbf{x}(0 : t)|y(1 : t)) \triangleq q(\mathbf{x}(t)|\mathbf{x}(0 : t - 1), y(1 : t))q(\mathbf{x}(0 : t - 1)|y(1 : t - 1)) \quad (5.3.13)$$

then the samples $\mathbf{x}^i(0 : t) \sim q(\mathbf{x}(0 : t)|y(1 : t))$ may be obtained by augmenting each of the existing samples $\mathbf{x}^i(0 : t - 1) \sim q(\mathbf{x}(0 : t - 1)|y(1 : t - 1))$ with new state $\mathbf{x}^i(t) \sim q(\mathbf{x}(t)|\mathbf{x}(0 : t - 1), y(1 : t))$. To derive the weight update equation, the probability density function $p(\mathbf{x}(0 : t)|y(1 : t))$ is first expressed in terms of $p(\mathbf{x}(0 : t - 1)|y(1 : t - 1))$, $p(y(t)|\mathbf{x}(t))$, and $p(\mathbf{x}(t)|\mathbf{x}(t - 1))$:

$$\begin{aligned} p(\mathbf{x}(0 : t)|y(1 : t)) &= \frac{p(y(t)|\mathbf{x}(0 : t), y(1 : t - 1))p(\mathbf{x}(0 : t)|y(1 : t - 1))}{p(y(t)|y(1 : t - 1))} \\ &= \frac{p(y(t)|\mathbf{x}(t))p(\mathbf{x}(t)|\mathbf{x}(t - 1))}{p(y(t)|y(1 : t - 1))}p(\mathbf{x}(0 : t - 1)|y(1 : t - 1)) \end{aligned} \quad (5.3.14)$$

$$p(\mathbf{x}(0 : t)|y(1 : t)) \propto p(y(t)|\mathbf{x}(t))p(\mathbf{x}(t)|\mathbf{x}(t - 1))p(\mathbf{x}(0 : t - 1)|y(1 : t - 1)) \quad (5.3.15)$$

Using Bayes' rule (Equation (5.3.4)) and substituting (5.3.13) and (5.3.15) into (5.3.12) yields the weight update equation

$$\begin{aligned}
w^i(t) &\propto \frac{p(y(t)|\mathbf{x}^i(t))p(\mathbf{x}^i(t)|\mathbf{x}^i(t-1))p(\mathbf{x}^i(0:t-1)|y(1:t-1))}{q(\mathbf{x}^i(t)|\mathbf{x}^i(0:t-1), y(1:t))q(\mathbf{x}^i(0:t-1)|y(1:t-1))} \\
&= w^i(t-1) \frac{p(y(t)|\mathbf{x}^i(t))p(\mathbf{x}^i(t)|\mathbf{x}^i(t-1))}{q(\mathbf{x}^i(t)|\mathbf{x}^i(0:t-1), y(1:t))} \quad (5.3.16)
\end{aligned}$$

If $q(\mathbf{x}(t)|\mathbf{x}(0:t-1), y(1:t)) = q(\mathbf{x}(t)|\mathbf{x}(t-1), y(t))$, then the importance density becomes only dependent on $\mathbf{x}(t-1)$ and $y(t)$. This is particularly useful in the case when only a filtered estimate of posterior $p(\mathbf{x}(t)|y(1:t))$ is required at each time step, as is the case in this work. In such a case $\mathbf{x}^i(0:t-1)$ and the history of observations, $y(1:t-1)$ can be discarded leading to a modified weight update equation

$$w^i(t) \propto w^i(t-1) \frac{p(y(t)|\mathbf{x}^i(t))p(\mathbf{x}^i(t)|\mathbf{x}^i(t-1))}{q(\mathbf{x}^i(t)|\mathbf{x}^i(t-1), y(t))} \quad (5.3.17)$$

and the posterior density $p(\mathbf{x}(t)|y(1:t))$ is then approximated as

$$p(\mathbf{x}(t)|y(1:t)) \approx \sum_{i=1}^N w^i(t) \delta(\mathbf{x}(t) - \mathbf{x}^i(t)) \quad (5.3.18)$$

whereby, as $N \rightarrow \infty$, (5.3.18) approaches the true posterior $p(\mathbf{x}(t)|y(1:t))$. Therefore, particle filtering consists of recursive propagation of importance weights $w^i(t)$ and support points $\mathbf{x}^i(t)$ as each measurement is received sequentially.

The choice of importance density is crucial in the design of particle filters and is significant to filter performance. This function must have the same support as the probability density function to be approximated. Generally, the closer the importance function to the distribution, the better the approximation to the approximated probability density function. A widely used choice of the importance function which will be

adopted in this chapter is given as

$$q(\mathbf{x}(t)|\mathbf{x}^i(t-1), y(1:t)) = p(\mathbf{x}(t)|\mathbf{x}^i(t-1)) \quad (5.3.19)$$

This choice of importance function implies that it is necessary to sample $p(\mathbf{x}(t)|\mathbf{x}^i(t-1))$ and that the importance weights from (5.3.18) can be updated by

$$w^i(t) \propto w^i(t-1)p(y(t)|\mathbf{x}^i(t)) \quad (5.3.20)$$

The importance sampling weights indicate the level of importance of the corresponding particle. A relatively small weight implies that the sample is drawn far from the main body of the posterior distribution and has a small contribution in the final estimation. Such a particle is said to be ineffective. If the number of ineffective particles is increased, the number of particles contributing to the estimation of states is decreased, so the performance of the filtering procedure deteriorates. The degeneracy can be avoided by a resampling procedure. Resampling is a procedure that eliminates the particles with small weights and replicates those with large weights according to their weights. A suitable measure of degeneracy of the algorithm is given by the effective sample size \hat{N}_{ef} [90],

$$\hat{N}_{ef} = \frac{1}{\sum_{i=1}^{N_s} (w^i(t))^2} \quad (5.3.21)$$

Whenever a significant degeneracy is observed (i.e. when \hat{N}_{ef} falls below some threshold N_{th}), resampling is performed.

5.4 Deriving a signal suitable for peak-picking from the AR process by Kalman and particle filtering based approaches

The AR process (5.2.1) can be written as

$$y(t) = \mathbf{y}(t-1)^T \mathbf{a}(t) + u(t) \quad (5.4.1)$$

where

$$\mathbf{a}(t) = (a_1(t), \dots, a_M(t)) \quad (5.4.2)$$

$$\mathbf{y}(t) = (y(t), \dots, y(t-M+1)) \quad (5.4.3)$$

A simple state-space representation of the univariate AR process in (5.4.1) that is suitable for recursive estimation of the AR parameters can be given by the following state and observation equations

$$\mathbf{a}(t) = \mathbf{a}(t-1) + \mathbf{v}(t) \quad (5.4.4)$$

$$y(t) = \mathbf{y}(t-1)^T \mathbf{a}(t) + u(t) \quad (5.4.5)$$

Since the dynamic behavior of $\mathbf{a}(t)$ is not known, it can be assumed that it performs a random walk ([91], [92]). That is, the AR parameters vary according to a simple Markov process. This is modelled by adding the noise process $\mathbf{v}(t)$, of known distribution, in Equation (5.4.4). Using the Kalman filter algorithm and the standard assumptions therein, the state estimate of $\mathbf{a}(t)$, $\hat{\mathbf{a}}(t|t)$, can then be recursively computed according to (5.3.7). The particle filter algorithm on the other hand, can

be outlined as follows,

- initialize particles and the corresponding weights $\{\mathbf{a}^i(0), w^i(0)\}_{i=1}^N$, then for each time step t repeat the following steps
- for $i = 1, \dots, N$, obtain samples $\{\mathbf{a}^i(t)\}$ from importance function $p(\mathbf{a}(t)|\mathbf{a}^i(t-1))$
- for $i = 1, \dots, N$, update the importance weights by

$$w^i(t) = w^i(t-1)p(\mathbf{a}(t)|\mathbf{a}^i(t)) \quad (5.4.6)$$

- normalize the weights according to

$$w^i(t) = \frac{w^i(t)}{\sum_{i=1}^N w^i(t)} \quad (5.4.7)$$

- resample to obtain particles of equal weights

It is possible however that since the state of the system is conditionally Gaussian in terms of the Kalman filter and nonGaussian when considering the particle filter, the parameter estimates can be of high variance. Therefore, the resulting estimates from both algorithms may need smoothing. A recursive nonlinear filter of the form

$$\bar{a}(t+1) = (1 - v(t))\bar{a}(t) + v(t)\check{a}(t+1) \quad (5.4.8)$$

$$v(t) = \frac{C(\check{a}(t+1) - \bar{a}(t))^2}{1 + C(\check{a}(t+1) - \bar{a}(t))^2} \quad (5.4.9)$$

is proposed for each component $\check{a}(t)$ of the estimated coefficient vector $\check{\mathbf{a}}(t)$, where C is a suitable constant and, $v(t) \in (0, 1)$ defines a low pass

filter.

5.4.1 Simulation results

In this section it is demonstrated how an evolution signal, with more definition than the actual heart sound signal (HSS), can be derived by simply tracking the evolution of its AR parameters. The heart sound signal, obtained from the *R.A.L.E.* [67], is first mixed with white Gaussian noise (WGN), with signal-to-ratio (SNR) equal to 5dB and 20dB. The WGN models the interference, possibly the lung sound, that can be picked up by digital stethoscopes during heart sound signal recordings (a typical noisy heart sound signal is shown on Fig.(5.2)). In practice such a signal would be recorded closer to the person's heart location or at any place on the body where the heart sound is perceived dominant. This noisy heart sound signal is modelled by a time-varying AR process whose evolution is tracked. After tracking the evolution of the parameters along the AR process each parameter is smoothed according to (5.4.8). For reasons that will become apparent in the following subsections, a much better signal to consider is the evolution of the norm of the parameters. The Kalman filter and the particle filter algorithms are considered for tracking the parameters. In both algorithms, the functions $\mathbf{G}(t - 1)$ and \mathbf{h} in (5.3.5) and (5.3.6) are assumed to be identity functions and the covariances \mathbf{Q} and r in the Kalman filter are assumed to be $\sigma_q \mathbf{I}$ and σ_r respectively. Whereas in the particle filter the covariance of noise matrices \mathbf{Q}_p and r_p are assumed to be $q_p \mathbf{I}$ and r_p respectively, where $\sigma_q \mathbf{I}$, σ_r , $q_p \mathbf{I}$, and r_p are known and constant parameters, and \mathbf{I} is the identity matrix. The parameters σ_q and σ_r , in the case of the Kalman filter and, q_p and r_p for the particle

filter, need proper adjusting in order to obtain good results. In this work, these parameters were set as follows; $\sigma_q = 1$, $\sigma_r = 0.01$, $q_p = 0.1$ and $r_p = 0.1$.

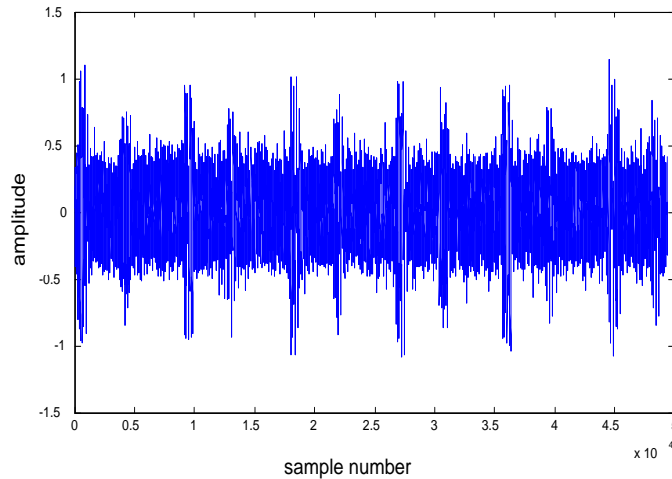


Figure 5.2. A typical noisy heart sound signal.

5.4.2 Using Kalman filtering

Here the norm of the parameters and the innovation signal that results from using the Kalman filter are considered. At SNR of 20dB, Figs. 5.3 and 5.4 show the evolution of the norm of unfiltered and low-pass filtered parameters respectively, while Fig. 5.5 depicts the evolution of the innovation signal. By comparing Fig. 5.2 with 5.4, it is seen that in Fig. 5.4, the peaks are more defined and this is a prerequisite for signal detection algorithms. The innovation signal (Fig. 5.5) is less interesting and is not considered. It is seen that even at SNR of 5dB, some very interesting results are still obtained for the norm of the smoothed parameters as depicted by Fig.5.7. Figs. 5.6 and 5.8, depicting the evolution of the norm of unfiltered parameters and the evolution of the innovation respectively, are presented for completeness.

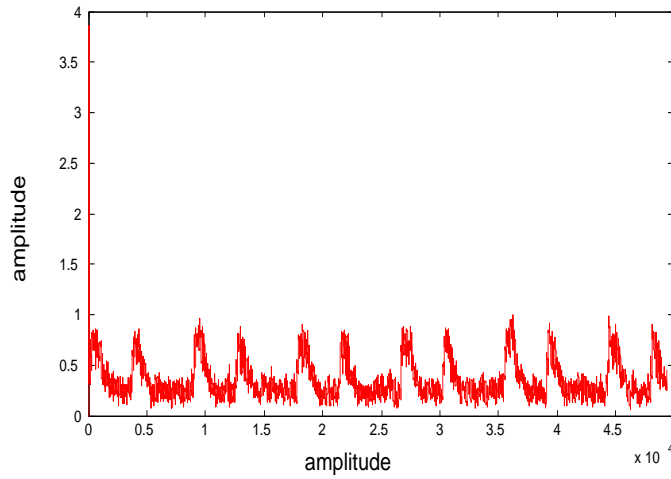


Figure 5.3. Unsmoothed evolution of the norm of parameters obtained by Kalman filtering at 20dB SNR. This shows high variance in the AR parameter estimates and therefore requires smoothing.

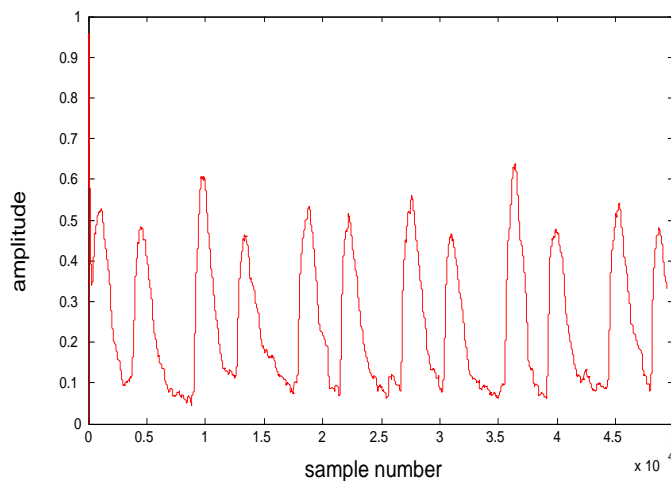


Figure 5.4. Smoothed evolution of the norm of parameters obtained by Kalman filtering at 20dB SNR. The smoothed evolution signal is a result of recursive nonlinear filtering according to Equation (5.4.8). The signal is cleaner and has clear distinct peaks which can easily be detected by peak detection algorithm.

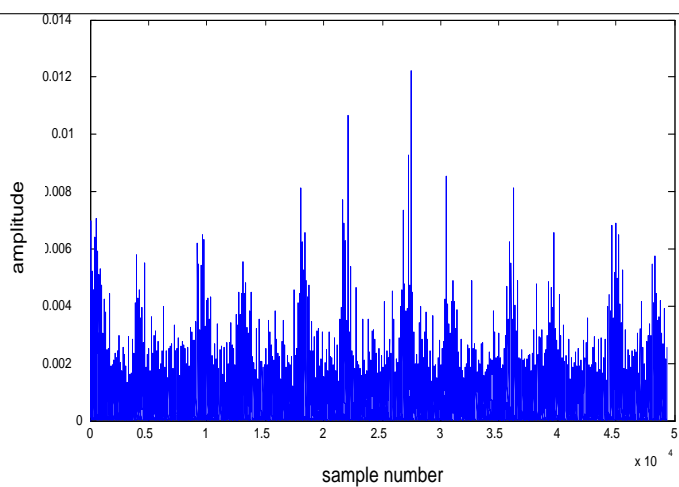


Figure 5.5. Evolution of the innovation signal obtained by Kalman filtering at 20dB SNR. This signal is noisy and therefore less interesting for peak detection.

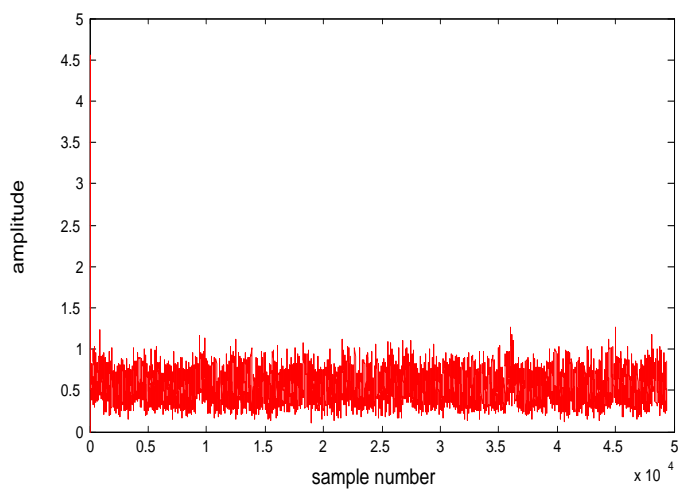


Figure 5.6. Unsmoothed evolution of the norm of parameters obtained by Kalman filtering at 5dB SNR. The AR parameter estimates require more smoothing.

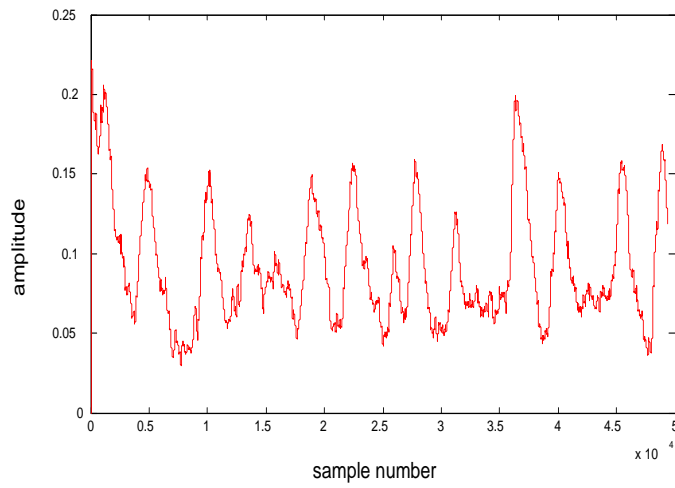


Figure 5.7. Smoothed evolution of the norm of parameters obtained by Kalman filtering at 5dB SNR. Even at 5dB SNR, some very interesting results are obtained.

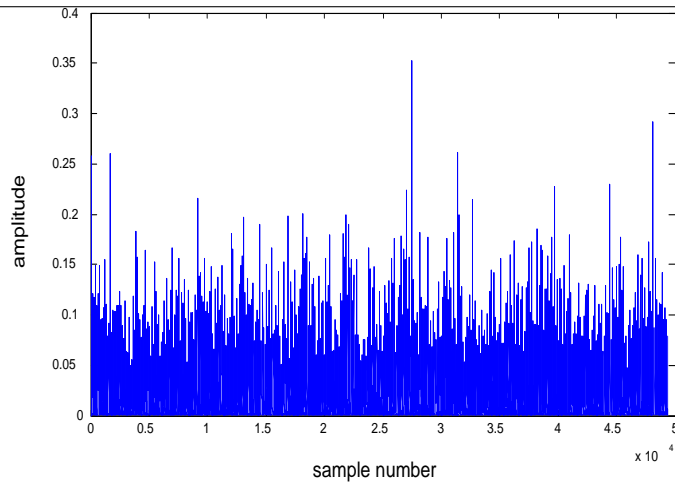


Figure 5.8. Evolution of the innovation signal by Kalman filtering at 5dB SNR. This signal is noisy and hence less interesting for peak detection.

5.4.3 Using particle filtering

In this simulation, a simple choice of the importance function, $p(\mathbf{a}(t)|\mathbf{a}(t-1)^i)$, was used with 500 particles. Here, the driving noise sequence $\mathbf{u}(t)$, is assumed to be non-Gaussian and is modelled according to (5.2.2). Figs. 5.9 and 5.10 show the evolution of the norm of the smoothed parameters at SNR of 20dB and 5dB respectively. As seen from the two figures, the particle filter performs well even when non-Gaussian noises are considered especially at higher SNR.

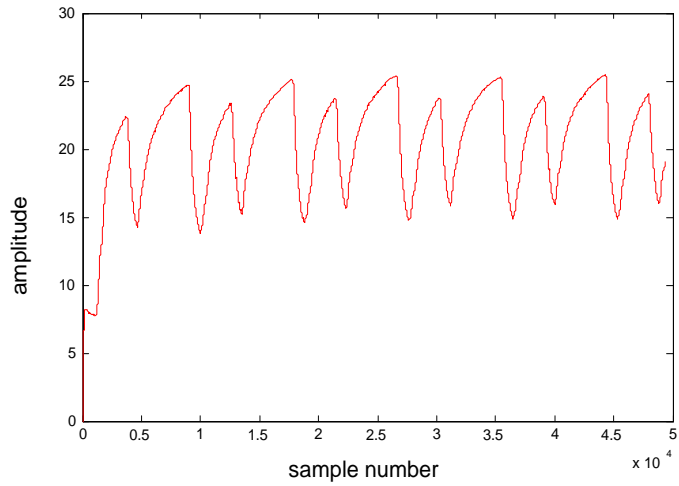


Figure 5.9. Smoothed evolution of the norm of parameters obtained by particle filtering with SNR of 20dB. The smoothed evolution signal is a result of recursive nonlinear filtering according to Equation (5.4.8). The signal is cleaner and has clear distinct peaks which can easily be detected by peak detection algorithm.

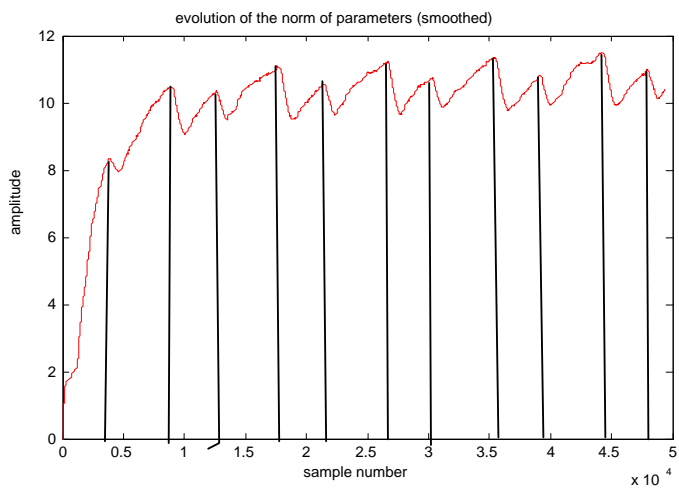


Figure 5.10. Smoothed evolution of the norm of parameters obtained by particle filtering with SNR of 5dB. The positions of the peaks are indicated by vertical lines on the figure.

5.5 Chapter summary and conclusion

In this chapter, it has been shown that rather than picking the peaks of an HSS by an eye-balling procedure, this HSS can be represented by the evolution signal of the norm of its AR parameters, which has more defined peaks that are suitable for *automatic* peak picking by established peak detection algorithms. The noisy HSS is thus modelled by a time-varying AR process whose parameters are trackable through non-linear Bayesian filtering techniques. In particular, two Bayesian filtering candidates were considered, namely, the Kalman filter and the particle filter. The Kalman filter is suitable when the associated noises in the state-space equations are assumed Gaussian and for nonGaussian noises the particle filter is exploited. The solution for *automatic* peak picking, presented in this chapter, means that there is no need to rely on the ECG signal (recorded simultaneously with HSS) for detecting HSS peaks and that a recording of HSS is essentially sufficient for detecting its peaks. In the following chapter, the ideas expressed here are incorporated and provide a complete solution for sequential blind source extraction of quasi-periodic signals with time-varying period.

**PROPOSED COMPLETE
SOLUTION FOR
SEQUENTIAL BLIND
SOURCE EXTRACTION OF
QUASI-PERIODIC SIGNALS
WITH TIME-VARYING
PERIOD**

This chapter presents a potential complete solution for sequential blind source extraction of quasi-periodic signals with time-varying period. The solution is a result of the combination of the blind source extraction algorithm presented in Chapter 4 and the ideas proposed in Chapter 5 for automating pick-peaking of the signal to be extracted.

6.1 Introduction

It has already been mentioned in Chapter 5 that the sequential blind extraction (SBE) algorithm developed in [85] and presented in Chapter 3 relies heavily on detecting the peaks of the signal of interest (SoI) in order to extract it from mixtures. If the signal has clear distinct peaks, as the ECG signal, then detecting its peaks can easily be performed automatically through peak detection algorithms. The peak information thereby obtained can then be used in the SBE algorithm for extraction purposes. However, if the signal peaks are less obvious (as is the case with the HSS) and pose problems when trying to detect them using peak detection algorithms, one can only rely on prior knowledge about the separation time of the peaks to approximate peak location and manually pick the peak locations through eye-balling. This necessary peak information can then be fed into the SBE to extract the SoI. It has been shown in Chapter 5 that a signal such as the HSS, which exhibits some degree of ambiguity about its peak location, can be represented by the evolution of the norm of its parameters. Such an evolution signal, as seen in Chapter 5, has more defined peaks. This is a much more desired feature if the peak detection algorithm is to be employed for picking the locations of signal peaks.

The reason for this chapter is to show how the ideas presented in Chapter 5 can be incorporated in the SBE algorithm presented in Chapter 4 so that rather than picking the peaks of the signal of interest manually through eye-balling or using some reference signal that is recorded simultaneously with the SoI as suggested in [85], the peak picking procedure is *automated* and performed by using only the SoI. Thus, a complete solution for sequential blind source extraction of quasi-periodic

signals with time-varying period incorporating automatic peak picking is presented in this chapter. In the following section a model of the approach for the proposed complete solution is presented, followed by the results of incorporating the ideas developed in Chapter 5 into the algorithm presented in Chapter 4.

6.2 Model of approach

The schematic diagram of the proposed complete solution to sequential extraction of quasi-periodic signal with time-varying period is shown on Fig.6.1. The signal of interest in this case is the heart sound signal (HSS) which is known to be quasi-periodic and somewhat nonstationary. The goal is to extract the HSS from the interfering lung sounds. Digital stethoscopes are used as sensors to pick up the heart/lung sound mixtures through a suitable interface that records the mixtures as they are measured. It is proposed that sensor 1 be located closer to the person's heart location while sensor 2 can be placed anywhere appropriate on the body where both heart and lung sounds can be picked up by the sensor. This arrangement ensures that mixture 1 from sensor 1 contains heart sound as the dominant sound and mixture 2 can contain heart and lung sounds in any proportion. Mixture 1 is fed into the Kalman/particle filtering to derive the evolution signal (as discussed in Chapter 4) which is then used for peak detection. The peak information is then used, together with the two mixtures, in the extraction algorithm to extract the heart sound signal. An enhanced lung sound measurement, free of HSS, is thereby obtained to aid in diagnosis. The dotted signal flow indicates an alternative procedure using the ECG signal recorded simultaneously with the two mixtures for peak picking.

The beauty of sequential Bayesian estimation stage proposed is that it replaces the eye-balling procedure and the use of the ECG signal by providing a signal suitable for use by the peak detection algorithm and thereby effectively automates the whole process of peak-picking.

The limitation in practical implementation of the proposed method is that a complete new stethoscope would need to be designed. The stethoscope would have two sensors for capturing the two mixture signals. The sensors would be connected to a processing system (possibly a digital signal processor (DSP)) that implements the proposed algorithm. An enhanced lung sound measurement, free of HSS, would then be used in diagnosis.

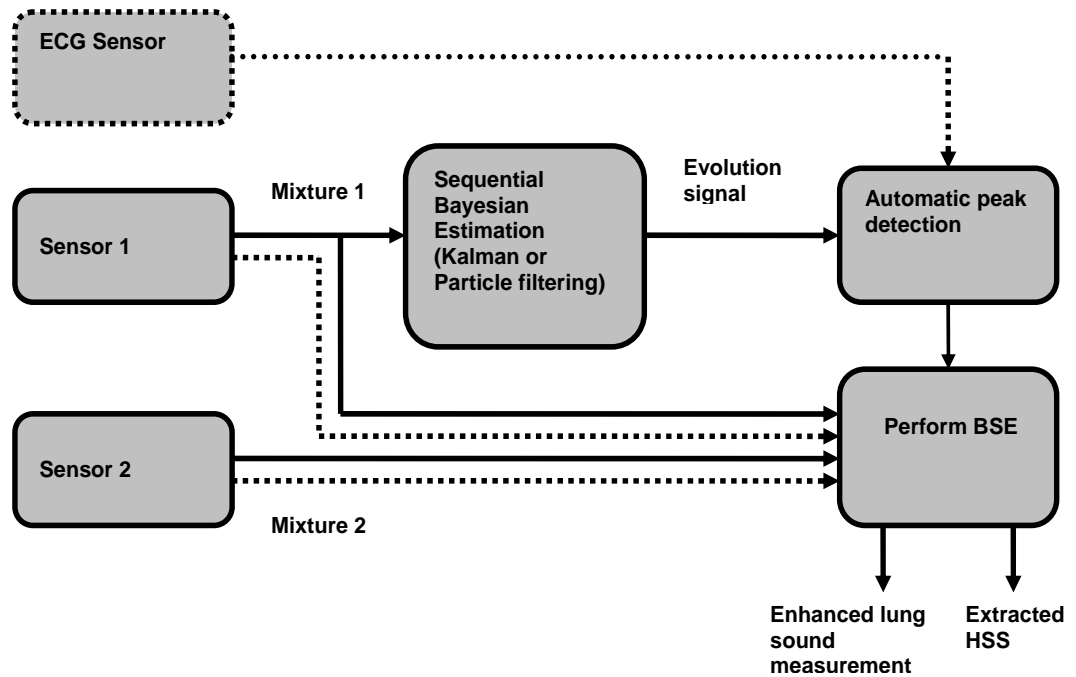


Figure 6.1. Schematic diagram of the proposed complete solution to sequential extraction of quasi-periodic signal with time-varying period. In practice, the HSS is the signal to be extracted from lung sound recording. Digital stethoscopes are used as sensors to pick up lung sound recordings (mixtures). The solid signal flow lines indicate the proposed procedure while the dotted lines indicate an alternative procedure when using the ECG signal for peak information.

6.2.1 Simulation results

In this simulation a signal is derived as in Section 5.4.1 from a real recorded noisy heart sound signal and the peak detection algorithm is used to detect its peaks. The peak information obtained is used in the SBE algorithm to extract the heart sound signal from a linear mixture. An example discussed in Section 4.3.1 of Chapter 4, where HSS was mixed with LSS by a matrix with elements drawn from a standardized Gaussian distribution, is considered again in this chapter. The original HSS and LSS together with their mixtures are shown on Fig. 6.2 top and bottom subplots respectively. This figure has been brought forward from Chapter 4 for ease of reference. The resulting HSS extracted from the mixtures of HSS and LSS, obtained through the proposed procedure used on the algorithm developed in [85] and presented in Chapter 4, is shown on Fig.6.3. As seen from the figure, accurate reconstruction is achieved. Comparing Fig.6.3 with the extraction results obtained in Section 4.3.1 of Chapter 4 (Fig.6.4), it is seen that essentially the same results are obtained although departure from strict periodicity degrades performance as seen from Fig.6.4.

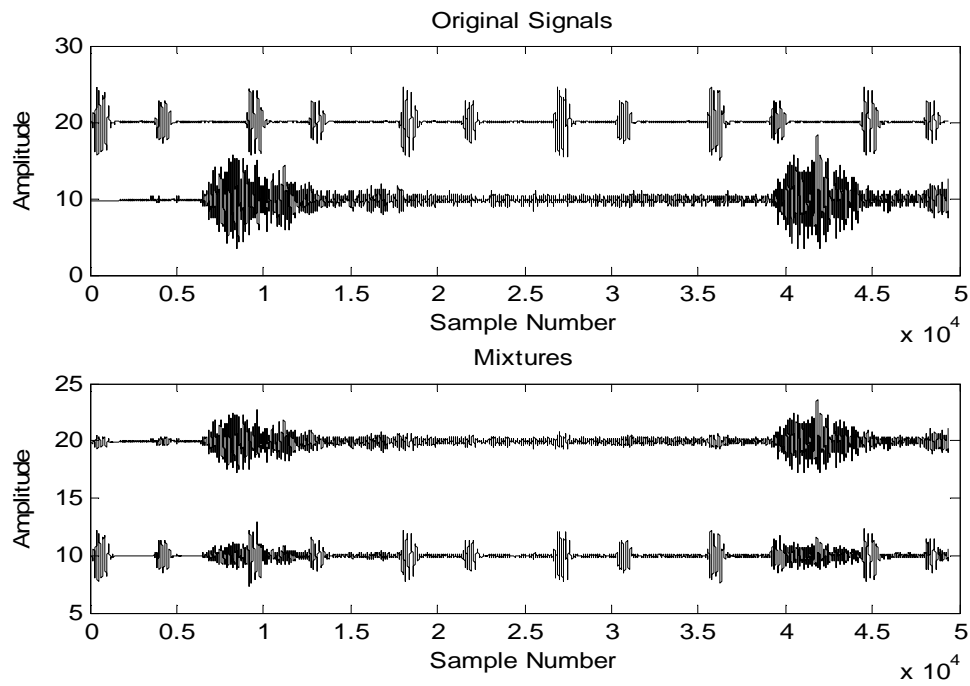


Figure 6.2. HSS and LSS before mixing (top), and the linear mixtures (bottom) (brought forward from Section 4.3.1 of Chapter 4 for ease of reference). Mixing is achieved by a matrix with elements drawn from a standardized Gaussian distribution.

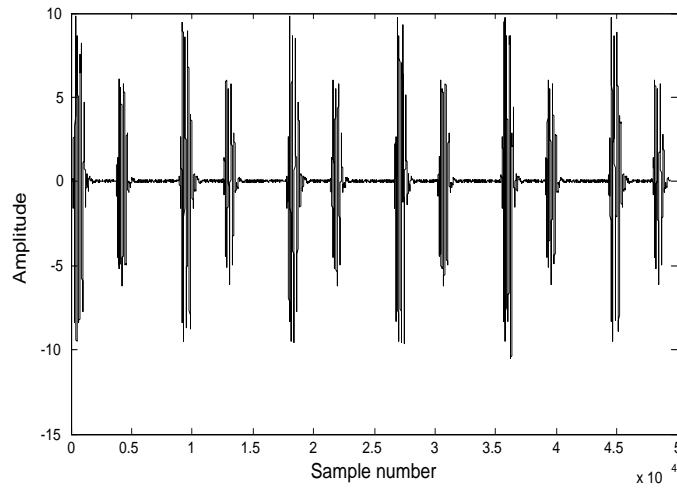


Figure 6.3. Extracted HSS by the new algorithm with automatic peak detection incorporated. By using the new algorithm, which accounts for nonstationarity of the signal of interest and incorporating automatic peak detection, a clean HSS is extracted.

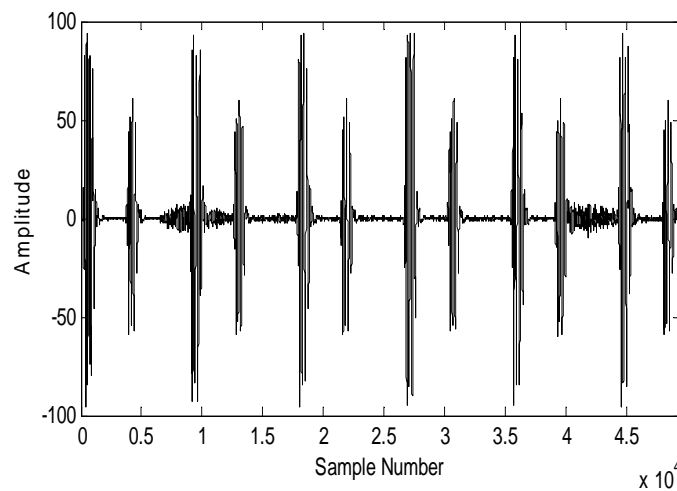


Figure 6.4. Extracted HSS by a fixed-period algorithm (brought forward from Section 4.3.1 of Chapter 4 for ease of reference). It is seen that the performance is degraded since the HSS extracted is noisy.

6.3 Chapter summary and conclusion

In this chapter, a potential complete solution for sequential blind source extraction of quasi-periodic signals with time-varying period is pre-

sented. This is achieved by replacing the eye-balling procedure and the use of a separate ECG in peak picking by using the evolution signal derived from the recorded signal mixture by nonlinear sequential Bayesian filtering techniques. The simulation results confirm the utility of the proposed solution. Using the ECG signal to approximate heart sound peaks would require additional equipment (ECG recording machine) and, although the heart sound signal is considered to follow the ECG signal, there is still a possibility for error since in actual fact the heart sound signal happens immediately after the ECG. This delay may be accounted for by introducing some time delay in the ECG signal. In practice, however, this delay would be variable due to nonstationarity of the heart sound and the ECG signal and hence may not be easily estimated. On the other hand, relying on eye-balling is not suitable for online-processing.

CONCLUSION AND FURTHER RESEARCH

7.1 Summary and conclusions

This study has presented novel signal processing approaches leading to a complete solution to the problem of extraction of quasi-periodic, nonstationary signals with time-varying period. The emphasis is on biological signals such as the heart sound signal (HSS) and the electroencephalogram (ECG). The contributions can be summarized as follows:

1. A novel approach using an adaptive line enhancer (ALE) exploiting periodicity of the signal of interest (SoI).
2. A novel blind source extraction based on second-order statistics (SOS) approach exploiting periodicity of the signal of interest.
3. Development of a new algorithm suitable for the extraction of a quasi-periodic signals with time varying period.
4. Automating periodic signal peak-picking.
5. A proposed complete solution to the problem of extraction of quasi-periodic, nonstationary signals with time-varying period.

The first contribution illustrates how the adaptive line enhancer (ALE) can be used to enhance an approximately periodic signal such as the heart sound signal (HSS) in the presence of coloured noise signal such as the lung sound signal (LSS). There are three very important parameters that determine the performance of the ALE, notably, the adaptive filter length L , the prediction distance del and the adaptation algorithm convergence parameter μ . In choosing the ALE parameters, several performance criteria are considered including: the adaptation rate, the excess mean square error (EMSE) and the frequency resolution required. All these are controlled by the choice of both μ and L . The prediction distance del has to be chosen such that decorrelation between the periodic signal (to be enhanced) and the “noise” component is achieved. Normally it is chosen as the sample number at which the autocorrelation function of the “noise” component decays to a small value relative to the zero lag $z(0)$. Therefore, for the best results to be achieved, the ALE parameters have to be chosen carefully, and this may be impractical in a real-time system.

The second contribution is based on a blind source extraction (BSE) algorithm by second-order statistics (SOS) that exploits the periodicity of the signal of interest (HSS) in order to extract it from its mixtures. The extraction is based on jointly diagonalizing the autocorrelation matrices at integer multiples of the fundamental period (if it is known) of the HSS. This hinges on the fact that if the fundamental period is, say, τ samples, then its autocorrelation matrix will theoretically have the same value at time lags corresponding to integer multiples of τ . A method such as the heart instantaneous frequency (HIF) estimation can be applied to the SoI to determine its period. It should be noted that

any errors in period estimation could lead to erroneous results, and any departure from strict periodicity due, for example, to nonstationarity of the signal of interest (SoI) may impact performance. This subject and considering the effect of error in the period estimation given nonstationary HSS are the focus of the third contribution.

In the third contribution, a novel sequential algorithm using second-order statistics for the blind source extraction of quasi-periodic source signals, which exploits the temporal, time-varying, quasi-periodicity of the source signals, has been developed. The algorithm is based on partial approximate joint diagonalization of autocorrelation matrices at time-varying lag τ_t corresponding to period variation, which is recalculated on a cycle-by-cycle basis. Most importantly, the time-varying lag τ_t information is captured by detecting the peaks of the signal of interest (in this case, the HSS). Peak detection may be performed manually or by using a suitably clean ECG signal in conjunction with established automatic peak-detection algorithms. The ECG proposed would be synchronous with the underlying heart sound within the phonocardiogram signals. Alternatively, rather than extracting the HSS peak information manually or using the ECG, a more suitable signal can be derived from the HSS itself. Such a signal should be cleaner with more defined peaks than the HSS such that it can be fed into the peak detection algorithm, and thereby automate the whole process of peak-picking/detection. This is the focus of the fourth contribution of this work. In conclusion, however, the work presented in this chapter is nonetheless a step forward in overcoming the time-varying periodic characteristic of many nonstationary biomedical measurements such as the heart sound signals, thereby allowing separation using information

about the periodicity of a signal.

The fourth contribution presents an approach based on Bayesian filtering techniques notably, Kalman filtering and particle filtering, to derive a signal (from the HSS) that is suitable for *automatic* peak-picking/detection by established peak detection algorithms. The solution for *automatic* peak picking, presented in this contribution, means that there is no need to rely on the ECG signal (recorded simultaneously with HSS) for detecting HSS peaks and that a recording of HSS is essentially sufficient for detecting its peaks. In the following contribution, the ideas expressed here are incorporated in the previous contribution to provide a complete solution for sequential blind source extraction of quasi-periodic signals with time-varying period.

The last but not least contribution presents a complete solution for sequential blind source extraction of quasi-periodic signals with time-varying period. Here, pick-peaking procedures by eye-balling or by using a separate ECG are replaced by the use of the evolution signal derived from the recorded signal mixture by nonlinear sequential Bayesian filtering techniques.

7.2 Future research

The cost function in (4.2.5), proposed in [68] has some limitations. Firstly, its convergence is rather difficult to prove analytically in the time domain. Secondly, there are some questions regarding its exact formulation and constraints imposed on the associated vector norms. This, together with exploring other algorithms based on cost functions that do not exhibit the aforementioned shortcomings forms part of the proposed future work.

The lung is an echoic environment. Therefore extraction of the HSS from the LSS recording leaves the LSS still contaminated with some echoes and possibly some noise from instruments. In order to obtain an enhanced lung sound, free of any echos and other noises, the resulting LSS from blind source extraction stage needs to be applied to an echo canceller to remove any echos. Thus, an echo canceller could be proposed.

A more robust approach for future work entails considering the lung as a time-varying echoic mixing system used in the context of non-linear blind source separation or extraction, possibly constrained by physiological aspects. Thus a hybrid blind source separation/extraction (BSS/E)-adaptive noise (echo) cancellation system for detection of lung and heart sounds could be proposed.

After detecting and separating the HSS and the LSS, the next step would be to classify them in terms of conditions that course them. Localizing the lung sounds is another aspect that could form part of the future work. Here, time-frequency techniques combined with complex image processing techniques could be employed to show where the sounds originates in the human body. This would go a long way in improving lung diagnosis of lung and heart diseases.

BIBLIOGRAPHY

- [1] F. H. Martini and E. F. Bartholomew, *Essentials of anatomy and physiology*. New Jersey, USA: Prentice Hall, 2003.
- [2] H. Pasterkamp, S. S. Kraman, and G. R. Wodicka, “Respiratory sounds: Advances beyond stethoscope,” *Am. J. Respir. Crit. Care Med.*, vol. 156, no. 3, pp. 975–977, January 1997.
- [3] H. Pasterkamp, R. Fenton, A. Tal, and V. Chernick, “Interference of cardiovascular sounds with phonopneumography in children,” *Am. Rev. Respir. Disc.*, vol. 131, no. 1, pp. 61–64, January 1985.
- [4] L. Yang-Sheng, L. Wen-Hui, and Q. Guang-Xia, “Removal of the heart sound noise from breath sound,” in *Proc. 10th Ann. Int. Conf. IEEE EMBS*, pp. 175–176. 1988.
- [5] L. Guangbin, C. Shaoqin, Z. Jingming, C. Jinzhi, and W. Shengju, “The development of a portable breath sound analysis system,” in *Proc. 14th Ann. Int. Conf. IEEE EMBS*, pp. 2582–2583. 1992.
- [6] V. K. Iyer, P. A. Ramamoorthy, H. Fan, and Y. Ploysongsang, “Reduction of heart sounds from lung sounds by adaptive filtering,” *IEEE Trans. Biomed. Eng.*, vol. 33, no. 12, pp. 1141–1148, April 1986.
- [7] L. Yip and Y. T. Zhang, “Reduction of heart sounds from lung sounds

- recording by automated gain control and adaptive filtering techniques,” in *Proc. 23rd Ann. Int. Conf. IEEE EMBS*, pp. 2154–2156. 2001.
- [8] M. Kompis and E. Russi, “Adaptive heart-noise reduction of lung sounds recorded by a single microphone,” in *Proc. 14th Ann. Int. Conf. IEEE EMBS*, pp. 691–692. 1992.
- [9] J. Gnitecki, Z. Moussavi, and H. Pasterkamp, “Recursive least squares adaptive noise cancellation filtering for heart sound reduction in lung sounds recordings,” in *Proc. 25th Ann. Int. Conf. IEEE EMBS*, pp. 2416–2419. 2003.
- [10] L. J. Hadjileontiadis and S. M. Panas, “A wavelet-based reduction of heart sound noise from lung sounds,” *Int. J. Med. Info.*, vol. 52, no.1-3, pp. 183–190, June 1998.
- [11] M. T. Pourazad, Z. Moussavi, and G. Thomas, “Heart sound cancellation from lung sound recordings using time-frequency filtering,” *IEEE Trans. Biomed. Eng.*, vol. 44, no. 4, pp. 216–225, April 2006.
- [12] E. Braunwald, D. Zipes, P. Libby, and R. Bonow, *Braunwalds Heart Disease: A Textbook of Cardiovascular Medicine*. Philadelphia, USA: Saunders, 2004.
- [13] Z. Syed, D. Leeds, D. Curtis, F. Nesta, R. A. Levine, and J. Guttag, “A Framework for the Analysis of Acoustical Cardiac Signals,” *IEEE Trans. Biomed. Eng.*, vol. 54, no. 4, pp. 651–662, April 2007.
- [14] S. S. Kraman, “Determination of site of production of respiratory sounds by subtraction phopneumography,” *Am. Rev. Respir. Disc.*, vol. 122, no. 5, pp. 303–309, April 1980.

- [15] H. Pasterkamp, R. E. Powell, and I. Sanchez, "Characteristics of lung sounds at standardized air flow in normal infants, children and adults," *Am. J. Respir. Crit. Care Med.*, vol. 154, no. 2, pp. 424–430, March 1996.
- [16] C. Jutten and J. Héroult, "Blind separation of sources, Part I: An adaptive algorithm based on a neuromimetic architecture," *Signal Processing*, vol. 24, no. 1, pp. 1–10, July 1991.
- [17] E. Moreau and O. Macchi, "Self-adaptive source separation Part II: Comparison of the direct, feedback, and mixed linear network," *IEEE Trans. Signal Processing*, vol. 46, no. 1, p. 3950, Jan 1998.
- [18] H. H. Yang and S. I. Amari, "Adaptive on-line learning algorithms for blind separation Maximum entropy and minimum mutual information," *Neural Computation*, vol. 9, no. 5, pp. 1457–1482, Jan 1997.
- [19] A. Mansour and C. Jutten, "Fourth-order criteria for blind sources separation," *IEEE Trans. Signal Processing*, vol. 43, no. 8, pp. 2022–2025, August 1995.
- [20] B. C. Ihm and D. J. Park, "Blind separation of sources using higher-order cumulants," *Signal Processing*, vol. 73, no. 3, pp. 267–276, March 1999.
- [21] U. A. Lindgren and H. Broman, "Source separation using a criterion based on second-order statistics," *IEEE Trans. Signal Processing*, vol. 46, no. 7, pp. 1837–1850, July 1998.
- [22] N. Delfosse and P. Loubaton, "Adaptive blind separation of independent sources: A deflation approach," *Signal Processing*, vol. 45, no. 1, pp. 59–83, July 1995.

-
- [23] A. Hyvrinen and E. Oja, "Simple neuron models for independent component analysis," *Int. J. Neural Syst.*, vol. 7, no. 6, pp. 671–687, December 1996.
- [24] A. Cichocki, S. I. Amari, and R. Thawonmas, "Blind signal extraction using self-adaptive nonlinear Hebbian learning rule," in *Proc. Int. Symp. Nonlinear Theory Appl.*, pp. 377–380. 1996.
- [25] R. Thawonmas and A. Cichocki, "Blind extraction of source signals with specified stochastic features," in *Proc. IEEE Int. Conf. Acoust. Speech, Signal Process.*, pp. 3353–3356. 1997.
- [26] A. Cichocki, R. Thawonmas, and S. Amari, "Sequential blind signal extraction in order specified by stochastic properties," *Electron. Lett.*, vol. 33, no. 1, pp. 64–65, January 1997.
- [27] R. Thawonmas, A. Cichocki, and S. Amari, "A cascade neural network for blind extraction without spurious equilibria," *IEICE Trans. Fund.*, vol. E81-A, no. 9, pp. 1–14, September 1998.
- [28] Z. Malouche and O. Macchi, "Adaptive unsupervised extraction of one component of a linear mixture with a single neuron," *IEEE Trans. Neural Networks*, vol. 9, no. 1, pp. 123–135, January 1998.
- [29] A. Cichocki and S. Amari, *Adaptive blind signal and image processing: Learning algorithms and applications*. West Sussex, England: John Wiley & Sons, INC, 2002.
- [30] A. Hyvrinen, J. Karhunen, and E. Oja, *Independent Component Analysis*. West Sussex, England: John Wiley & Sons, INC, 2001.

-
- [31] S. M. Naqvi, Y. Zhang, T. Tsalaile, S. Sanei, and J. A. Chambers, “A multimodal approach for frequency domain independent component analysis with geometrically-based Initialization,” in *Proc. Int. Conf. EUSIPCO*. 2008.
- [32] S. Roberts and R. Everson, *Independent Component Analysis*. Cambridge, England: Cambridge University Press, 2001.
- [33] J. Cardoso, “Blind signal separation: statistical principles,” in *Proc. IEEE, Special issue on blind identification and estimation*, pp. 2009–2025. 1998.
- [34] S. Amari, A. Cichocki, and H. H. Yang, “A new learning algorithm for blind signal separation,” in *Proc. Adv. Neural inf. Process. Syst.*, pp. 752–763. vol. 8, 1996.
- [35] A. Belouchrani, K. Abed-Meraim, J. F. Cardoso, and E. Moulines, “A blind source separation technique using second-order statistics,” *IEEE Trans. on Signal Processing*, vol. 45, no. 2, pp. 434–444, February 1997.
- [36] L. Tong, R. W. Liu, V. C. Soon, and Y. F. Huang, “Indeterminacy and identifiability of blind identification,” *IEEE Trans. on Circuits and Systems*, vol. 38, no. 5, pp. 499–509, May 1991.
- [37] L. Parra and C. Spence, “Convolutive blind separation of non-stationary sources,” *IEEE Trans. on Speech and Audio Processing*, vol. 8, no. 3, pp. 320–327, May 2000.
- [38] J. F. Cardoso and A. Souloumiac, “Blind beamforming for non-Gaussian signals,” in *Proc. Inst. Elect. Eng*, pp. 3362–3370. vol. 140, 1993.

-
- [39] Z.-L. Zhang and Z. Yi, "Extraction of a source signal whose kurtosis value lies in a specific range," *Neurocomputing*, vol. 69, no. 3, pp. 900–904, July 2006.
- [40] J. C. A. Van-Der-Lubbe, *Information Theory*. Cambridge, England: Cambridge University Press, 1997.
- [41] A. J. Bell and T. J. Sejnowski, "An information-maximisation approach to blind separation and blind deconvolution," *Neural Computation*, vol. 7, no. 6, pp. 1129–1159, 1995.
- [42] S. Haykin, *Adaptive Filter Theory (4th edition)*. Englewood Cliffs, N.J.: Prentice Hall, Inc., 2002.
- [43] Mathworks inc., "Wavelet Tool Box User's Guide, Chapter 1. Wavelets: A New Tool for Signal Analysis". 1996 Edition.
- [44] R. C. Gonzalez and R. E. Woods, *Digital Image Processing*. New Jersey, USA: Prentice Hall, 2002.
- [45] L. J. Hadjileontiadis and S. M. Panas, "Separation of Discontinuous Adventitious Sounds from Vesicular Sounds Using a Wavelet-Based Filter," *IEEE Trans. Biomed. Eng.*, vol. 44, no. 12, pp. 1269–1272, December 1997.
- [46] S. W. Smith, *The scientist and engineer's guide to signal processing. 2nd Ed.* San Diego, USA: California Technical Publishing, 1999.
- [47] L. T. Hall and J. L. Maple, "Sensor system for heart sound biomonitor," *Microelectronics Journal*, vol. 31, no. 7, pp. 583–592, July 2000.

-
- [48] M. Obaidat, “Phonocardiogram signals: techniques and performance comparison,” *Journal of medical engineering and technology*, vol. 17, no. 6, pp. 221–227, November 1993.
- [49] M. Kutz, *Standart handbook on biomedical engineering and design. 1st Ed.* New York, USA: McGraw-Hill, 2003.
- [50] S. R. Messer, J. Agzarian, and D. Abbot, “Optimal wavelet denoising for phonocardiograms,” *Microelectronics Journal*, vol. 32, no. 12, pp. 931–941, December 2003.
- [51] S. M. Debbal and F. Bereski-Reguing, “Heart sound analysis with the wavelet transform,” *Journal of mechanics in medicine and biology*, vol. 4, pp. 133–141, March 2004.
- [52] S. Mann and S. Haykin, “The Chirplet Transform: Physical considerations,” *IEEE Trans. Signal Processing*, vol. 43, no. 11, pp. 2745–2761, November 1995.
- [53] G. Davis, S. Mallat, and M. Avellaneda, “Adaptive Greedy Approximations,” *Constructive Approximation*, vol. 13, no. 1, pp. 57–98, March 1997.
- [54] A. Bultan, “A four-parameter atomic decomposition of chirplets,” *IEEE Trans. Signal Processing*, vol. 47, no. 3, pp. 731–745, March 1999.
- [55] S. G. Mallat and Z. Zang, “Matching pursuit with time-frequency dictionaries,” *IEEE Trans. Signal Processing*, vol. 41, no. 12, pp. 3397–3415, December 1993.
- [56] R. Gribonval, “Fast matching pursuit with multiscale dictionaries

- of Gaussian chirps,” *IEEE Trans. Signal Processing*, vol. 49, no. 5, pp. 994–1001, May 2001.
- [57] J. Cui and W. Wong, “The Adaptive Chirplet Transform and Visual Evoked Potentials,” *IEEE Trans. Biomed. Eng.*, vol. 53, no. 7, pp. 1378–1380, July 2006.
- [58] B. Widrow, J. M. McCool, J. Kaunitz, C. S. Williams, R. H. Hearn, J. R. Zeidler, E. Dong, and R. C. Goodlin, “Adaptive noise cancelling: Principles and applications,” in *Proc. Ann. Int. Conf. IEEE*, pp. 1692–1716. 1975.
- [59] Naval Undersea Centre, San Diego, CA, *Principles and applications of adaptive filters: A tutorial view*. 1977 Edition.
- [60] J. R. Zeidler, E. Satorius, D. Chabries, and H. Wexler, “Adaptive enhancement of multiple sinusoids in uncorrelated noise,” *IEEE Trans. Acoustics, Speech, and Signal Processing*, vol. 26, no. 3, pp. 240–254, January 1978.
- [61] L. G. Griffiths, “Rapid measurement of digital instantaneous frequency,” *IEEE Trans. Acoustics, Speech, and Signal Processing*, vol. 23, no. 2, pp. 207–222, April 1975.
- [62] L. Griffiths, F. Smolka, and L. Trembly, “Adaptive deconvolution: A new technique for processing time-varying seismic data,” *Geophysics*, vol. 42, no. 4, pp. 742–759, Jun 1977.
- [63] D. Morgan and S. Craig, “Real-time adaptive linear prediction using the least mean squares gradient algorithm,” *IEEE Trans. Acoustics, Speech, and Signal Processing*, vol. 24, no. 6, pp. 494–507, December 1976.

-
- [64] B. Widrow and M. Holf, “switching circuits,” in *IRE WESCON Conv. Rec.*, pp. 96–104. 1960.
- [65] J. Zeidler, “Performance analysis of LMS adaptive prediction filters,” in *Proc. Ann. Int. Conf. IEEE*, pp. 1784–1793. 1990.
- [66] J. Rickard and J. Zeidler, “Second-order output statistics of the adaptive line enhancer,” *IEEE Trans. Acoustics, Speech, and Signal Processing*, vol. 27, no. 1, pp. 31–39, February 1979.
- [67] “R.a.l.e. repository.” [online], <http://www.rale.ca/Recordings.htm>.
- [68] X. Li and X. Zhang, “Sequential blind extraction adopting second-order statistics,” *IEEE Signal Process. Lett.*, vol. 14, no. 1, pp. 58–60, January 2007.
- [69] R. Sameni, C. Jutten, and M. B. Shamsollahi, “Multichannel electrocardiogram decomposition using periodic component analysis,” *IEEE Trans. on Biomedical Engineering*, vol. 55, no. 8, pp. 1935–1940, August 2008.
- [70] A. Hyvrinen and E. Oja, “Independent component analysis: algorithms and applications,” *Neural Networks*, vol. 13, no. 4, pp. 411–430, March 2000.
- [71] P. Comon, “Independent component analysis, a new concept?,” *Signal Processing*, vol. 36, no. 3, pp. 287–314, April 1994.
- [72] K. Matsuoka, M. Oya, and M. Kawamoto, “A neural net for blind separation of nonstationary signals,” *Neural Networks*, vol. 8, no. 3, pp. 411–419, November 1995.

- [73] D. T. Pham and J. F. Cardoso, "Blind separation of instantaneous mixtures of non stationary sources," *IEEE Trans. on Signal Processing*, vol. 49, no. 9, pp. 1837–1848, September 2001.
- [74] L. Molgedey and H. G. Schuster, "Separation of a mixture of independent signals using time delayed correlations," *Phys. Rev. Lett.*, vol. 72, no. 23, pp. 3634–3637, June 1994.
- [75] S. Choi and A. Cichocki, "Blind separation of nonstationary sources in noisy mixtures," *Electron. Lett.*, vol. 36, no. 9, pp. 848–849, April 2000.
- [76] A. Belouchrani and A. Cichocki, "A robust procedure in blind source separation context," *Electron. Lett.*, vol. 36 no. 24, pp. 2050–2051, November 2000.
- [77] M. G. Jafari, W. Wang, J. A. Chambers, T. Hoya, and A. Cichocki, "Sequential blind source separation based exclusively on second-order statistics developed for a class of periodic signals," *IEEE Trans. Signal Process.*, vol. 54, no. 3, pp. 1028–1040, March 2006.
- [78] R. T. Behrens and L. L. Scharf, "Signal processing applications of oblique projection operators," *IEEE Trans. Signal Process.*, vol. 42, no. 6, pp. 1413–1424, June 1994.
- [79] R. Sameni, C. Jutten, and M. B. Shamsollahi, "What ICA provides for ECG processing: Application to noninvasive fetal ECG extraction," in *Proc. of the International Symposium on Signal Process. and Information Technology (ISSPIT06)*, pp. 656–661. 2006.
- [80] G. H. Golub and C. F. V. Loan, *Matrix Computation, 3rd edition*. USA: Johns Hopkins Series in the Mathematical Sciences, 1996.

- [81] T. Tsalaile, S. M. Naqvi, K. Nazarpour, S. Sanei, and J. A. Chambers, "Blind source extraction of heart sound signals from lung sound recordings exploiting periodicity of the heart sound," in *Proc. IEEE Int. Conf. on Acoustics, Speech, and Signal Processing (ICASSP08)*, pp. 461–464. vol. 3, Las Vegas, Nevada, April 2008.
- [82] J. F. Yip and A. Souloumiac, "Blind beamforming for non Gaussian signals," in *Proc. Ann. Int. Conf. IEE*, pp. 362–370. 1993.
- [83] A. K. Barros and N. Ohnishi, "Heart instantaneous frequency (HIF): an alternative approach to extract heart rate variability," *IEEE Trans. on Biomedical Engineering*, vol. 48, no. 7, pp. 850–855, August 2001.
- [84] R. Sameni, G. D. Clifford, C. Jutten, and M. B. Shamsollahi, "Multichannel ECG and Noise Modeling: Application to Maternal and Fetal ECG Signals," *EURASIP Journal on Advances in Signal Process.*, Article ID 43 407, 14 pages.
- [85] T. Tsalaile, R. Sameni, S. Sanei, C. Jutten, and J. Chambers, "Sequential blind source extraction of quasi-periodic signals with time-varying period," *IEEE Trans. on Biomedical Engineering*, doi=10.1109/TBME.2008.2002141.
- [86] B. Ristic, S. Arulampalam, and N. Gordon, *Beyond the Kalman filter: Particle filters for tracking applications*. Boston . London: Artech house publishers.
- [87] L. Ljung and T. Söderström, *Theory and practice of recursive identification*. MIT Press, 1983.

-
- [88] H. H. Chen and L. Guo, *Identification and stochastic adaptive control*. Birkhäuser, 1991.
- [89] A. Doucet, S. Godsill, and C. Andrieu, “On sequential Monte Carlo sampling methods for Bayesian filtering,” *Statistics and Computing*, vol. 10, pp. 197–208, 2000.
- [90] J. S. Liu and R. Chen, “Sequential Monte Carlo methods for dynamical systems,” *J. Amer. Statist. Assoc.*, vol. 93, pp. 1032–1044, 1998.
- [91] P. J. Harrison and C. F. Stevens, “Bayesian forecasting,” *J. Roy. Statist. Soc. Series B. Methodological*, vol. 38, pp. 205–228, 1976.
- [92] S. Haykin, *Adaptive filter theory, 3th Ed.* Prentice Hall, 1996.